BIOLOGY OF AAV VECTORS IN THE CENTRAL NERVOUS SYSTEM

Giridhar Murlidharan

A dissertation submitted to the faculty at the University of North Carolina at Chapel Hill in partial fulfillment of the requirements for the degree of Doctor of Philosophy in the Curriculum in Genetics and Molecular Biology in the School of Medicine.

Chapel Hill
2016

Approved by:

Aravind Asokan

Juan Song

Garret Stuber

Jian Liu

Mark Heise

ABSTRACT

Giridhar Murlidharan: Biology of AAV vectors in the central nervous system
(Under the direction of Aravind Asokan)

Adeno-Associated Viruses (AAV) have emerged as the vector platform of choice for therapeutic gene transfer towards multiple genetic disorders with neurological manifestations. My doctoral thesis was focused on a) evaluating CNS spread, transduction profiles, receptor interactions and clearance; and b) understanding the physiological and biochemical checkpoints governing AAV biologics in the CNS. In our first study, we engineered an AAV4 variant (AAV4.18) that shows expanded tropism from ependymal cells to migrating progenitors in the developing brain. AAV4.18 revealed a striking shift in glycan engagement from 2,3-linked Sialic acid (SA) to 2,8-linked Polysialic acid (PSA). PSA is an important biomarker of neurogenesis. We also report opposing roles of SA and PSA on CNS transduction of AAV4. Overall, carbohydrate content can be exploited to regulate viral tropism in the brain. We then evaluated a lab-derived chimeric AAV2g9, developed through rational vector design. Direct brain injections of AAV2g9 resulted in widespread neuronal transduction with reduced glial tropism. As compared to AAV9, AAV2g9 displayed minimal systemic leakage and off-target gene expression within peripheral organs. We utilized AAV2g9 for brain-specific deletion of ubiquitously expressed MIR137 schizophrenia risk gene using CRISPR/Cas9 technology. Our approach exemplifies control over AAV tropism at both cellular and organ levels to potentially improve vector safety. Lastly, AAV mediated

CNS gene therapy requires a deeper understanding of factors affecting transduction efficiency and clearance. Dysfunction in aquaporin-4 (AQP4) mediated CSF flux during aging or disease is correlated with ineffective solute clearance from the brain. Aged mice showed mislocalized AQP4 expression and increased AAV9 deposition following intraCSF administration. We further compared wildtype (WT) and AQP4 knockout (AQP4-/-) mouse CNS. Minutes after intraCSF administration, AQP4-/- mice exhibited highly restricted spread of fluorophore labeled AAV9. Transgene expression was markedly increased 2 weeks post AAV9 administrations in AQP4-/- mice. Further, AQP4-/- mice showed markedly reduced AAV biodistribution and transgene expression in peripheral organs. This suggests that AQP4-deregulation affects CNS spread, transduction efficiency and systemic leakage of AAV vectors. We hypothesize that altered CSF flux under conditions of aging, CNS disease or injury can impact AAV residence time and gene transfer efficiency.

To my parents Mr. S. Murlidharan and Mrs. Jaya Murlidharan
&
My fiancé Suguna Jairam

ACKNOWLEDGEMENTS

Coming from an engineering background, I have always been drawn to devising elegant solutions for problems. To this end, the spectrum of scientific questions being asked and the bandwidth of studies being conducted at the Asokan lab immediately resonated with my research interests. As a PhD advisor, Dr. Aravind Asokan offered the right mix of effective mentorship and friendly approachability to his students. One of Aravind's key attributes is his ability to inculcate a sense of ownership in his team of researchers, for their work. His commitment to train students on conducting day-to-day experiments while keeping the big picture in sight at all times, is truly commendable. In addition to constantly providing direction to my research, Aravind was very patient and equipped me with the skills I required to showcase my findings and connect with various audiences. Overall, having known Aravind as his PhD mentee and as a friend, I will always try to emulate his scientific perseverance and his ability to think objectively at all times. Lastly, I am grateful to him for offering me a position in his lab and advising me on issues related to work and life; and his family for treating me, Suguna and Khushi as one of their own.

My special thanks to my thesis committee members Dr. Mark Heise, Dr. Jian Liu, Dr. Garret Stuber, Dr. Richard Jude Samulski, Dr. Juan Song and Aravind. Their expertise and knowledge in the fields of virology, glycobiology, neuroscience, and gene

therapy have enabled me to complete a comprehensive body of research work and publish my findings in a timely fashion. I specifically want to thank them for taking time off their busy schedules for ensuring my progress during my committee meetings. Their ability to critically analyze my experimental findings, to applaud the positives and criticize the shortcomings has shaped me into a thorough scientist. They ensured that I achieve the important milestones along the way of completion of my PhD. My heartfelt thanks to all of them.

I would also like to thank the curriculum in Genetics and Molecular Biology, our program director Dr. Jeff Sekelsky and administrative coordinators John Cornett and Cara Marlow for helping me fulfill all the graduate school requirements and ensuring smooth completion of my PhD training.

Growing up, my dad once said achievements are only as valuable as the struggle and sacrifice they demand. Coming from a family of academicians on both my parents' sides, I was exposed to hard work, patience and a curiosity to learn from very early on. Some of the most vivid memories of my childhood include listening to my mother give Indian classical music lessons to kids from the neighborhood, against the backdrop of a constant clamor from my dad's old Remington typing machine, as he wrote articles for his weekly columns in newspapers. I truly believe that good parenting by way of setting examples goes a long way in one's life. My parents always strived to put my happiness before anything else, and I am deeply grateful to them. What I am today is thanks to the efforts and love of my mom and dad.

I met my fiancé Suguna Jairam during the first year of undergraduate college in Tamilnadu, India. She is the love of my life, a constant source of inspiration and an

unfaltering support system. As I complete this chapter in my life and embark on a new journey, I consider myself lucky to have her by my side.

While I was undergoing my PhD training here at UNC, Suguna was pursuing hers at University of Florida. During one of my visits to Florida in the 4th year of my PhD, our friends Sherry and Corky introduced us to a beautiful one month old beagle-mix from their pet rescue. Suguna and I did not have to think twice before we decided to bring her into our life. Small wonder, bringing 'Khushi' home also brought us the most happiness. The final stretch of graduate school work was made easy knowing that at the end of the day, when I go back home, the happiest being on earth was waiting to greet me, every single day.

The collaborative atmosphere at Asokan lab truly helped cultivate a sense of positivity and maximized my productivity. When I joined the Lab, Shen Shen, Nagesh Pulicherla and Eric Horowitz were extremely helpful and open to sharing ideas, reagents, protocols and techniques. This enabled me to get a head start with my various projects and I am really thankful for their gesture. As a junior graduate student in lab, I watched Shen successfully cross hurdles, present her findings at scientific meetings, publish manuscripts and finally defend her PhD work. The experience was both rewarding and a great learning opportunity overall. I would like to specifically thank Shen for her friendly and approachable demeanor.

I am very thankful to other graduate students that overlapped with me during my time at Asokan Lab-Erin, Garret, Blake, Vicky, Patrick and Rita have been instrumental in keeping the atmosphere at work happy and life outside lab fun! A special mention to

Erin and Garret who joined the PhD program along with me in 2011. It has been a pleasure making these great friends and grow as a scientist alongside them!

The postdoctoral scholars Ruth, Sven and Victor have been extremely helpful in sharing their knowledge and providing constructive criticisms while I wrote manuscripts and designed experiments. Special thanks to Victor for keeping everyone around him laughing all the time (one of the funniest people I know); Sven and Cheryl for organizing the best movie/game nights at their home; and Ruth for bringing her kids to work from time to time! It was wonderful working with these people.

I would also like to thank the extremely talented set of past and present postbac and undergraduate researchers I have had the pleasure of working with over the years- Andrew, Sarah, Leo, Joey, Ryan, Sebastian, Lavanya, Travis, Michael, Danny, Rob, Dasean, Kelly, Kelsey, Julianne and Becca. A special shout-out to Travis, Lavanya and Danny for helping me with animal experiments which were instrumental in completion of my manuscripts.

Lastly, my heartfelt thanks to our director of research, Tara Britt, our lab mom! For ensuring everyone's wellbeing and constantly bringing us amazing food! And to my friends and family back home in India and the huge family of friends that I have made in the US, for all their love and support.

I have always aspired to see 'PhD' written next to my name. In addition to the sense of achievement for this cherished goal, I will leave Asokan lab with some of the happiest memories, great friends, and a promise to keep visiting as often as I can.

Giri Murlidharan

TABLE OF CONTENTS

LIST OF FIGURES xii

LIST OF TABLES xiv

LIST OF ABBREVIATIONS xv

CHAPTER 1: INTRODUCTION 1

1.1 Disorders of the Central Nervous System 1

1.2 Therapeutic Approaches to CNS disorders 2

1.3 Recombinant Adeno-Associated Viral Vectors 3

1.4 Biology of AAV cell entry and implications for CNS gene transfer 6

1.5 Clinical routes of AAV administration for CNS applications 7

1.5.1 Direct AAV administration into the CNS 7

1.5.2 Intravenous AAV administration for CNS Gene Transfer 11

1.6 AAV transport within the CNS 13

1.7 Gene Therapy of CNS Disorders using Recombinant AAV vectors 16

1.7.1 Gene therapy of Movement disorders 16

1.7.2 Gene therapy of CNS disorders arising from metabolic defects 25

1.8 Safety aspects of AAV-mediated CNS gene therapy 36

CHAPTER 2: EXPLOITING GLYCAN SIGNATURES TO REGULATE ADENO-ASSOCIATED VIRAL TROPISM IN THE DEVELOPING BRAIN 45

2.1 Overview 45

2.2 Introduction 46

2.3 Materials and Methods 48

2.4 Results 52

2.5 Discussion 59

CHAPTER 3: LIMITED SYSTEMIC BURDEN AND BRAIN-SPECIFIC GENE DELETION WITH A NOVEL AAV VECTOR 72

3.1 Overview 72

3.2 Introduction 73

3.2 MATERIALS AND METHODS 77

3.3 RESULTS AND DISCUSSIONS 82

CHAPTER 4: AQUAPORIN 4 REGULATES THE PARAVASCULAR CLEARANCE OF AAV VECTORS FROM THE BRAIN 109

4.1 Overview 109

4.2 Introduction 110

4.3 Materials and Methods 112

4.4 Results 116

4.5 Discussion 123

Chapter 5: SYNOPSIS AND FUTURE DIRECTIONS 134

5.1: The Big Picture 134

5.2: Future Directions 137

REFERENCES 145

LIST OF FIGURES

Figure 1: Schematic representation of AAV genomes 39

Figure 2: Differential spread of CNS transduction from AAV4 or AAV9 vectors packaging TdTomato fluorescent reporter transgene in neonatal mouse brain 40

Figure 3: Effects of substrate-specific neuraminidases on AAV4/4.18 transduction *in vitro* 64

Figure 4: Ependymal transduction in the neonatal mouse brain by AAV4 and the AAV4.18 mutant. 65

Figure 5: The AAV4.18 mutant exhibits selective tropism for migrating progenitors 66

Figure 6: AAV4.18 particles show enhanced CNS spread. 67

Figure 7: SA and PSA play opposing roles in AAV4 transduction within the neonatal mouse brain. 68

Figure 8: Removal of PSA expands AAV4 tropism to mature OB neurons. 69

Figure 9: The AAV4.18 mutant selectively exploits polysialic acid (PSA) to transduce migrating progenitors. 70

Figure 10: AAV4.18 selectively transduces migrating progenitors expressing polysialyated NCAM and GFAP. 71

Figure 11. Comparison of transgene (GFP) expression and cellular tropisms displayed by AAV9 and AAV2g9 vectors with a ubiquitous promoter after ventricular (ICV) injection. 94

Figure 12. Comparison of transgene (GFP) expression and cellular tropisms displayed by AAV9 and AAV2g9 vectors with cell type-specific promoters after ventricular (ICV) injection. 96

Figure 13. Quantitative assessment of transduction following ICV administration of AAV9 and AAV2g9 vectors. 97

Figure 14. Heparan sulfate interactions are critical towards preferential neuronal transduction by AAV2g9 vectors. 98

Figure 15. CNS transduction profile of a gal-binding AAV9 mutant (W503R) and AAV9 following ventricular (ICV) administration. 99

Figure 16. CNS transduction profile and cellular tropisms displayed by AAV8 and gal-binding AAV8g9 vectors following ventricular (ICV) injection. 101

Figure 17. Comparison of transgene (GFP) expression and cellular tropism displayed by AAV9 and AAV2g9 vectors following intrathecal infusion. 103

Figure 18. Comparison of systemic biodistribution and off-target transgene (GFP) expression displayed by ICV/IT injected AAV9 and AAV2g9 vectors. 105

Figure 19. Comparison of blood circulation/pharmacokinetic profiles AAV9 and AAV2g9 vectors in adult mice post IT administration. 107

Figure 20. CNS-restricted gene disruption of MIR 137 within Cas9 transgenic mouse using AAV2g9. 108

Figure 21. Comparison of AAV vector accumulation within juvenile and aging mouse brains. 126

Figure 22. Aged mice display abnormal AAV accumulation and altered AQP4 localization in the brain. 128

Figure 23. Comparison of AAV vector spread within wildtype and aquaporin-4 knockout mouse CNS. 129

Figure 24. Comparison of AAV transduction efficiency following intraCSF administration in WT and AQP4-/- mouse brains. 130

Figure 25. Comparison of off-target transduction and biodistribution of AAV vectors following intracranial administrations in WT and AQP4-/- mice. 132

Figure 26. Comparison of AQP4 expression in WT and AQP4-/- mouse brain. 133

LIST OF TABLES

Table 1. Capsid-receptor interactions, transduction profiles and axonal transport properties of some of the well characterized Adeno-associated viral serotypes in the mammalian CNS. 41

Table 2. Clinical gene therapy of some neurological disorders using AAV vectors 42

LIST OF ABBREVIATIONS

6-OHDA	6-hydroxydopamine
α-syn	alpha-synuclein
β-GUSB	β-glucuronidase
AADC	L-amino acid decarboxylase
AAP	Assembly activating protein
AAT	Alpha-1 Antitrypsin
AAV	Adeno-associated virus
Aβ	Amyloid beta
AD	Alzheimer's disease
ALS	Amyotrophic lateral sclerosis
AQP4	Aquaporin-4
BBB	Blood-brain barrier
BDNF	Brain derived neurotrophic factor
BMT	Bone marrow transplant
BrdU	5-bromo-2'-deoxyuridine
CBA	Chicken beta actin
CBh	Chicken beta hybrid
CC	Corpus callosum
CED	Convection-enhanced delivery
circRNA	Circular RNA
CMV	Cytomegalovirus

CNS	Central nervous system
CRISPR	Clustered regularly interspaced short palindromic repeats
CSF	Cerebrospinal fluid
CT	Cortex
DA	Dopaminergic
DAB	Diaminobenzidine
DCX	Doublecortin
DMEM	Dulbecco’s modified eagle’s medium
DNA	Deoxyribonucleic acid
DRG	Dorsal root ganglia
EDTA	Ethylenediaminetretraacetic acid
Endo-N	Endoneuraminidase-N
EPO	Human erythropoietin
ERT	Enzyme replacement therapy
FBS	Fetal bovine serum
FITC	Fluorescein isothiocyanate
GABA	Gamma (γ)-amino butyric acid
GAD	Glutamic acid decarboxylase
GAG	Glycosaminoglycans
Gal	Galactose
GAN	Giant axonal neuropathy
GDNF	Glia derived neurotrophic factor
GFAP	Glial fibrilary acid protein

GFP	Green fluorescent protein
GLD	Globoid-cell leukodystrophy
gRNA	Guide RNA
GUSB	β-glucuronidase
GWAS	Genome-wide association study
HC	Hippocampus
HD	Huntington's disease
HEK293	Human embryonic kidney 293
HSPG	Heparan sulfate proteoglycans
HSV	Herpes simplex virus
hSYN	Human synapsin
HTL	Hypothalamus
ICV	Intracerebroventricular
ISF	Interstitial fluid
ISTR	Intrastriatal
IT	Intrathecal
ITR	Inverted terminal repeats
IV	Intravenous
KSHV	Kaposi's sarcoma associated herpesvirus
LINCL	Late infantile neuronal ceroid lipofuscinosis
LSD	Lysosomal storage disorder
LV	Lateral ventricle
MENβ	Multiple endocrine neoplasia β

miR	MicroRNA
MPS	Mucopolysacharidoses
MVM	Minute virus of mice
MWCO	Molecular weight cut-off
NaGlu	N-acetylglucosaminidase
NCAM	Neural cell adhesion molecule
NCL	Neuronal ceroid lipofuscinosis
Neu	Neuraminidase
NeuN	Neuronal antigen N
NGF	Nerve growth factor
NHP	Non-human primate
NTN	Neurturin
OB	Olfactory bulb
ORF	Open reading frame
P0	Postnatal day 0
PCR	Polymerase chain reaction
PD	Parkinson’s disease
PEI	Polyethylenimine
PET	Positron emission tomography
PFA	Paraformaldehyde
PH3	Phospho-histone H3
PRV	Pseudorabies virus
PSA	Polysialic acid

QPCR	Quantitative polymerase chain reaction
RMS	Rostral migratory stream
ROI	Region of interest
RT PCR	Reverse transcription PCR
SA	Sialic acid
SEZ	Subependymal zone
Sc	Self-Complementary
SMA	Spinal muscular atrophy
SNPc	Substantia Nigra Pars Compacta
ss	Single-Stranded
STN	Subthalamic nucleus
TBI	Traumatic brain injury
TdTom	TdTomato
TH	Tyrosine hydroxylase
THL	Thalamus
UTR	Untranslated region
VM	Ventral mesencephalic
VP	Viral protein
VTA	Ventral tegmental area

CHAPTER 1: INTRODUCTION[1]

1.1 Disorders of the Central Nervous System

Mammalian central nervous system (CNS) is a complex and precise connectivity of intertwining neurons nourished and supported by glial cells- astrocytes, oligodendrocytes, and microglia. Smooth functioning of the CNS is orchestrated by excitation and inhibition of neuronal firing/action potential i.e. relay of potential difference traveling between the cell body (soma) and its projections at the axonal terminus/ni. Neurons are decorated with receptors for neurotransmitters like glutamate and gamma (γ)-amino butyric acid (GABA), which are specifically associated with excitatory or inhibitory responses (1).

While timely excitation and inhibition of regional subpopulations of neurons controls motor, behavioral, hormonal, sensory and cognitive outcomes; unregulated neuronal activity and selective loss of neuronal or glial subgroups has been associated with CNS disorders. Such disorders can arise from drug abuse, injuries, genetic, epigenetic and environmental factors. Loss of functionality in affected cell types within the brain can often be attributed to defects in single genes. For instance, a range of

[1]This chapter includes original publications that appeared in the journal Frontiers in Molecular Neuroscience and the book Translational Neuroscience. Full citations are as follows: Murlidharan, G., Samulski, R.J., Asokan, A. Biology of adeno-associated viral vectors in the central nervous system, Frontiers in Molecular Neuroscience, 2014, 89:0076.
Murlidharan, G, Samulski, R.J., Asokan, A. Gene therapy of CNS disorders using recombinant AAV vectors, Translational Neuroscience-Fundamental approaches for neurological disorders, 2016 (9-32)

neurological disorders arise from the inability of cells in the CNS to break down metabolic end products (e.g. lysosomal storage disorders (LSDs)). One such example of LSDs with fatal manifestations includes Globoid-cell leukodystrophy (GLD) or Krabbe disease in which mutations in galactosylceramidase leads to accumulation of the toxin 'psychosine' in the CNS (2). This disease shows early-onset of symptoms like demyelination, astrocyte gliosis etc. and progresses to the death of patients within 2 years of age (3). Other examples of LSDs include Fabry disease, Gaucher disease, GM1/GM2 Gangliosidosis, Mucopolysacharidoses disorders, Pompe disease and Neuronal Ceroid Lipofuscinosis amongst others (4, 5).

Another major class of neurological disorders manifest themselves as loss of motor skills e.g. Parkinson's disease (6), Huntington's disease (7), epilepsy (8), Tourette's syndrome (9, 10) and amyotrophic lateral sclerosis (ALS) (11); cognitive skills e.g. Alzheimer's disease (11), and Autism (12); or can rarely even be lethal very early on in life e.g. Canavan's disease (13). A common theme among patients suffering from such diseases includes difficulties in performing day to day activities amounting to exceptional loss in quality of life; disruption of social life; heavy financial burden of treatment; and in most cases, absence of curative options.

1.2 Therapeutic Approaches to CNS disorders

To ameliorate such disease phenotypes, tremendous effort has been directed towards pharmacological regulation of events such as neurotransmitter signaling e.g. by synthesizing receptor agonists/manipulating receptor domains by genetic reprogramming etc. (14). Although successful reversal of pathology is not common,

such interventions often provide symptomatic relief for short periods of time and are therefore approved for clinical use. Unfortunately, side-effects of pharmacological agents; irreversible nature of most genetic alterations; restricted ability of CNS cells to replenish themselves; and complicated clinical procedures make CNS disease therapy an exceptionally difficult endeavor.

Gene therapy is being utilized for treating severely debilitating diseases by delivering healthy cargo of genetic information to afflicted cell/tissue types. Within the CNS, replenishment of biomolecules that are depleted as a result of disease (e.g. catabolic enzymes); protection of neurons and glia from premature death; and even utilization of cells as bio-factories for production of neurotransmitters and their biological co-factors have been demonstrated using gene therapy. Viral vector mediated gene therapy offers the ability to perform efficient *in vivo* gene transfer of therapeutic transgenes directed to the CNS. In particular, Adeno-Associated Viruses (AAV) have emerged as promising tools for clinical gene transfer in a broad range of genetic disorders with neurological manifestations (15). Throughout this chapter, I have attempted to bridge the current understanding of the biology of different AAVs with their properties such as transduction efficiencies, cellular tropism and transport within the CNS.

1.3 Recombinant Adeno-Associated Viral Vectors

Adeno-associated viruses (AAV) are non-enveloped, helper-dependent parvoviruses with an icosahedral capsid architecture ~25 nm in diameter. AAVs

package ~4.7 kb genome flanked by ~145 bp inverted terminal repeats (ITRs) on the 5' and 3' ends (16). The wildtype AAV (wtAAV) genome is a linear single stranded DNA consisting of two open reading frames (ORFs). AAV ORFs encode four replication proteins (Rep) and three capsid proteins (Cap/VP) and an assembly activating protein (AAP) (17). In addition, wtAAV requires co-infection by Adenoviruses or Herpes Simplex viruses for successful replication and production of viable AAV particles (16).

Three advancements have been instrumental in enabling the use of AAV as a recombinant vector for gene transfer applications: a) the ability to pseudotype AAV vectors by employing AAV capsids of natural or synthetic origin (18-21); b) cloning and characterization of adenoviral helper genes that are minimally required for generation of infectious AAV particles (22); and c) understanding that inverted terminal repeats (ITRs) are the only *cis*-acting molecular signature for successful packaging of transgenes within an AAV capsids (23). These streamlined components are now used to manufacture recombinant AAV (rAAV) vectors packaging a broad spectrum of promoter elements and transgene cassettes for different gene transfer applications (24). It is noteworthy that due to the aforementioned discoveries, we are now able to manufacture AAV vectors with minimal contamination of the wildtype virions. This technology allows us to package the transgene of interest into an AAV serotype with desirable properties in either single stranded (ss) or self-complementary (sc) configuration (**Figure 1**).

Different AAV serotypes exhibit a range of properties pertaining to antigenicity, *in* vivo tropism and receptor interactions based on their capsid structures (17). Capsids of different AAV strains bind a spectrum of cell surface glycan receptors and utilize co-receptors for infection (25). These differences in capsid-receptor interactions play a

major role in determining the regional and cellular transduction efficiencies of AAV strains across different mammalian organs. Additionally, a recent *in vitro* genetic screen has revealed the type I transmembrane protein, KIAA0319L as an important receptor for AAV infection (26). Continued progress in understanding the biology of AAV infection over the past two decades has provided the scientific and clinical community with an arsenal of AAV strains that offer desirable features for CNS gene transfer (27). In addition to natural isolates, several laboratory-derived AAV strains have been engineered or evolved for specific CNS gene transfer applications. These efforts have yielded novel AAV vectors for targeting a) glioblastoma cells (28); b) rat, mouse and human neural stem cells (29); and c) specific regions (piriform cortex and ventral hippocampus) of blood-brain barrier (BBB) compromised rats (30).

In order to showcase differences in CNS transduction profiles of AAV vectors, we injected two structurally and functionally distinct strains- AAV4 and AAV9 packaging TdTomato (TdTom) fluorescent reporter gene driven by chicken β actin (CBA) promoter in the neonatal mouse brain. Intraventricular injections (white arrows, **Figure 2**) of AAV4 resulted in TdTom expression (red) close to the site of injection (ependyma) (AAV4-CBA-TdTom, **Figure 2**). On the other hand, AAV9 administration resulted in widespread TdTom expression across multiple regions of the brain parenchyma (AAV9-CBA-TdTom, **Figure 2**). These results suggest that AAV vectors can be utilized to achieve either restricted or widespread transgene expression in the CNS. We discuss the existing inventory of AAV vectors and their characterization within the CNS later.

1.4 Biology of AAV cell entry and implications for CNS gene transfer

Successful transduction by AAV vectors is contingent on many key steps like cell surface receptor binding, endocytic uptake, endosomal escape, subsequent nuclear entry, capsid uncoating, genome release, second strand synthesis and subsequent transcription. Surface exposed regions on the AAV capsids dictate the interactions with the host cell surface (25). Cell surface glycans have been identified as the preferred primary receptors for many natural AAVs (31). Accordingly, differences in glycan architecture have been attributed to variations in the efficiency of gene transfer by AAV capsids in different organs. AAV serotypes 1,5 and 6 bind *N*-linked sialic acid (SA), whereas AAV4 is the only natural AAV isolate that binds *O*-linked SA moieties on mammalian cell surfaces (32-34). AAV2, 3 and 6 bind Heparan Sulfate (HS) proteoglycans, whereas AAV9 requires N-terminal galactose residues to perform successful gene transfer (35-38).

Direct injection of HS binding AAV2 in the CNS leads to a largely neuronal transduction profile, whereas Sialic acid (SA) binding vectors like AAV1 and AAV5 perform efficient neuronal and some glial transduction (39-41). The preferential neuronal tropism of AAV2 was later identified to correlate with the comparatively larger availability of Heparan sulfate proteoglycans (HSPGs) on the surface of neurons than glia (42, 43). Interestingly, in addition to enabling the neurotropic bias of AAV2, HS binding has also been associated with restriction of the CNS volume that is effectively targeted by AAV vectors.

It is now known that the lysine residue at position 531 on AAV6 capsid plays an indispensable role in HS binding (44, 45). By creating HS binding and non-binding

variants of AAV1 (AAV1E531K) and AAV6 (AAV6K531E) respectively, Arnett and colleagues demonstrated antagonistic effect of HS binding on CNS transduction of intracranially injected AAVs (46). Supporting these point mutation studies, co-injection of safe doses of soluble heparin also led to substantial increase in the CNS transduction by AAV2 (47, 48).

On the other hand, N-terminal galactose binding AAV9 is one of the most efficient vectors for CNS gene transfer. AAV9 has been shown to perform extensive neuronal and glial transduction from different routes of injection in small and large animal models (49-56). In addition to important features on the capsid surfaces, efficiency of AAV vector mediated gene transfer can be affected by several post-entry, trafficking and genome-related events within the CNS (26). Studies pertaining to some of these aspects of AAV biology have been performed within the context of the CNS and discussed later. Prior to cell surface binding, the transduction profiles of different AAV strains also appear to be affected by the route of CNS administration. These aspects are first discussed below.

1.5 Clinical routes of AAV administration for CNS applications

1.5.1 Direct AAV administration into the CNS

Direct injections of AAV vectors into the CNS have been used to achieve high levels of transgene expression across different animal models (57-60). This strategy of AAV vector administration can be broadly classified into intra-cerebrospinal fluid (CSF) administration and intra-parenchymal administration. The CSF plays a multi-functional role by providing nutrients; molecular and physical cues for important processes like

stem cell migration; and removal of interstitial solutes from the brain parenchyma (61, 62). An extensive characterization of CSF clearance of brain interstitial solutes and its effects on intracranially administered AAV biologics can be found in chapter 4 of this thesis. The CSF is housed within the subarachnoid space, cerebral ventricles, cisterna magna, openings under the cerebellum (foramena), and is in close contact with the spinal cord and brain tissue in the rostrocaudal axis (63, 64). Understandably, efficient delivery of reporter/therapeutic transgenes to large areas of the CNS has been achieved using AAV injections into cerebral ventricles, cisterna magna or intravertebral lumbar puncture (65-75).

Serotypes such as AAV9 and rh.10 exhibit inherently superior ability to spread within the brain parenchyma. These vectors have been used to achieve widespread and long term expression of corrective transgenes from intra-CSF injections towards disease models of spinal muscular atrophy and Krabbe disease (73, 74). On the other hand, some AAV vectors exhibit highly cell-specific transduction profiles from intra-CSF injections. For instance, intracerebroventricular (ICV) administration of AAV4 leads to selective targeting of astrocytes in the ependymal zone surrounding the cerebral ventricles (71, 76, 77). The ependyma consists of adult neural stem cells that have the ability to perform lifelong migration, differentiation and repopulation of functionally defined regions in the brain (78). Due to this natural propensity for ependymal cells, we used AAV4 as a platform to engineer a migrating neural progenitor targeting AAV4.18 vector, as shown in chapter 2. Indeed, targeted delivery of neurogenic cargo, e.g. noggin and brain derived neurotrophic factor (BDNF) packaged in AAV4 has shown long-term rescue of mouse models of severely debilitating CNS disorders like

Huntington's disease (76, 79). In addition to these *in vivo* studies, biophysical analysis of the AAV4 capsid has revealed distinct structural features and low capsid homology among other natural AAV isolates (80, 81).

Due to the advantages offered by the CSF connectivity of the brain and the spinal cord, AAV vector administration has also been extensively characterized through intrathecal injections (IT). Traditionally, these injections have been performed by exposing the subarachnoid space at the suboccipital cisterna magna region or the intravertebral space at lumbar region. In general, applications requiring enhanced transduction at the motor, sensory and nociceptive neuronal subpopulations (e.g. within dorsal root ganglia (DRG)) utilize lumbar punctures. AAV serotypes 1, 5, 8 and 9 have shown extensive transduction in the spinal cord and DRG neurons from IT injections at the intravertebral lumbar region (82-84). In an independent study, Snyder and colleagues compared IT injections of AAV vectors 1, 6, 8 and 9 for transduction of motor neurons in the spinal cord and brain stem, and reported superior transduction properties of AAV6 and 9 (85). From studies conducted in large animals like pigs and non-human primates (NHPs), a single IT injection of AAV9 has emerged as the candidate procedure for clinical correction of motor neuron disorders affecting the different regions of the spinal cord (86, 87). As with all these studies, it remains to be seen how vectors pseudotyped with these different capsids respond in a human setting and more importantly, in manifestations of human brain disease.

Direct parenchymal injections of AAV vectors in rodents and non-human primates have been traditionally used to achieve transduction within, focused, spatio-functionally distinct regions of the brain (88-90). AAV2 shows minimal ability to spread

from the parenchymal site of injection and performs preferential gene transfer in the neurons (71). Unlike other capsid-receptor interactions, the high affinity for HSPGs has been shown to be detrimental to the spread of AAV2 in the brain parenchyma (48). As discussed above, another vector that lacks the ability to spread from the site of intracerebral injection is the NHP isolate AAV4 (71). In another study performed in adult rats, Burger and colleagues demonstrated that *N*-linked SA binding AAV1 and AAV5 are superior to AAV2 in terms of spread of transduction from a single parenchymal microinjection into the hippocampus, substantia nigra, globus pallidus, striatum and spinal cord (89). Widespread transgene expression was also achieved by parenchymal injections of AAV7, 8 and 9 in rodents (90, 91). On a cellular level, these vectors preferentially transduced neurons in the adult rodents from clinically relevant stereotaxic injections into the hippocampus, thalamus, cortex and striatum (90). Interestingly, in addition to capsid serotype, other parameters like age of the animal also seem to affect cellular tropism of AAV vectors from direct brain injections. Using ICV injections of AAVs 1, 8 and 9, Chakrabarty and colleagues demonstrated, that injections performed on postnatal day 0 (P0) leads to preferential neuronal tropism. On the other hand the same vectors showed neuronal and astrocytic transduction profiles from injections performed on P1 or later (72).

Against this backdrop of AAV isolates and serotypes that have been extensively characterized for their receptor interactions, novel AAV serotypes isolated from human beings- AAVhu32, 37, 11, 48R3; and non-human primates- AAVrh.8 and 10 have been evaluated in neonatal and adult rodents (55, 92). Preliminary studies have confirmed the ability of these vectors to perform transduction comparable to AAV9 in rodents,

expanding the AAV vector toolkit for CNS gene transfer. For instance, a recent study conducted head to head comparison of AAV 2, 5, 8 and rh.10 for therapeutic delivery of functional ‘CLN2’ transgene in a late infantile neuronal ceroid lipofuscinosis (LINCL) mouse model. Among different serotypes, AAVrh.10 demonstrated comparatively larger spread of transgene expression and restoration of functional levels of the enzyme tripeptidyl-peptidase I, originally lost as a result of mutations in the CLN2 gene. Improvement in motor activities like gait, balance and grip; and amelioration of seizures led to enhanced survival of the treated mice from a single direct brain parenchymal injection (93). More recent studies evaluating AAVrh.10 administered through different routes in primates have been reviewed in detail in the context of AAV transport within the CNS later.

1.5.2 Intravenous AAV administration for CNS Gene Transfer

Systemic administration of viral vectors has the potential to achieve ubiquitous gene transfer of the CNS from a single injection. Additionally, the minimally invasive nature of intravenous (IV) injections adds great value to clinical administration of AAV vectors via the bloodstream. Two major roadblocks currently impede our ability to utilize this technique for therapeutic gene transfer of the CNS. The first major concern is the broad biodistribution of AAV vector particles into off-target tissues such as the liver, spleen and kidneys during IV administration of AAVs. For instance, IV injections of AAV9 achieves exceptional transduction of neurons and glia in rodents and non-human primates, but also leads to enrichment of viral genomes (~10 fold or more) in the liver and spleen as compared to the brain (94). Careful optimization and use of safe dosages of AAV vectors can lead to reduced systemic leakage and associated viral clearance

due to neutralizing antibodies (94). Another approach to reduce peripheral organ toxicity is the occlusion of blood flow into organs like liver and spleen during IV injections of AAVs (95).

Clearly, the use of such techniques requires meticulous optimization of complicated surgical procedures during vector administration before being approved for the clinic. However, it should also be noted that several of these techniques are already approved for use with other drugs/treatments in the clinical setting. Another important problem is the inability of the majority of well-characterized AAV vectors to efficiently cross the blood-brain barrier (BBB) and transduce cells within the CNS. In order to successfully transduce cells in the CNS, systemically injected virions are thought to undergo receptor mediated transcytosis to cross the brain microvasculature. Tight junctions in the endothelial cells, astrocytic endfeet and pericytes are collectively thought to constitute the BBB (96, 97). Intra-arterial infusion of mannitol leads to transient opening of the BBB without eliciting any permanent damage (67). Short-term disruption of these checkpoints by administration of mannitol led to effective CNS transduction by IV injections of AAV2 which is unable to cross the BBB (67, 98).

A recent study compared CNS transduction from injections of AAVs 1, 2, 5, 6, 7, 9, Rh.10, Rh.39 and Rh.43 into the superficial temporal vein of neonatal mice (P1). Successful, but differential levels of CNS transduction were reported from all tested vectors (except AAVs 2 and 5) (96). Additionally, some leading examples of intravenous administration of AAV vectors that have been tested in adult rodents and non-human primates include AAVs 8, 9, Rh.8 and Rh.10 (97, 99). These results clearly indicate that many AAV serotypes have been associated with a range of cellular and regional CNS

gene transfer properties from systemic injections. A better understanding of capsid structural motifs that allow certain AAV strains to traverse the blood brain barrier is critical. For instance, using directed evolution, Gray and colleagues have engineered two AAV capsids capable of crossing seizure compromised-BBB in rats. The original library of AAVs from which the candidate capsid was isolated included AAVs 1-6, 8 and 9. Comparison of the parental and evolved capsid sequences further provided some insights into capsid domains possibly involved in CNS transduction after IV administration (30). Along similar lines, peptide motifs have been identified that impart AAV capsids with the ability to cross the brain microvasculature. IV injection of a peptide modified version of the AAV2 packaging β–glucuronidase was used to achieve significant clearance of lysosomal storage burden, leading to cognitive benefits and prolonged survival in a mucopolysacharidoses VII mouse model (100). It is noteworthy that IV administration of the corrective transgene packaged in AAV9 capsid was unable to confer therapeutic benefits. It was later identified using fluorescein labeled *Sambucus Nigra* lectin that enhanced SA depositions in the MPS VII affected mouse CNS might be detrimental for AAV9-mediated CNS transduction (100). Such results demonstrate that the biology of different AAV strains can be affected by specific disease phenotypes that alter the molecular composition(s) of different cell types within the brain.

1.6 AAV transport within the CNS

Subsequent to vector administration and engagement of cell surface attachment factors such as glycans, AAV vectors appear to undergo interstitial as well as intracellular transport within the CNS. For instance, recent studies in the primate brain

have demonstrated that AAVrh.10 displays distinct transduction patterns following different routes of administration (101). Of the five routes tested, delivery to parenchyma resulted in more efficient gene transfer than intraventricular or intraarticular routes of administration. Another study in marmosets demonstrated that intravenous administration of AAVrh.10 is capable of efficient CNS transduction (97). These results highlight the potential diversity in AAV vector transport mechanisms not only in the context of brain physiology, but also possibly due to vector serotype, receptor usage and animal models.

Although not completely understood, two mechanisms, namely paravascular CSF transport and axonal transport appear to play a role in controlling the spread of AAV vectors within the CNS. It has been established that the paravascular transport of CSF plays a major role in the spread of interstitial fluid (ISF) within the CNS. One of the earliest studies demonstrated that proteins accumulate along highly vascularized regions of forebrain and brainstem within minutes of ICV injections (102). Further, medically induced blood pressure fluctuations have been directly shown to control the spread of nanoparticles including AAVs in the brain (103). The brain is distinct from other organs in that it lacks lymphatic circulation (104, 105). To understand compensatory mechanisms, Iliff and colleagues performed CNS-injections of differently sized (between 750 da and 2000 kda) molecular tracers. Using compelling visual evidence provided by 2-photon microscopy, the authors concluded that paravascular movement of CSF clears solutes from the CNS (62). Specifically, the para-arterial influx and the paravenous efflux of subarachnoid CSF drain accumulations of metabolic end products and other solutes within the brain parenchyma. These results suggest that

mechanisms like the CSF transport can possibly play a role in determining the extent of spread of viruses within the CNS. Clearly, understanding the structure-function correlates of AAV capsids and host factors that might dictate their ability to spread within the CNS will be valuable.

Another known pathway that viruses utilize to spread within the CNS is axonal transport post-entry into host neurons. Viruses can travel long distances by getting transported across synaptic connections in various sectors of mammalian central and peripheral nervous system (106, 107). Over the years, Herpes simplex virus (HSV) and Pseudorabies virus (PRV) have been used to visualize axonal transport and the resulting patterns of viral infections in the CNS milieu (108). Although accurate neuronal tracing has been achieved using these viruses, a major disadvantage is the loss of gene expression and neuronal death observed in the labeled cells between 5 days to 2 weeks post infection (109-111). In case of AAVs, both unidirectional and bidirectional axonal transport has been observed depending on the viral strain (112, 113). During retrograde transport, intact virions are taken up at the axonal projections and are transported to the neuronal cell body (soma), where the virus enters the nucleus to carry out transduction. Conversely, a successful anterograde transport requires virions to enter the neuronal soma and travel along the length of the axon to finally get released at the projections. The released virions are then free to transduce new cellular subpopulations in the region.

Understandably, directional axonal transport of AAV can be utilized to achieve safe and targeted gene delivery in spatially and functionally distinct neuronal subpopulations. For instance, AAV2 specifically undergoes anterograde transport (114,

115). On the other hand, AAV6 exhibits exclusive retrograde transport in both rat and primate brain (116). In addition, AAV9 has been shown to efficiently travel in both anterograde and retrograde directions (117-119). Specifically, Castle and colleagues visualized dye-conjugated AAV9 vectors during their anterograde and retrograde movements within cultured rat cortical neurons. These studies showed that axonal transport of AAV9 occurs in Rab7 positive late endosomal/lysosomal compartments. Further, cytoplasmic dynein and kinesin-2 were identified as being critical for successful retrograde and anterograde transport, respectively (118, 120).

The aforementioned strides made in context of AAV biology within *in vitro* and *in vivo* experimental systems have been instrumental in the field of CNS gene therapy. We now focus on therapeutic usage of AAV biologics for CNS disorders. The following sections elaborate on the progress made towards AAV mediated therapeutic intervention for two major classes of neurological diseases- movement disorders and storage disorders.

1.7 Gene Therapy of CNS Disorders using Recombinant AAV vectors

1.7.1 Gene therapy of Movement disorders

The timely firing of neurons projecting within corticostriatal, nigrostriatal and thalamocortical circuits of the brain orchestrate events leading to motor control. Under the umbrella of movement disorders, therapeutic gene transfer using rAAVs has shown promise in animal models e.g. Huntington’s disease (HD) and Parkinson’s disease (PD), amongst others. For the purpose of this chapter, we will focus on PD and assess the use of AAV vectors in understanding and treating the multifactorial CNS disorder.

Familial, environmental and idiopathic factors result in selective loss of dopaminergic (DA) neurons leading to Parkinsonism (121). PD patients exhibit bradykinesia (slow movements), akinesia (no movements) and tremors among other symptoms exemplifying disrupted motor function. During normal conditions, DA neurons at the basal ganglia (Substantia Nigra Pars Compacta (SNPc) region) send inhibitory inputs to the subthalamic nucleus (STN) through enhanced GABA signaling (6). Such inhibitory inputs received at the STN are important for the controlled excitation of the projections to motor associated regions of the cortex. Detailed descriptions of the neuronal subtypes and comprehensive analyses of the circuitry that governs the states of normalcy and disease have been reviewed elsewhere (6, 121). On a cellular level, PD features loss of DA neurons at the SNPc leading to reduced inhibition of the STN causing unregulated inputs reaching motor areas further downstream. Understandably, the dysfunction of two major checkpoints i.e. loss of DA neurons/dopamine and reduction of GABAergic input to the STN result in disease. Over the years, gene therapy research has focused on both of these checkpoints to develop strategies that can reverse PD pathology.

One of the hallmarks of PD is the appearance of aggregated synaptic protein alpha-synuclein (α-syn) in the surviving dopaminergic neurons (122, 123). Such aggregations called ‘Lewy bodies’ are not restricted to PD. A similar phenotype occurs in Alzheimer’s disease (AD) where aggregations of the proteins amyloid-β ($A\beta$) and *tau* have been associated with loss of hippocampal neurons resulting in learning and memory defects (124). In case of PD, the phosphorylation of the protein α-syn at the Serine-129 position has been associated with potent disease pathology (125-128). A

key mechanistic insight of the association between PD pathology and α-syn aggregation was provided by the work of Gorbatyuk and colleagues (129). The authors performed nigral injections of rats with AAV5 vectors packaging three versions of α-syn i.e. wt α-syn, phosphorylated α-syn S129A or non-phosphorylated α-syn S129D. The enzyme TH is a biomarker for DA neurons as it is required for the conversion of L-tyrosine to levodopa, a precursor of dopamine (130). The study demonstrated that the AAV mediated delivery of S129A mutant was highly toxic to the TH immunopositive (TH+) DA neurons resulting in loss of striatal dopamine levels in the brain. Intermediate loss of TH+ neurons was also observed due to AAV mediated overexpression of wildtype α-syn. More importantly, the study reported that the unphosphorylated form of α-syn (S129D) was not toxic to dopaminergic neurons and was incapable of causing PD pathology. In summary, this *in vivo* study utilized AAV vectors to demonstrate that PD pathology due to α–syn aggregation is dependent on its phosphorylation state at the S129 position (129).

The use of AAV vectors to achieve controlled biosynthesis of dopamine *in vivo* has been reported by Li and colleagues (131). Briefly, AAV2 vectors packaging dopamine synthesizing enzyme TH, flanked by LoxP loci were generated. In the event of Cre-recombination, the transgene expression would be lost, leading to a loss of TH gene expression in the transduced neurons. To incorporate temporal control of TH expression in their system, the authors packaged 4-hydroxytamoxifen inducible version of Cre ($CreER^{TS}$) into another AAV vector (132). The authors speculated that such AAV mediated regulation of TH expression would alter the dopamine levels in both *in vitro* and *in vivo* settings. Transfection of AAV2 vectors packaging the LoxP flanked-TH

transgene led to efficient production of dopamine which was significantly lost after subsequent superinfection of AAV2-Cre/CreER^{TS} recombinases in cell culture. This confirmed proper functioning of constitutively active and inducible Cre systems *in vitro*.

The authors then tested their system in Parkinsonian rats. Specifically, neurotoxin 6-hydroxydopamine (6-OHDA) was injected into rat brain to induce lesions in the dopaminergic areas of the CNS, generating a Parkinsonian rat model. Such rats then received individual/combinations of the above mentioned AAV vectors in the striatum and were assessed for biochemical and behavioral outcomes associated with PD. Significantly increased dopamine production in the animals that received AAV2 vectors packaging TH encoding transgene was reported. Subsequent Cre-recombinase mediated loss of dopamine production led to significant disruption of motor skills during apomorphine-induced rotation tests and spontaneous limb movement tests.

During low levels of dopamine availability, the compensatory mechanism employed by the brain involves conversion of dopamine precursor levodopa into usable dopamine using L-amino acid decarboxylase (AADC) enzyme. The Cre-recombinase mediated loss of TH expression led to significant reduction of dopamine levels, but did not affect the cellular expression of AADC in the rats that received oral levodopa. This suggested that the inherent compensatory mechanism of dopamine production is unaffected by the AAV treatments. These results demonstrated a system wherein AAV gene therapy was used to achieve temporally controlled induction and rescue of PD pathology *in vivo* (131).

Gene therapy mediated replenishment of the levels of AADC enzyme in the brain is a potential strategy to ameliorate PD pathology by way of bolstering the

compensatory mechanism for dopamine production. A phase 1 clinical trial reported the use of tracer dependent positron emission tomography (PET) to track the spread of AADC transgene delivered using AAV2 in 6 PD patients who underwent putaminal injections of the vectors (133). The patients were given oral levodopa for continuous supply of the enzymatic substrate. PET analysis revealed a 56% increase in the bioavailability of AADC for up to 96 weeks post injections. 6 months post injections, the authors observed ~46% improved Unified Parkinson's Disease Rating Scale scores. These results show that the AAV vectors can be utilized for potential therapeutic intervention for PD pathology, but is also safe and well tolerated in a human disease setting (133).

The combinatorial intracranial delivery of the therapeutic enzyme AADC along with oral administration of levodopa is not free of side-effects. Continuous intake of levodopa leads to complications associated with loss of impulse control leading to uncontrolled motions (Dyskinesia) among other symptoms (134-136). Cederfjall and colleagues hypothesized that gene therapy can be used to achieve focused biosynthesis of dopamine in therapeutically relevant regions of the brain (137). For this, two rate-limiting enzymes involved in the conversion of tyrosine from human diet to DOPA (3,4- Dihydroxyphenylalanine) were packaged in the same AAV vector. Intrastriatal delivery of AAV5 vectors encoding the transgenes tyrosine hydroxylase (TH) and GTP-cyclohydrolase-1 (GCH1) led to efficient production of DOPA and its cofactor 5,6,7,8- tetrahydro-L-biopterin (BH4), respectively. The previously discussed 6-OHDA induced PD rat model was used to assess the efficacy of AAV mediated gene therapy.

Efficient expression of TH and GCH1 were reported at the striatum and SN. The authors speculated anterograde transport of the vector to be responsible for this transgene expression profile in the rat brains. AAV treated PD rats in the study exhibited supraphysiological levels of BH4 expression along with accumulation of synthesized DOPA in the forebrain regions, possibly due to the saturation of available AADC enzyme. Furthermore, AAV-treated rats exhibited motor and behavioral benefits from PD pathology, not seen in the lesion control animals. Specifically, the motor skills were compared using amphetamine-apomorphine induced rotation tests; and corridor and staircase tests. Significant therapeutic benefit with forelimb akinesia, sensorimotor control and symmetry of movements was reported. In short, widespread biochemical reversal of PD pathology (DOPA production) in the AAV5 treated 6-OHDA lesioned rat brains resulting in functional recovery of motor control was observed (137). Another comprehensive study was recently conducted by the same research group utilizing administration of the aforementioned AAV5 vectors. This study surprisingly reported the inability of their previous strategy of vector administration used in the PD rat model to directly translate therapeutic benefit in higher order mammals. In NHPs, such AAV5 administration led to increase in the GCH1 levels but not TH levels. It was speculated that other important parameters like promoter/enhancer elements were to be optimized so as to dissect the molecular basis of the incoherence seen between gene therapy of rats and monkeys (138).

In addition to accentuation of dopamine levels by delivering enzymes that partake in its biosynthesis, gene therapy could be used to reverse another aspect of PD pathology, neurodegeneration. Gasmi and colleagues have extensively characterized

the neuroprotective factor Neurturin (NTN) or Glia derived neurotropic factor (GDNF) towards amelioration of PD pathology (139). The authors packaged NTN in AAV2 vectors and performed intra-striatal injections in a 6-OHDA induced rat model of PD. NTN gene expression was reported as early as 2 days post injections and lasted till the last time point of the study i.e. 1 year post administration. Further evaluation of the kinetics of the AAV gene transfer reported both the bioavailability of the enzyme and the expression of the transgene stabilized in 4 weeks post striatal injections. The effect of NTN transduction on the dopaminergic neurons was further evaluated at the SN via immunostaining for TH. A significant increase ($p<0.001$) in the neuroprotection of the TH-immunopositive (TH+) SN neurons as compared to the control animals was reported. Similar promising results were reported during intra-striatal injections of AAV2 packaging the neurotrophic factor Pleiotrophin (PTN). PTN has a protective and nourishing effect towards nigrostriatal dopaminergic neurons lost during PD. Studies have shown that PTN expression is associated with differentiation of mesencephalic TH+ neurons and neuroprotection of surviving DA neurons during PD (140, 141). To utilize such properties of PTN towards gene therapy of PD, intrastriatal delivery of AAV1 encoding the PTN transgenes was performed by Gombash and colleagues (142). Interestingly, this led to restricted transduction of neurons at the striatum and SNPc leading to efficient neuroprotection of DA neurons and reversal of PD phenotype in the 6-OHDA rat model.

It is clear that the injection of neuroprotective agents like GDNF has a stimulatory effect on DA neuronal growth at the site of injection. While functional reversal of PD pathology from intrastriatal injections of AAV vectors packaging GDNF has been shown,

SN injections of such AAV vectors has been associated with ‘aberrant sprouting’. Specifically, intracranial administration of viral vectors packaging GDNF has been shown to cause innervation of DA neurons in unspecific regions around the site of injection (143). The unprecedented increase of DA synthesizing neurons at random projection regions has been associated with counter-beneficial behavioral side-effects in the animals (144).

Fetal ventral mesencephalic (VM) cells are precursors of DA neurons in the mammalian CNS. Direct injections of fetal VM tissue implants have shown reversal of PD pathology via integration and striatal-innervation of mature DA neurons. Functional turnover of dopamine biosynthesis leading to reversal of behavioral pathology in PD animal models has been reported from such treatments (145-147). A combination of gene and cell therapy strategies was used by Redmond Jr. and colleagues in an attempt to augment the benefits individually achieved by both (148). AAV5 vectors packaging the GDNF transgene were co-administered with VM tissue grafts into the caudate and putamen striatal regions of MPTP induced PD model of NHPs. A head to head comparison of the gene and cell therapy based systems individually and in tandem was performed. Striatal levels of both DA and GDNF were significantly higher in animals that received the dual treatment in comparison to either individual procedure. Interestingly, during the phenotypic evaluation conducted over a span of 8 months post-treatments, the dual treatment did not show a significant increase in the amelioration of PD pathology as compared to the singular treatments.

The authors speculated that these discrepancies in the biochemical and functional outcomes could be accounted for by events like downregulated TH

expression at innervations of DA termini and aberrant sprouting events in the treated NHPs (148). These results indicate that gene and cell therapeutic interventions that are autonomously capable of reversing PD pathology do not always complement one another. Such results need to be taken into consideration before clinical translation of such combinatorial procedures.

Human erythropoietin (EPO) enhances the production of red blood cells and is therefore an unlikely candidate for gene therapy of neurodegenerative disorders in CNS. However, recent research has indicated strong neuroprotection of dopaminergic neurons achieved by EPO expression in the brain. Mechanistically, the protein is known to have anti-inflammatory and anti-apoptotic effects among others leading to protection from neuronal loss during experimental neurodegeneration (from hypoxia induced ischemia); or toxic insults (e.g. MPTP and 6-OHDA abuse) *in* vivo. (149-152). In an attempt to utilize the aforementioned therapeutic properties of the EPO protein, Xue and colleagues packaged human EPO transgene into AAV9 vectors and injected them into the rat striatum (153). The authors reported neuroprotection of DA neurons due to widespread transduction of EPO in the striatum and SN. The behavioral PD pathology was also attenuated in the rats injected with AAV9-EPO, as demonstrated in the rotation test and the test for spontaneous use of forelimbs.

Taken together, such experimental and clinical outcomes have characterized three main strategies routinely used in gene therapy of PD i.e. dopamine biosynthesis (154); functional growth, protection and innervation of DA neurons (155, 156); and neurochemical inhibition of STN (157, 158). Clearly, it is important to restrict the aforementioned processes to functionally relevant regions of the brain by choosing the

optimal site of injection, dosage and the right AAV serotype during PD gene therapy. Other challenges associated with CNS gene therapy in the clinic include neutralizing antibodies, long-term bioactivity and aggregation of the protein product. It is important to note that none of these concerns have posed serious adverse effects in the last decade of research in PD gene therapy (159-163). A comprehensive perspective on gene therapy of PD with special focus on predictive animal models, clinical trial design, safety, patient selection, and the current limitations has been recently provided by Bartus and colleagues (164).

1.7.2 Gene therapy of CNS disorders arising from metabolic defects

Mammalian cells constantly break down complex biomaterials into simpler end products that make up for cellular nutrients or act as transient precursors for subsequent metabolic activities. Such biomaterials originate from dietary intake or preceding enzymatic degradations. Lysosomes are enzyme rich digestive compartments inside a cell that are specifically designed to break-down such buildup. Understandably, dysfunctional lysosomes cause steady accrue of undigested enzymatic substrates, ultimately leading to cell death. Organs with continuously dividing cells are often able to compensate for this loss by replenishing themselves with new cells over time. On the other hand, once fully formed, the CNS undergoes very little cell division and reorganization. This makes it vulnerable to loss of functional tissue from such cellular distress. CNS disorders arising from metabolic storage burden have largely been classified as lysosomal storage disorders (LSDs). Another class of disorders

called neuronal ceroid lipofuscinosis (NCLs) presents a similar phenotype and originates from the inability of the cells to breakdown the metabolite lipofuscins.

The first association of a metabolic storage disorder with debilitating human disease was Pompe's disease (Glycogen storage disease type II) characterized by severe progressive myopathy (165). We are now cognizant of 50 LSDs that affect humans, most of which target CNS tissue (5). It is worth mentioning that majority of LSDs and NCLs are transmitted in an autosomal recessive fashion, which accounts for their rare occurrence in the human population (166). The molecular bases of many such disorders have been uncovered in the last few decades and have been reviewed elsewhere (5). Such efforts have been important in the development of strategies to employ gene therapy towards disease treatment and amelioration. During normal conditions, catabolic enzymes utilize specific cellular macromolecules as substrates.

Typically, LSDs and NCLs occur due to 'loss of' or 'mutations in' functional genes that encode such enzymes. Mucopolysacharidoses (MPS) are a broad range of LSDs branching from the common incapability of breaking down mucopolysaccharides resulting in fast deterioration of CNS milieu. Pharmacological enzyme replacement therapy (ERT) only provides short-lived and localized respite from the cellular buildup due to inefficient penetration of CNS tissue and inability of recombinant enzymes to cross checkpoints like the blood-brain barrier (BBB) (167). A complete reversal of disease pathology demands continuous production and secretion of the lost enzymes in both CNS and peripheral organs. AAV gene therapy provides the necessary genomic elements to the patient's functional tissue for biosynthesis of lost enzyme(s) in a cell autonomous/non-autonomous fashion. In addition, the combinatorial spread of AAV

vectors and the translated protein results in efficient penetration of the disease-afflicted CNS and peripheral organs. We have focused our discussion on major MPS disorders as case studies outlining progress towards understanding prominent metabolic storage disorders affecting the CNS and the use of AAV gene transfer towards their therapy.

MPS type VII (Sly disease) is a severely debilitating form of LSD that occurs as a result of accumulation of glycosaminoglycans (GAGs) due to the deficiency of β-glucuronidase (GUSB) enzyme. The disease symptoms include skeletal deformations, mental retardation, loss of sensory skills (vision and hearing), distorted features and a short life span (168). In one of the first attempts at utilizing AAV gene therapy towards amelioration of MPS VII in a mouse model, AAV2 vectors were engineered to package the GUSB transgene. Intravenous delivery of AAV2-GUSB led to reversal of disease phenotypes pertaining to bone length, retinal function and vacuole clearance in the MPS VII mouse model at an early age of postnatal day 2 (P2) (169, 170). In theory, utilizing the blood stream for delivering pharmacological agents to multiple organs is attractive, although, it is not always the best route for administration of certain AAV serotypes for gene therapy.

Early studies conducted by Elliger and colleagues concluded that i.v. administration of the AAV2 vectors resulted in modest levels of CNS transduction and higher transgene expression in the peripheral tissues i.e. heart and liver (171). Recent research has demonstrated that AAV2 vectors are unable to cross the BBB (96). Therefore, the clearance of GAG accumulation from CNS tissue observed in these initial studies using AAV2 is possibly due to secreted enzymes crossing the brain microvasculature or entering the parenchyma via aquaporin mediated interstitial fluid

clearance (62, 172). Further supporting this argument, direct CNS administration of AAV2-GUSB via intrathecal injections in adult mice was demonstrated to achieve increased enzyme levels and decreased vacuole formations in the CNS tissue (171). This study underscores the importance of pairing an AAV serotype with its optimal route of administration for CNS gene therapy applications. Widespread diffusion of the GUSB enzyme product in the CNS tissue was achieved by Skorupa and colleagues (173). Their report demonstrated that direct injections of AAV2-GUSB into four sites in the adult rodent brain namely: striatum, cortex, thalamus and hippocampus achieves maximal spread of the enzyme. The authors reported clearance of lysosomal storage burden across the complete neuraxis in the ipsilateral hemisphere from such injections (173).

More recently, the use of multiple intracranial injections to achieve efficient biodistribution of therapeutic enzyme has been replaced by other strategies that are more amenable to clinical translation. To this end, a single striatal injection in the adult MPSVII affected rat brain was shown to produce enzyme expression in 10% of the brain volume leading to loss of the storage burden for ~16 weeks by Bosch and colleagues (174). An alternative strategy towards achieving enhanced levels of transduction is to incorporate genetic elements like the promoter and enhancer, from other infectious mammalian viruses. The work of Sferra and colleagues demonstrated enhanced transduction efficiency of murine β-GUSB transgene, when driven by cytomegalovirus promoter-enhancer elements. ~50-240% spread of enzyme expression across the CNS, resulting in metabolic storage benefit for up to 3 months of age was reported by the authors (175).

Progressive loss of vision due to retinal degeneration is a characteristic clinical phenotype of MPSVII in humans. In an attempt to correct this pathology, AAV2-GUSB was injected into adult MPSVII mice via the intravitreal route by Hennig and colleagues (176). The enzyme activity was observed in areas of the brain receiving visual inputs from the eye e.g. thalamus and tectum. Interestingly, neighboring non-visual areas like hippocampus and visual cortex also exhibited GUSB activity. The transduction profile suggested the combined role of synaptic vector transmission and diffusion of the translated product (176).

Understandably, expression of the GUSB transgene in large 3-dimensional spaces of the CNS is important for rapid lysosomal clearance and associated symptomatic benefits from MPSVII. Primate derived AAV strains 7, 8, 9 and rh10 were injected into adult mouse brain regions cortex, striatum, thalamus and hippocampus by Cearley and colleagues to assess their properties as CNS gene transfer vectors (90). The authors reported that all tested serotypes showed preferential transduction of neurons and not astrocytes and oligodendrocytes. While AAV7 performed efficient gene transfer in cortex, thalamus and hippocampus, AAV9 and AAV Rh.10 outperformed other serotypes in spread and transduction of both ipsilateral and contralateral hemispheres. Specifically, the assessment of AAV9 injected rodent brains demonstrated reversal of lysosomal clearance at 2 months post injections in multiple regions of the brain. The authors also observed AAV9 mediated transduction across neuronal projections in the hippocampal commissure, providing supportive evidence for the vector’s ability to undergo axonal transport to cover large distances in the CNS (90).

Although AAV mediated gene therapy in the postnatal *in vivo* animal models successfully reverses clinical manifestations of LSDs, survival of such animals is still significantly lower than their wildtype counterparts. In one of the first attempts to introduce therapeutic intervention in an *in vivo* embryonic stage, AAV1 vector encoding the GUSB transgene was administered at embryonic day 15.5 (E15.5) by Karolewski and colleagues (177). Vector mediated CNS transduction resulting in enzymatic spread across the entire brain and spinal cord was observed. Low levels of GUSB activity was also observed in peripheral organs like liver, spleen, kidneys and gonads. Interestingly, no vector genomes were detected at such off-target locations. The authors further discussed that the peripheral leakage of the enzyme was possibly due to uptake of CSF metabolites into the venous system. The CNS-specific therapeutic intervention was enough to confer benefit from lysosomal storage lesions for up to one year post injections and improved the survival comparable to wildtype controls. Surprisingly, some of the clinical manifestations like facial and skeletal deformations were not rectified post-treatment. Such mixed results indicate room for improvement in areas like vector design and route of AAV administration (177).

Some of the most daunting challenges with clinical translation of gene therapy are related to surgical procedures during vector administration in the clinic. Major advances have been made towards reduction of invasiveness during therapeutic vector administration targeting the CNS. Intra-CSF injections like ICV injections, intracisternal injections (IC) and intrathecal lumbar puncture (IT) are all viable strategies to achieve maximal contact with the CNS tissue from a single dose of administration. In addition, viruses are also known to utilize axonal transport to cover long distances via inter-

synaptic relay. AAV strains have different efficiencies and preferred directionalities of movement across neuronal connections (112). In this regard, utilizing regions of heavy afferent and efferent 'wiring' within the brain can be a useful strategy. A comparative assessment of AAVs 1, 9 and Rh.10 injected into a major hub of neuronal projections, ventral tegmental area (VTA) was reported by Cearley and colleagues (55). The authors compared VTA injections of the AAV vectors to conventional striatal injections. While an increase in spread of transduction to distal regions of the brain was reported from all three AAV serotypes, the maximal spread was seen in case of AAV9 vectors. The authors then used the strategy to deliver GUSB transgene packaged in AAV9 vectors in the MPSVII mouse model. The study reported widespread transduction of the therapeutic transgene, leading to expanded biodistribution of the enzyme in the entire brain from a single 1 ul injection of ~10^{10} total viral genomes (vg) (55).

On the behavioral front, MPSVII patients display mental retardation due to neuronal and glial cell death. Frisella and colleagues hypothesized that AAV mediated GUSB transgene delivery would achieve successful restoration of lost cognitive function. To this end, intracranial administration of AAV2-GUSB was performed in the MPSVII mice by the authors that led to long-lasting supply of the enzyme in the CNS. The authors then utilized the Morris water maze test to show that the mice treated with the AAV vector exhibit near wildtype levels of cognitive skills (178). The loss of cognitive acumen is often related to dysfunction of the hippocampus e.g. deteriorated learning and memory, difficulties in fear conditioning etc.

Preclinical evaluations of the extent of cognitive benefit seen in MPSVII mice due to AAV mediated gene therapy was performed by Liu and colleagues (179). The authors

administered AAV5 packaging β-GUSB via bilateral intrastriatal injections in adult MPS VII mice. AAV5 has been previously demonstrated to be a highly neurotropic vector capable of transducing a larger area of the CNS than AAV2 (71). AAV5 mediated intrastriatal delivery of the corrective GUSB transgene provided cognitive benefits in MPS VII mice as demonstrated in repeated acquisition and performance chamber (RAPC) assay. Specifically, the MPSVII affected adult mice underwent RAPC assay before and after the vector administration. Post administration, the mice displayed a significant reduction in the learning errors and latency period to reach the reward. Furthermore, the authors identified a specific loss of glutamate receptor on the surface of hippocampal neurons in the MPSVII affected mice. Specifically, 40-60% depletion of glutamate receptors GluR1, GluR2 and NR1 was observed in the hippocampal neurons which could be linked to the learning deficits. Furthermore, the authors demonstrated that the glutamate receptor levels of AAV5-β–GUSB treated mice was indeed restored comparable to the levels of heterozygous littermates, thereby providing the molecular basis of the therapeutic benefit (179).

MPSIIIB/Sanfilippo syndrome is a rare, genetically transmitted LSD where patients suffer from intracellular accumulation of glycosaminoglycan heparan sulfate. The disorder stems from the deficiency of α-N-acetylglucosaminidase (NaGlu) enzyme in the CNS. The disease features fast deterioration of CNS and peripheral tissues leading to severe mental retardation and premature death in patients (Neufeld and colleagues 2001, Metabolic and Molecular basis of inherited diseases). Enzyme biosynthesis using gene therapy confers successful protection of neuronal and peripheral tissue and provides symptomatic relief in the MPS IIIB mouse model. One of

the earliest examples of therapeutic AAV gene transfer was reported by Fu and colleagues (180). AAV2 vectors packaging the NaGlu transgene was engineered. The transgene was driven by either a constitutive cytomegalovirus (CMV) promoter or a neuron specific enolase (NSE) promoter. Successful transduction of AAV2 in human MPS IIIB patient fibroblasts and mouse somatic and primary brain cells, resulting in significant degradation of GAGs was demonstrated. A low dose (~10^7) of viral genomes of AAV2-NSE-NaGlu was then injected into the adult MPS IIIB mouse brain and successful NaGlu expression leading to correction of GAG storage in a broad CNS area was observed(180).

Cressant and colleagues assessed the effects of AAV mediated gene transfer of the NaGlu transgene on the behavioral outcomes of MPS IIIB (181). It is now clear that certain AAV serotypes like AAV2 have the preferential ability to undergo axonal transport in the anterograde direction (115). Regions of extensive synaptic connectivity are attractive sites of injection for AAVs packaging corrective transgenes to target a large area of the brain from a single injection. In the mammalian CNS, axonal projections to multiple regions originate at the caudate putamen. In this report, the authors compared putaminal injections of AAV2 and AAV5 vectors in adult 6-week old MPS IIIB mice and demonstrated that AAV5 mediated transduction spreads more than AAV2 (181). AAV5 binds *N*-linked sialic acid as cell surface attachment factors whereas AAV2 requires the availability of Heparan Sulfate proteoglycans (HSPG) to perform successful gene transfer (34, 182).

The interaction of AAV2 with its cognate receptor (HSPG) is one of the rare occurrences where cellular receptor binding is detrimental to the spread of the AAV

vectors in the CNS (172). This phenomenon might explain the enhanced ability of AAV5 vectors to spread and transduce CNS tissue in the distant regions from the site of injection. Both AAV vector injections resulted in the enzyme bioavailability above untreated controls leading to reversal of disease phenotype in the neurons, microglia and perivascular cells. Additionally, a complete reversal of behavioral symptoms from both AAV2 and AAV5 treatments was reported (181). The assessment of behavioral recovery was performed using a circadian cycle controlled open field test. Parameters such as mouse activity during light and dark time periods; explorative and habituated navigations, were monitored during the course of the sessions. To summarize, these tests provide a fair assessment of the success of gene therapy towards reversal of cellular pathology and behavioral outcomes seen in MPS IIIB patients featuring anxiety, restlessness, hyper-excitability and aggressiveness (181).

Many natural and engineered AAV isolates are being discovered with attractive properties like the ability to spread and transduce large CNS volumes. In an attempt to achieve widespread correction of the MPS IIIB disease pathology in the CNS, AAV2 mediated NaGlu gene transfer was performed by Fu and colleagues in BBB compromised mice *in vivo* (183). Specifically, the authors utilized intra-arterial injection of mannitol post AAV administration that led to transient opening of the BBB. While there is no measurable permanent damage inflicted upon the BBB due to this treatment, efficient entry of viruses, antibodies and large macromolecules has been widely documented due to such treatment (98, 183, 184). The authors demonstrated that combined intravascular and intra-cerebrospinal fluid (CSF) vector administration led to successful and long term correction of the disease pathology and a significant increase

in the lifespan of the mice (from 7.9-11.3 months in untreated mice to 11.1-19.5 months in treated mice).

Simultaneous use of CSF and blood connectivity led to successful gene transfer not only in the CNS tissue but in peripheral organs as well. Virtually the entire brain and spinal cord tissue are connected with the combination of the CSF and blood vessels. The CSF constantly provides nutrients and molecular signals to, and drains interstitial fluids from, the brain and spinal cord tissue via the sub-arachnoid space, cerebral ventricles, cerebellar foramena and the cisterna magna (61-64). The blood vessels on the other hand provide constant supply of oxygenated blood due to the combination of arterial influx and venous efflux in the CNS tissue. The authors of this study speculated that the success of their therapeutic AAV administration could be attributed the routes of administration (183). The transient opening of the BBB clearly assisted the CNS spread of AAV vectors. Moving forward, the time span between intra-arterial mannitol infusion and the i.v. administration of AAV vectors was optimized by McCarty and colleagues. The authors demonstrated that injections performed exactly 8 min after the mannitol infusions led to significantly enhanced viral transduction resulting in reversal of the disease phenotype in the MPS IIIB mice (98).

Combinatorial use of other strategies of therapeutic intervention can have a synergistic effect on AAV mediated gene therapy of the CNS. Exploring such a hypothesis, AAV gene transfer in combination with bone marrow transplant and assessment of correction of MPS IIIB was performed by Heldermon and colleagues in mice. Specifically, the authors performed intracranial AAV5-NaGlu administration with/without the transplant of NaGlu transduced bone marrow cells in the MPS IIIB

mouse model. The bone marrow transplant (BMT), by itself, was the least efficacious of all three strategies and the report surprisingly concluded an antagonistic effect of the combination treatment on survival and motor skills in the disease affected mice (185). Such outcomes provide cautious optimism and direction for the future use of AAV towards CNS gene therapy of metabolic storage disorders.

1.8 Safety aspects of AAV-mediated CNS gene therapy

Recombinant AAV vector genomes display inefficient integration into the host chromosome and predominantly persist in episomal form (186). This reduces the risk of insertional mutagenesis, often associated with other viral vectors like retroviruses (187). The vector genomes subsequently require the host cellular machinery to carry out second strand synthesis, transcription and translation (188, 189). Safety aspects pertaining to persistence of AAV vector genomes have been reviewed elsewhere (27, 186, 190).

Another important safety consideration is the observation that rAAV mediated overexpression of non-self transgenes can elicit immune responses due to antigen presentation of the expressed transgene product. . For instance, direct primate brain infusion of AAV1 packaging a humanized *Renilla* GFP transgene triggered an immune response against the translated reporter product (191). Similarly, a cell mediated immune response and neuronal loss was observed in rats injected with AAV9 vectors packaging the GFP reporter transgene or a human L-amino acid decarboxylase transgene (192). More recently, certain AAV serotypes have been shown to undergo

systemic leakage resulting in off-target biodistribution in organs like liver and spleen (94, 97, 101). Crucially, AAV vector engineering can also be employed to design elegant solutions to contain peripheral organ accumulation of CNS-targeted AAV biologics. To this end, we have engineered and extensively characterized the AAV2g9 vector that performs widespread neuronal gene transfer with minimal systemic leakage, peripheral tissue biodistribution and systemic tissue gene transfer. These findings have been elaborated in the chapter 3 of this thesis.

These preliminary observations in animal models highlight the need to better understand the parameters that determine potential toxicity/biodistribution profiles and immune response in AAV-mediated CNS gene transfer. It is also important to acknowledge that aspects related to manufacturing, downstream processing and purity of AAV vector preparations are critical towards ensuring the safety of AAV vectors. A comprehensive comparison of different viral gene transfer vectors for parameters such as packaging capacity, host chromosomal integration and other biosafety aspects can be found elsewhere (27, 190).

As of early 2014, 5.3% of world-wide clinical trials involving gene therapy have utilized Adeno-associated viruses (AAVs) (109 ongoing trials) (Journal of Gene medicine). Only a few of these trials are aimed at treating diseases with CNS manifestations. In this chapter, I attempted to provide an overview of various parameters that might play a role in determining the success of AAV mediated therapeutic gene transfer to the CNS. Interactions of AAV vectors with different primary receptors, directional transport and cellular tropisms following different routes of administration are summarized in **Table 1**. Although we were unable to cover every

contribution to the field of CNS gene therapy, the information provided not only highlights potential gaps in our understanding of AAV-host interactions within the CNS, but will assist with continued vector development for CNS-directed gene transfer applications in the clinic.

Some of the prominent applications of AAV mediated CNS gene therapy that are currently undergoing various stages of clinical trials as reported in the National Institutes of Health's database (https://clinicaltrials.gov/) have been listed in **Table 2**. Although we were unable to discuss gene therapy of many other CNS disorders and several other outstanding scientific contributions; through this chapter, we have attempted to bring clarity to the advantages and challenges associated with the therapeutic use of AAV vectors in the CNS.

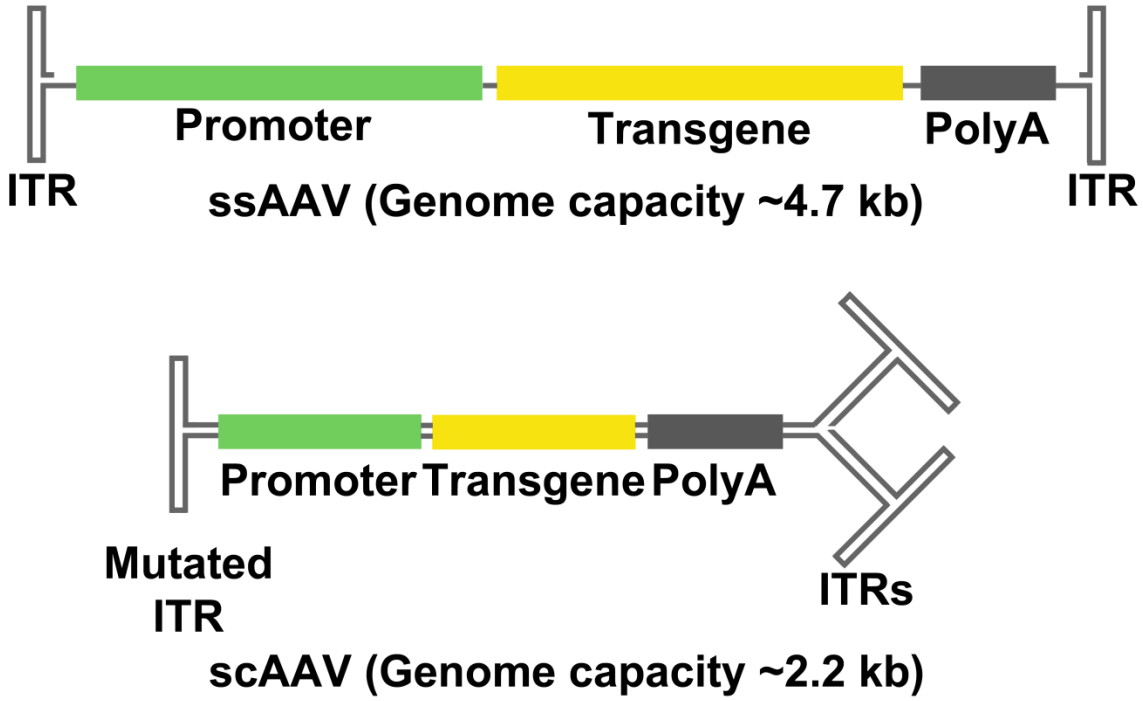

Figure 1: Schematic representation of recombinant AAV genomes: The promoter, transgene and polyadenylation signal (PolyA) are flanked by inverted terminal repeats (ITRs) in single stranded (ss) or self-complementary (sc) configurations.

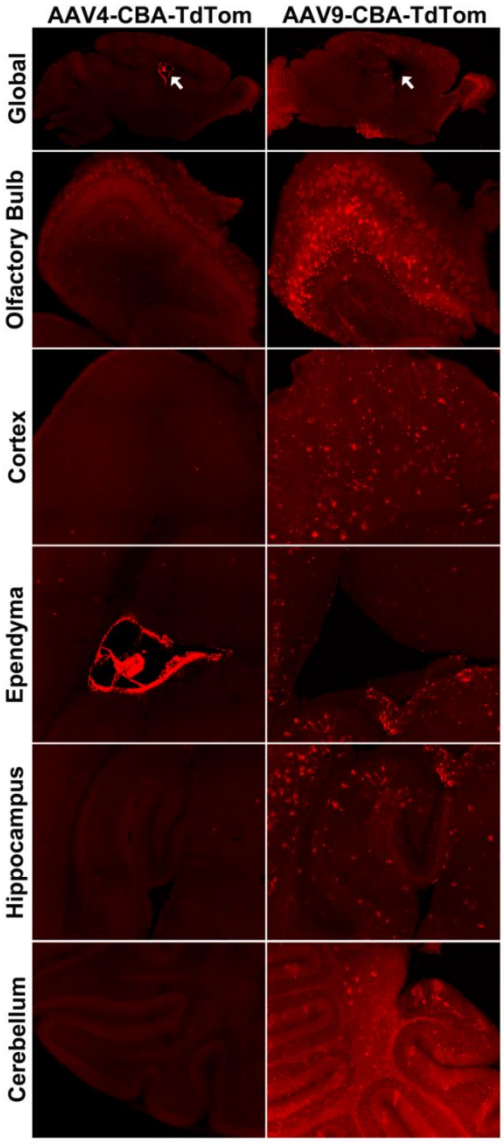

Figure 2: Differential spread of CNS transduction from AAV4 or AAV9 vectors packaging TdTomato fluorescent reporter transgene in neonatal mouse brain: P0 mice were injected with $1x10^9$ vg of AAV4 or AAV9 packaging a CBA-TdTom reporter transgene into the left lateral ventricle. At 2 weeks post injections, mice were sacrificed and paraformaldehyde fixed brains were sectioned. Brain sections were imaged using a Zeiss CLSM 700 confocal laser scanning microscope. Confocal micrographs show TdTom transgene expression (red) in 50 μm vibratome section of the mouse brain (global) and higher magnification images of individual regions in the rostrocaudal axis of the brain parenchyma.

Table 1. Capsid-receptor interactions, transduction profiles and axonal transport properties of some of the well characterized Adeno-associated viral serotypes in the mammalian CNS.

Serotype	Primary Receptor	Intra-CSF or Intra-parenchymal Administration		Intravascular Administration		Axonal Transport
		Neuronal Transduction	Glial Transduction	Neuronal Transduction	Glial Transduction	
AAV1	α2,3/α2,6 N-linked SA	++	+	+	+	A-,R+
AAV2	Heparan Sulfate	+	-	-	-	A+,R-
AAV4	α2,3 O-linked SA	-	+	-	-	?
AAV5	α2,3 N-linked SA	++	+	-	-	?
AAV6	α2,3/α2,6 N-linked SA/heparan sulfate	++	-	+	+	A-,R+
AAV8	?	++	++	++	++	A+, R+
AAV9	Galactose	+++	++	+++	+++	A+,R+
AAVRh.8	?	++	++	+++	+++	?
AAVRh.10	?	+++	+	+++	+++	?

? Receptor usage/Axonal transport has not been characterized; **+** Low levels of transduction; ++ Moderate levels of transduction; +++ High levels of transduction; - No transduction; ? A+ or R+ (AAV vector undergoes axonal transport in the anterograde (A) or retrograde (R) direction during *in vivo* characterization)

Table 2. Clinical gene therapy of some neurological disorders using AAV vectors.					
Category	**Disorder**	**Transgene**	**AAV Serotype, Route and Dosage**	**Clinical Status**	**Summary**
Metabolic Storage Disorders	Batten's Disease	Human CLN2 gene	AAV2- Intracranial injections	Phase 1 (NCT00151216)	Expression of CLN2 transgene to replenish the levels of tripeptidyl transferase-1 (TPP1) enzyme.
			AAV Rh.10- Intracranial injections – 2.85 or 9 X 10^11 vg	Phase 2 (NCT01414985)	
	Pompe Disease	Human acid alpha-glucosidase (GAA) gene	AAV9- Intramuscular injections- 5X10^9 vg	Phase 1 (NCT02240407)	The enzyme GAA degrades cellular accumulation of glycogen which leads to severe neuromuscular pathology.
			AAV1- Intramuscular injections- 1-5X10^12 vg	Phase 2 (NCT00976352)	

	MPS III A (Sanfilippo's type A Syndrome)	Human SGSH and SUMF1 genes	AAV Rh.10- Intracranial injections	Phase 2 NCT01474343	Expression of N-Sulfoglucosamine Sulfohydrolase and Sulfatase modifying factor 1 leads to degradation of glycosaminoglycans (GAGs) accumulations in the CNS tissue
	Acute Intermittent Porphyria	Porphobilinogen deaminase (PBDG) gene	AAV5- Intravenous injections	Phase 1 (NCT02082860)	PBDG enzyme deficiency blocks heme-biosynthesis and causes severe neuropathic symptoms ranging from abdominal pain to seizures and psychotic episodes.
Movement Disorders	Parkinson's Disease	Human aromatic L-amino acid decarboxylase (AADC)	AAV2- Intracranial I(Striatal injections) – 9X10^10 – 3X10^11 vg total	Phase 1 (NCT00229736)	AADC mediated conversion of orally administered levodopa into dopamine
			AAV2- Intracranial (Striatal injections) – 7.5X10^11- 2.3X10^12 vg	Phase 2 (NCT01973543)	

			total		
		Glial cell line-derived neurotrophic factor (GDNF)	AAV2-Intracranial (Striatal injections) – 9X10^10-3X10^12 vg total	Phase 1 (NCT01621581)	Neuroprotection of dopaminergic neurons with GDNF
		Neurotrophic factor Neurturin (NTN)	AAV2-Intracranial (Putaminal Injections)	Phase 1 (NCT00252850)	Neurturin mediated neuroprotection of dopaminergic neurons
			AAV2-Intracranial (Putaminal and Substantia Nigral injections) – 4-5X10^11 vg or 24X10^11 vg	Phase 1 (NCT00985517)	
		Glutamic acid decarboxylase (GAD)	AAV-GAD intracranial injections (Subthalamic nucleus)	Phase 1 (NCT00195143)	GAD expression in the STN has an inhibitory effect due to GABA production

CHAPTER 2: EXPLOITING GLYCAN SIGNATURES TO REGULATE ADENO-ASSOCIATED VIRAL TROPISM IN THE DEVELOPING BRAIN[2]

2.1 Overview

Adeno-associated viruses (AAV) are thought to spread through the central nervous system (CNS) by exploiting cerebrospinal fluid (CSF) flux and hijacking axonal transport pathways. The role of host receptors that mediate these processes is not well understood. In the current study, we utilized AAV serotype 4 as a model to evaluate whether ubiquitously expressed 2,3-linked sialic acid and the developmentally regulated marker, 2,8-linked polysialic acid (PSA) regulate viral transport and tropism in the neonatal brain. Modulation of the levels of SA and PSA in cell culture studies using specific neuraminidases revealed possibly opposing roles of the two glycans on AAV4 transduction. Interestingly, upon intracranial injection into lateral ventricles of the neonatal mouse brain, a low affinity AAV4 mutant (AAV4.18) displayed a striking shift in viral tropism from 2,3-linked SA+ ependymal lining to 2,8-linked PSA+ migrating progenitors in the rostral migratory stream and olfactory bulb. In addition, this gain-of-function phenotype correlated with robust CNS spread of AAV4.18 through paravascular transport pathways. Consistent with these observations, altering glycan dynamics within the brain by co-administering SA and PSA specific neuraminidases resulted in striking changes to the cellular tropisms and transduction efficiencies of both

[2]This chapter includes the original publication that appeared in the journal of virology. The full citation is as follows: Murlidharan, G., Corriher, T., Ghashghaei, H.T., Asokan, A. Unique glycan signatures regulate adeno-associated virus tropism in the developing brain, Journal of Virology, 2015, 89(7):3976-3987 (PMID: 25631075).

AAV4 as well as AAV4.18 vectors. We postulate that glycan signatures associated with host development can be exploited to redirect AAV vectors to specific cell types in the brain.

2.2 Introduction

Viruses enter the CNS by exploiting a variety of transport pathways that hinge on preliminary infection of peripheral nerve endings or through the blood by infecting circulating leukocytes or brain endothelial cells. Subsequent spread within the brain is achieved by axonal transport and trans-synaptic spread (193). A key step in viral entry into the CNS and subsequent directional transport is the recognition of specific cell surface membrane glycoproteins as receptors. For instance, polioviruses utilize CD155 as a receptor (194), while alpha herpesviruses exploit nectin-1 for CNS entry (195), both members of the immunoglobulin superfamily. Several membrane-associated components have also been implicated in Rabies virus CNS entry (196). Prior to engagement of such host membrane proteins, viruses often bind to cell surface glycans for attachment. One of the most versatile host glycans that have been exploited as viral attachment factors are the family of sialic acids (SA) (197-199). For instance, SA receptors have been implicated in the neurovirulence of reovirus and polyomaviruses (200, 201). Modulating SA binding affinity has also been shown to influence the pathogenicity of the neurovirulent strain of the minute virus of mice (MVM) (25).

While no natural isolates from brain tissue have been reported thus far, adeno-associated viruses (AAV), which are helper-dependent parvoviruses, display a broad spectrum of CNS tropisms following intracranial or systemic administration in different

hosts (71, 89, 90, 92, 96, 97, 172). The cellular tropisms of different AAV strains observed in these studies were mostly neuronal, with a few exceptions that can transduce astrocytes and glia as well. Similar to their helper viruses such as Adenoviridae or Herpesviridae (193), AAV strains undergo interstitial as well as axonal transport within the CNS (172). However, the molecular bases of this diversity in AAV transport mechanisms and CNS tropisms are not well understood. Within this framework, AAV isolates have been shown to utilize three different glycans – SA, galactose (GAL) and heparan sulfate (HS) for cell surface attachment (25). In addition, several growth factor receptors, transmembrane proteins and integrins have been identified as being essential for AAV cell entry (26, 31). Our lab and others have recently demonstrated the role of SA and GAL in determining the systemic fate of different AAV serotypes in mouse models (38, 202, 203).

The African green monkey isolate, AAV serotype 4 is one of the evolutionarily and structurally most distinct serotypes known to date and displays selective tropism for the ependymal lining following intra-cerebroventricular (ICV) administration in neonatal and adult mice (77). In addition, AAV4 particles directly injected into the sub-ventricular zone can transduce astrocytes forming glial tubes within the RMS. The functional cell surface attachment factor for AAV4 is *O*-linked α2,3-SA (mucin) (34, 204, 205). We previously identified a novel AAV4 mutant (AAV4.18) that displays decreased affinity towards 2,3-SA and a transduction-deficient phenotype following systemic administration in mice (205). In the current study, we identify a novel glycan that differentially regulates the CNS transport and cellular tropism of AAV4 and the lab-derived mutant strain. Unlike AAV4, which displays restricted tropism for the ependymal

lining, the lab-derived AAV4.18 mutant spreads throughout the brain parenchyma and can selectively infect migrating progenitors in the rostral and caudal directions from a unilateral ICV injection in neonatal mice. Further biochemical characterization of AAV4 and AAV4.18 in the mouse brain confirmed a switch in receptor specificity from α2,3-linked SA to α2,8-linked PSA, a well-established marker of neurogenesis.

2.3 Materials and Methods

Recombinant AAV vector production. Recombinant AAV4 and mutant AAV4.18 vectors were generated using an updated triple plasmid transfection method (206). Briefly, this involved transfection of (a) the pXR4 helper plasmid (18) or the mutant pXR4.18 helper plasmid (205); (b) the adenoviral helper plasmid pXX6-80; and (c) pTR-CBA-tdTom or pTR-CBA-Luc plasmids encoding the tdTomato (tdTom) or Luciferase (Luc) reporter genes driven by the chicken beta actin (CBA) promoter and flanked by inverted terminal repeats (ITRs) derived from the AAV2 genome. Vector purification was carried out using cesium gradient ultracentrifugation and viral titers obtained by quantitative PCR using a Roche Lightcycler® 480 (Roche Applied Sciences, Pleasanton, CA) with primers (IDT Technologies, Ames, IA) designed for the CBA promoter (forward, 5'-CGT CAA TGG GTG GAG TAT TT-3' ; reverse, 5'-GCG ATG ACT AAT ACG TAG ATG-3').

In order to generate AAV particles packaging thymidine analog 5-bromo-2'-deoxyuridine (BrdU) labeled genomes, we adapted a modified vector production protocol described earlier (207, 208). Briefly, at 1hr post triple plasmid transfection, HEK293 producer cells were treated with a 10:1 molar mixture of BrdU and 5-fluoro-2'-

deoxyuridine at a final concentration of 10μg BrdU/ml of media (Invitrogen, Camarillo, CA). Vectors packaging BrdU-labeled genomes were purified and quantified as described above.

Cellular transduction assays. CV-1 cells (African green monkey kidney fibroblasts) were seeded at a density of $5x10^4$ cells per well in 24-well plates and were maintained at 37˚C and 5% CO_2. The cells were grown in Dulbecco's modified eagle's medium (DMEM) supplemented with 10% fetal bovine serum (FBS) and 100 U/ml penicillin, 100 μg/ml streptomycin and 2.5 μg/ml amphotericin-B (Sigma-Aldrich, St. Louis, MO). For transduction assays, cells were first exposed to the different enzymatic treatments as described below.

To cleave long PSA chains, cell cultures were treated with Endoneuraminidase-N (ABC Scientific, Los Angeles, CA) diluted to 1:5000 in DMEM supplemented with 10% FBS for 12 hrs at 37˚C and 5% CO_2. To cleave terminal SA residues, Neuraminidase III (Neuraminidase) (Sigma-Aldrich, St. Louis, MO) was diluted to 50 mU/ml in serum-free DMEM and cells treated for 3 hrs at 37˚C and 5% CO_2. After these treatments, cells were washed three times with phosphate-buffered saline (1XPBS) and the media replaced with fresh DMEM+10% FBS containing AAV4 or AAV4.18 vectors packaging the firefly luciferase transgene, driven by the CBA promoter at a multiplicity of infection (MOI) of 1000 viral genomes per cell (vg/cell). Cells were lysed at 24 hours post-transduction and luciferase transgene expression was quantified using Victor2 luminometer (PerkinElmer, Waltham, MA) with D-Luciferin as a substrate.

Intracerebroventricular (ICV) injections. All animal experiments were carried out with Balb/c mice bred and maintained in accordance to NIH guidelines and as approved by the UNC Institutional Animal Care and Use Committee (IACUC). Neonatal postnatal day 0 (P0) pups were rapidly anesthetized by hypothermia by placing on ice for 1 min followed by stereotaxic intraventricular cerebral injections. A Hamilton 700 series syringe with a 26s gauge needle (Sigma-Aldrich, St. Louis, MO) was attached to a KOPF-900 small animal stereotaxic instrument (KOPF instruments, Tujunga, CA) and the mice injected unilaterally in their left lateral ventricle with a dose of $1x10^9$ particles (volume 3 µl) of AAV4 or AAV4.18 vectors packaging the CBA-tdTom reporter cassette. Developing mouse brains (P14) were harvested, post-fixed and immunostained as described in detail below. For tracking bromodeoxyuridine (BrdU)-labeled viruses, $7.4x10^8$ vector genome-containing particles in a volume of 5 µL were injected into the left lateral ventricle of P0 mice. Neonatal brains were harvested 2 hours post-injection, post-fixed in paraformaldehyde, sectioned and immunostained as described below. For recombinant sialidase co-injection experiments, the vectors were mixed with either 5.2 mU of Neuraminidase type III (Sialidase, Sigma-Aldrich, St. Louis, MO) or 1.45U of Endoneuraminidase-N (ABC Scientific, Los Angeles, CA) to a total injection volume of 4.3µl. All neonatal injections were performed 0.5mm relative to the sagittal sinus, 2mm rostral to transverse sinus and 1.5mm deep. Following vector administration, mice were revived under a heat lamp and rubbed in the bedding before being placed back with the dam.

Tissue processing, confocal microscopy and immunofluorescence analysis. Two week old mice were sacrificed with an overdose of tribromoethanol (avertin) (0.2 ml/10 g of 1.25% solution) followed by transcardial perfusion of 4% paraformaldehyde in PBS. The brains were removed and post-fixed for 24 hr and 50µm thick sections were obtained using a Leica VT 1000S vibrating blade microtome (Leica VT 1000S, Leica Biosystems, IL). Free floating brain sections were blocked in 10% goat serum and 1% Triton X (Sigma-Aldrich, St. Louis, MO) in PBS for 1hr prior to overnight incubation with primary monoclonal antibodies at 4˚C. The following primary antibodies were utilized: rabbit anti- S100β (Sigma, 1:1000), mouse anti-GFAP (Abcam-10062, 1:1000), rabbit anti-Dcx (Abcam-18723, 1:1000), goat anti-phospho-histone H3 (Millipore, 1:1000), mouse anti-BrdU (Invitrogen-033900, 1:2500), rabbit anti-NeuN (Abcam-104225, 1:750), mouse anti PSA-NCAM (DSHB, 1:750) and mouse anti-Rc2/Nestin (DSHB, 1:750). Secondary antibodies were raised in goats and conjugated to Alexa 488 or Alexa 647 (Abcam, 1:500). For jacalin staining, we followed the blocking step with 1.5 hour incubation of free floating mouse brain sections in FITC-Jacalin at room temperature (Vectorlabs, Burlingame, CA, 1:40). Jacalin was diluted to a working concentration of 20 µg/ml in 3% goat serum in PBS-T. Immunostained brain sections were visualized using a Zeiss CLSM 700 confocal laser scanning microscope and analyzed with Zen® Black software. Colocalization (%) of tdTomato reporter expression with different cell type specific markers were derived from the ratio of the number of transduced cells (tdTom+) that were S100β/GFAP/Dcx/PH3+ and the total number of transduced cells (tdTom+). Cells were counted in non-overlapping fields of view of 200

μm^2 area in the subependymal zone, rostral migratory stream, olfactory bulb or other pertinent regions in the P14 mouse brain.

2.4 Results

Substrate-specific neuraminidases have differential effects on AAV4 transduction *in vitro*. In most mammalian tissues, SA occupies the terminal position originating from Asparagine linked (*N*-) or Serine/Threonine linked (*O*-) glycoprotein glycans. However, in the CNS, sialylated glycans are expressed in two forms, α2,3- or α2,6-sialylated glycosphingolipids (gangliosides) as well as long polymeric chains of α2,8-linked PSA bound to neural cell adhesion molecule (NCAM) (209) (**Fig. 3A**). Importantly, the expression of PSA is known to regulate neural plasticity and play an indispensable role in embryonic and adult neurogenesis in the mammalian brain (210).

It is well known that AAV4 utilizes α2,3-linked SA as the mammalian cell-surface receptor (34). In order to understand whether α2,8-linked PSA on cell surfaces could also affect AAV4 transduction, we performed specific neuraminidase treatments to alter the relative levels of cell surface SA and PSA *in vitro*. We chose parental African green monkey kidney CV1 cells (precursor to Cos cells) for these experiments due to their highly permissive nature towards AAV4 transduction (34). As depicted in **Fig. 3A**, two classes of neuraminidase enzymes were used - Neuraminidase (Neu), which specifically cleaves α2,3/2,6 linkages on SA and Endoneuraminidase-N (Endo-N), which targets α2,8 linkages on the polymeric PSA chain. We observed that cleavage of SA by Neuraminidase treatment significantly reduced AAV4 transduction (> 1 log order

of magnitude reduction in luciferase activity, $p < 0.005$, **Fig. 3B**). In contrast, Endoneuraminidase-N mediated cleavage of α2,8-linked PSA significantly enhanced AAV4 transduction (> 7 fold increase, $p < 0.05$, **Fig. 3C**). Taken together, these preliminary results suggested that levels of SA and PSA on cell surfaces might differentially regulate AAV4 transduction. In contrast to AAV4, we observed no significant changes in the *in vitro* transduction efficiency of AAV4.18 virions arising from Neuraminidase or Endoneuraminidase-N treatments (**Figs. 3D and E**). However, we interpreted these results with caution due to the inherently low transduction efficiency of the AAV4.18 mutant in these cells. Earlier studies from our lab have demonstrated that the mutant AAV4.18 is likely transduction-deficient *in vitro* due its low binding affinity for SA on the cell surface (205).

Ependymal transduction efficiency by AAV4.18 is similar to parental AAV4 in neonatal mice. Previous studies have demonstrated that ICV administration of AAV4 results in robust gene transfer in the ependymal cells and astrocytes lining the neonatal mouse cerebral ventricles (77). We injected P0 mice with identical titers of AAV4 or AAV4.18 packaging the tdTomato (tdTom) reporter gene driven by chicken beta actin (CBA) promoter via the ICV route. At 2 weeks post-injection, we carried out confocal microscopy analysis of sagittal mouse brain sections. Both vectors displayed efficient tdTom expression (tdTom+) in the sub-ependymal zone (SEZ) (**Figs. 4A & B**, Top row panels). In order to further characterize the tdTom+ cells at a cellular level, we performed immuno-colocalization with markers for ependymal cells (S100β) and primary astrocytes (GFAP). As seen in **Figs. 4D and E**, tdTom+ cells (red) within the SEZ in

both AAV4 and AAV4.18 injected mouse brains show significant colocalization with S100β+ cells (green). Similarly, comparable levels of colocalization of tdTom+ cells (red) and the GFAP+ cells (green) were also observed in the SEZs of AAV4 and 4.18 treated mice (**Figs. 4G & H**). These observations were further supported by quantitative and statistical analyses that showed no significant differences in tdTom+ cells within the SEZ (**Fig. 4C**) or the percentage (%) colocalization with cellular markers (S100β and GFAP) from AAV4 or AAV4.18 injections (**Figs. 4F & I**). These results indicate that both AAV4 and 4.18 vectors can efficiently transduce neonatal mouse ependyma. Although not relevant to the current study focused on the developing brain, it is noteworthy to mention that similar ependymal transduction profiles for AAV4 and AAV4.18 vectors were observed in adult mouse brains (data not shown).

The AAV4.18 mutant displays expanded tropism for migrating progenitors. Neuronal progenitors in the SEZ are known to migrate via the RMS to the OB, where they differentiate into interneurons of the granular and periglomerular layers in developing and adult rodent brains (78). Confocal microscopy analysis of sagittal sections of postnatal mouse brains imaged at 2 weeks post-injection revealed strikingly distinct patterns of transduction between AAV4 and AAV4.18 vectors. Notably, AAV4.18 injected mice showed significantly more tdTom expression in the RMS and OB (~3 and 6 fold increase respectively, n=4 mice) regions as compared to AAV4 injected mice (Top row panels, **Figs. 5A & B**). We then performed immunostaining for the migrating neuroblast marker doublecortin (Dcx) and proliferating cell marker phospho-histone H3 (PH3) to assess the cell types associated with the tdTom expression in the RMS and

OB. As seen in **Figs. 5D & E** (Middle row panels), tdTom+ cells (red) within the RMS and the OB in AAV4.18 injected mouse brains show significantly increased colocalization with Dcx+ cells (green) compared to AAV4 injected brains. A similar trend showing increased colocalization of tdTom+ expression with the PH3+ cells was observed in the RMS and to a lesser level in the OB of 4.18 injected brains (**Figs. 5G & H**; Bottom row panels). These observations were corroborated by quantitative and statistical analyses (**Figs. 5C, F & I**; *$p < 0.05$).

Mutant AAV4.18 virions display enhanced CNS spread. In order to understand the mechanisms underlying the selective tropism of AAV4.18 for progenitors and neuroblasts in the postnatal CNS, we tracked the distribution of each AAV vector in the mouse brain parenchyma following ICV injections. To achieve this, we injected AAV vectors packaging genomes that were labeled with the thymidine analog bromodeoxyuridine (BrdU) through ICV injections in neonatal mice. Brains were harvested as early as 2 hours post vector administration and immunostained with an anti-BrdU antibody to visualize the biodistribution of AAV genomes in the brain parenchyma. AAV4 injected mice exhibit robust BrdU staining in the immediate vicinity of the site of injection in the SEZ and the outer meninges of the neonatal brain, presumably due to CSF transport (**Fig. 6A**, middle column, arrow). In contrast, the AAV4.18 vector shows a remarkably diffuse distribution pattern of BrdU-labeled viral particles not only in the SEZ (**Fig. 6A**, far right column, arrow) but also through the brain parenchyma and particularly in the cortical regions (**Fig. 6A**, far right column, arrowhead). Immunostaining analysis of brain sections with the endothelial cell marker

CD31 revealed BrdU+ AAV4.18 genomes (green) arranged alongside CD31+ processes (red) in the cortical regions of the mouse brain (**Fig. 6B**, far right column). In contrast, AAV4 genomes did not show this phenotype in the cortex (**Fig. 6B**, middle column). It should be noted that despite the expanded spread of the AAV4.18 genomes, complete colocalization with endothelial cells was not observed (**Fig. 6B**, far right column, inset). This suggests that the selective tropism for migrating progenitors can, in part, be attributed to the ability of AAV4.18 to spread across the neonatal brain parenchyma.

Selective enzymatic removal of PSA expands CNS tropism of AAV4 vectors. The polysialylated form (PSA, 2,8-linked sialic acid) of neural cell adhesion molecule (NCAM) is expressed in migrating progenitor cells of the RMS during OB neurogenesis (211). PSA-NCAM plays a pivotal role in mediating rostral migration of olfactory bulb precursor cells whereas deficiencies in either PSA or NCAM cause accumulation of progenitor cells in the SEZ and RMS resulting in aberrant olfactory histogenesis (211, 212). We co-injected Neuraminidase, which selectively cleaves terminal SA residues or Endoneuraminidase-N, which cleaves the polymeric PSA chain with AAV4 packaging the CBA-tdTom reporter gene in neonatal P0 mice via the ICV route. Loss of terminal SA residues due to Neuraminidase treatment was confirmed by a significant reduction in fluorescein isothiocyanate (FITC)-labeled jacalin staining in the mouse brain (data not shown). Control injections of AAV4 alone resulted in highly localized tdTom+ expression in the ependymal lining, which was almost completely abrogated in Neuraminidase co-injected mice (**Figs. 7A and C**, left columns). We

observed minimal tdTom+ expression in migrating progenitors within the RMS and OB by AAV4, regardless of treatment with Neuraminidase (**Figs. 7A and C**, middle and right columns). Further, no colocalization with PSA-NCAM immunostaining was observed (**Figs. 7B and D**). In contrast, Endoneuraminidase-N treatments increased AAV4 mediated tdTom+ expression in the RMS, but more strikingly in the OB (**Fig. 7E**, middle and right columns) and without affecting ependymal tdTom+ expression. (**Fig. 7E**, left column). A concomitant and significant reduction in PSA-NCAM immunostaining in the RMS and OB upon Endoneuraminidase-N treatment is also observed (**Figs. 7D & F**). Taken together, these results suggest that 2,8-linked PSA negatively regulates AAV4 spread and potentially competes for 2,3-linked SA binding sites on the AAV4 capsid.

To further characterize the expanded transduction profile of AAV4 observed following Endoneuraminidase-N co-injections, we carried out immuno-colocalization with several cellular markers. As discussed above, PSA-NCAM immunostaining was abrogated due to efficient cleavage of PSA residues from such treatments (**Fig. 8A**) and no colocalization with tdTom+ cells was observed as expected. Interestingly, we observed that AAV4 mediated transgene expression (tdTom+) significantly colocalized with NeuN+ neurons in the OB (**Fig. 8B**, arrows, far right column). However, we did not observe colocalization of tdTom+ cells with the astrocytic marker, GFAP or the radial glial marker, RC2/Nestin (**Figs. 8C and D**). These results indicate that under conditions displaying reduced PSA levels, AAV4 can efficiently transduce mature OB neurons. This data is consistent with observations from cell culture studies described earlier.

Thus, it appears that modulation of PSA levels can influence AAV4 tropism in the mammalian brain.

The low affinity AAV4.18 mutant displays expanded tropism for migrating progenitors by exploiting high PSA levels. In order to dissect the possible mechanism underlying the expanded tropism displayed by AAV4.18 from ependymal cells towards migrating neuroblasts, we subjected the mutant strain to similar enzymatic modulation of SA and PSA levels. Similar to untreated controls (**Figs. 9A & B**), co-injection of Neuraminidase III with AAV4.18 did not alter the extent of co-localization between tdTom+ and PSA-NCAM+ cells in the RMS or the OB (**Figs. 9C & D**). In contrast, co-administration of Endoneuraminidase-N dramatically altered PSA-NCAM staining throughout the mouse brain, particularly within the migrating progenitor continuum and completely abrogated tdTom reporter gene expression in AAV4.18 injected mouse brains (**Fig. 9E and F**). Taken together, these results support the notion that the AAV4.18 has undergone a complete switch in glycan receptor specificity from terminal 2,3-linked SA to the polymeric 2,8-linked PSA chain owing to a loss in SA binding affinity. In turn, AAV4.18 appears to exploit the PSA glycosylation pattern in the developing brain to efficiently transduce migrating progenitors.

Further characterization of AAV4.18 treated mice co-injected with Neuraminidase revealed a striking correlation between the pattern of TdTom+ cells and PSA-NCAM staining along the migrating progenitor RMS-OB continuum (**Fig. 10A**). No apparent colocalization was observed with the mature neuronal marker, NeuN in the PSA-NCAM labeled region (**Fig. 10B**). Although, it is noteworthy to mention that some colocalization

was observed between tdTom+ and NeuN+ cells in the periphery of OB (data not shown). Several tdTom+ cells along the migratory pathway colocalized with the astrocyte marker, GFAP; but not the radial glial marker, RC2/Nestin in the RMS as well as OB (**Figs. 10C and D**). Taken together, these results corroborate the notion that modulating SA and PSA levels in the brain can be differentially exploited by AAV4 and AAV4.18 to attain strikingly distinct transduction patterns targeting the ependymal lining, neurons within the OB or migrating progenitors in the RMS and OB regions within the neonatal brain.

2.5 Discussion

Successful infection by parvoviruses such as AAV involves a series of carefully orchestrated events including cell surface receptor binding, endocytic uptake, capsid uncoating, nuclear entry and genome release followed by second strand synthesis and subsequent transcription. The first step, i.e., parvoviral attachment to the host cell surface is mediated by different glycans (25). In the brain, AAV capsid interactions with heparan sulfate (HS) have been particularly well-studied. Direct parenchymal injection of AAV serotype 2, which utilizes HS as a primary receptor (35), results in a prominently neuronal transduction profile (40, 41). Co-injection of soluble heparin has been shown to improve the CNS spread and consequently transduction efficiency of AAV2 following intracranial injections in rodent models (47, 48). The ability to bind HS also appears to restrict the CNS transduction profile of AAV serotype 6 (46). However, this effect can be reversed in part by mutating a lysine residue (K531) on the capsid surface, which

abolishes HS binding (45, 46). These earlier studies highlight the potential for glycan expression patterns to regulate viral spread and tropism in the brain.

In the current study, we have characterized a novel AAV mutant that selectively transduces migrating progenitors in the neonatal mouse brain. This mutant was originally discovered from a randomly mutated AAV4 capsid library and characterized as an SA-binding deficient mutant. When administered systemically, the AAV4.18 mutant displays attenuated cardiopulmonary tropism in mice due to the low binding affinity towards *O*-linked 2,3-SA, the cognate receptor for the parental AAV4 serotype (205). In the neonatal mouse brain, the natural isolate AAV4 exclusively transduces ependymal cells following ventricular injection (77). Interestingly, when injected directly into the SEZ, AAV4 can transduce type B astrocytes in the SVZ and glia overlying the RMS (77). Our results now show that this dichotomy potentially arises from the high binding SA and PSA affinity of AAV4 capsids, which likely restricts transduction to the ependymal lining following ICV administration.

In contrast, the low affinity AAV4.18 mutant can penetrate the ependymal barrier into the brain parenchyma following a single ICV injection and selectively transduce migrating neuroblasts and proliferating cells, apparently due to interactions with PSA alone (**Figs. 3-5**). It is noteworthy that the enhanced spread of AAV4.18 particles to distal regions of the mouse brain does not result in successful transduction of mature neurons within these regions. Rather, immunohistochemical analysis suggests that AAV4.18 particles that reach the cortex are closely associated with the brain microvasculature without actually transducing endothelial cells (**Fig. 6**). This observation suggests that interstitial solutes such as viral particles might exploit paravenous efflux or

the ‘glymphatic’ clearance pathway (62). Correspondingly, we postulate that low binding affinity AAV4.18 particles are more likely to be affected by interstitial fluid transport through white matter tracts and perivascular spaces leading to enhanced penetration of brain parenchyma.

We further expanded these findings by evaluating the effect of selective enzymatic removal of 2,3- or 2,8-linked SA from the murine brain by ICV injection of substrate-specific neuraminidases. While AAV4 transduction is completely abrogated by selective SA removal, AAV4.18 transduction of a subset of cells in the ependymal wall, the choroid plexus and PSA-NCAM+ migrating progenitors remains unaffected (**Figs. 7 - 9**). This selective requirement of polymeric 2,8-linked PSA chain rather than terminal SA residues for AAV4.18 transduction was clearly demonstrated by enzymatic removal. Taken together, these results support the notion that AAV4.18 can not only spread throughout the brain parenchyma, but also selectively exploit PSA (2,8-linked SA) to transduce postnatal migrating progenitors in the mouse forebrain.

The expanded receptor usage and selective cellular tropism displayed by AAV4.18 particles are not a mere coincidence. It is well known that the linear homopolymer of alpha 2,8-linked sialic acid (polysialic acid/PSA) plays an indispensable role in embryonic and adult neurogenesis. Two regions of the brain, namely OB and hippocampal dentate gyrus are persistently neurogenic and undergo constant progenitor chain migration into adulthood in rodents (213). Despite multiple differences between adult and embryonic neurogeneses, consistent PSA-NCAM expression is a feature observed in both of these regions through adulthood (214). The biochemical properties of PSA make it a potent negative regulator of cell-cell adhesion. This is

important for successful migration of precursor cells during neurogenesis (215). This is potentially the reason PSA-NCAM is highly expressed in the neuronal precursor cells during olfactory neurogenesis (215). Furthermore, the enzymatic removal of PSA using Endoneuraminidase-N treatment disrupts the RMS leading to neuroblast dispersion to unspecific regions like cortex and striatum (211). Thus, the selective transduction of migrating progenitors by AAV4.18 can be directly attributed to the expression patterns of this unique glycan attachment factor that can vary with the developmental stage of the host organism.

Certain gaps still remain in our understanding of the proposed AAV-PSA interactions. First, PSA does not appear to functionally influence the tropism or transduction efficiency of AAV4 or related mutants in physiological settings other than the CNS, such as the heart and lung following intravenous administration (205). It is likely that the developing brain provides a unique setting for this novel virus-glycan interaction. Secondly, the structural coordinates that mediate PSA recognition by AAV4 and the mutant virion remain to be determined. Preliminary structural modeling revealed altered surface electrostatics for the AAV4.18 mutant in comparison with the parental AAV4 strain (data not shown). It is tempting to speculate that manipulation of capsid surface charge density might decrease affinity for branched or linear 2,3-linked SA glycans, while simultaneously imparting the expanded potential to recognize the negatively charged PSA glycopolymer.

These hypotheses warrant further structural and biophysical analysis outside the scope of the current study. Nevertheless, our overall approach helps understand the functional implications of altering virus-glycan interactions in the CNS, impact of

developmentally regulated or disease-specific glycan expression profiles on virus neurotropism. Simultaneously, we provide a roadmap for engineering viruses to favor certain glycan architectures for gene transfer applications in the brain.

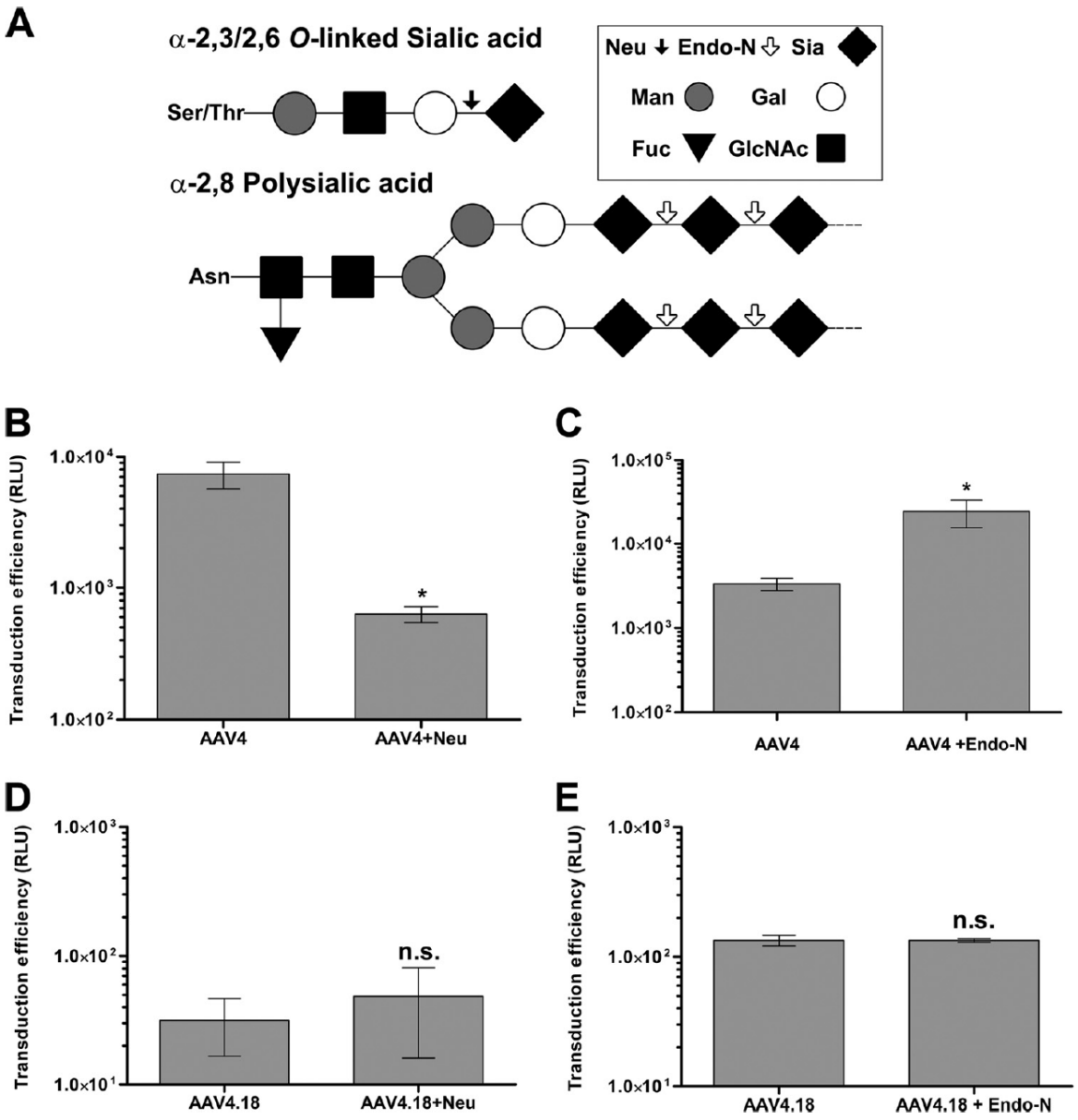

Figure 3: Effects of substrate-specific neuraminidases on AAV4/4.18 transduction *in vitro* (A) Schematic representation of *O*-linked α–2,3/2,6 Sialic acid (top) and α–2,8 Polysialic acid (bottom) on mammalian cell surfaces. Legend describes different glycan symbols. Black and white arrows represent the cleavage sites of Neuraminidase (Neu) and Endoneuraminidase-N (Endo-N) enzymes, respectively. Effects of Neuraminidase and Endoneuraminidase-N treatment on AAV4 **(B and C)** as well as AAV4.18 **(D and E)** are also shown. CV-1 cells pretreated with each enzyme were incubated with AAV4 or AAV4.18 vectors packaging a CBA-Luc transgene (MOI = 1000 vg/cell) and luciferase activity in relative light units (RLU) measured at 24 hrs post-infection. Error bars represent standard deviation (n = 3). (n.s., not statistically significant; *p < 0.05 as determined by student t-test).

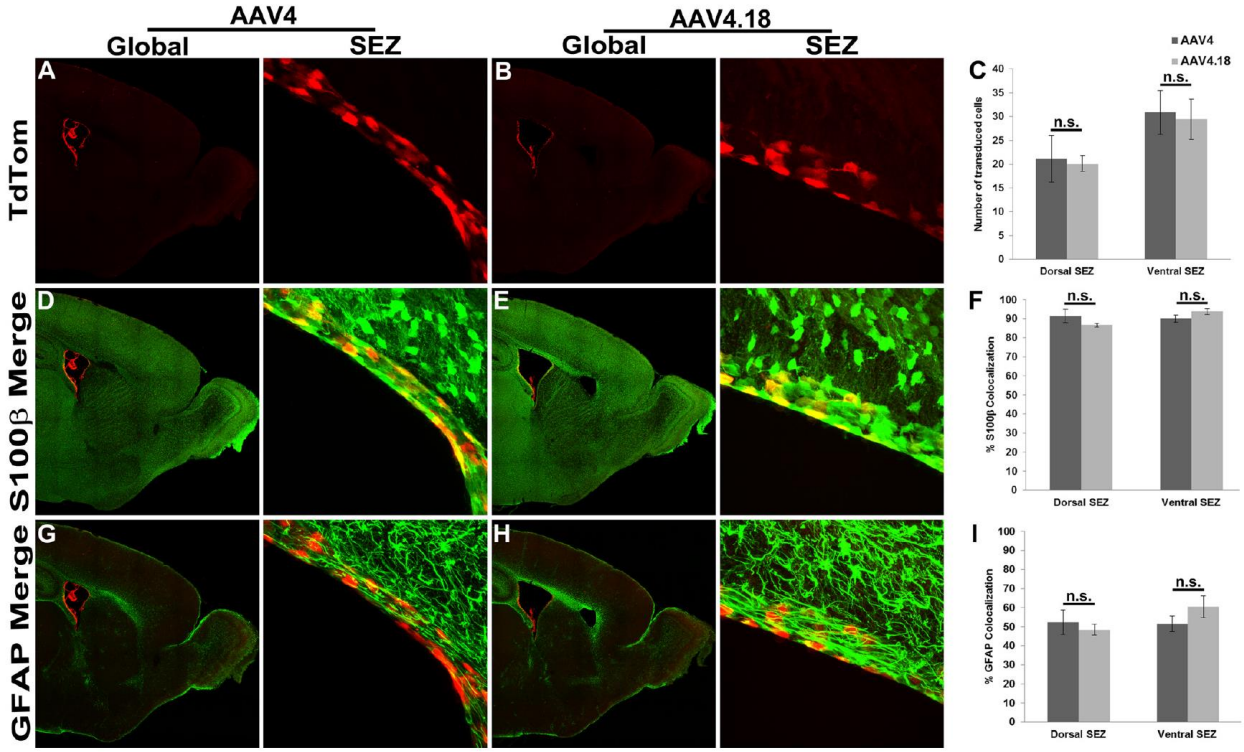

Figure 4: Ependymal transduction in the neonatal mouse brain by AAV4 and the AAV4.18 mutant. P0 mice were injected with 1x10^9 vg of AAV4 **(A)** or mutant AAV4.18 **(B)** packaging a CBA-tdTom transgene into the left lateral ventricle. At 2 weeks post-injections, mice were sacrificed and paraformaldehyde fixed brains were sectioned and immunostained. Brain sections were imaged using a Zeiss CLSM 700 confocal laser scanning microscope equipped with 488nm and 555nm excitation filters. Confocal micrographs show tdTom transgene expression in red. Global brain sections are confocal image stitches of representative 50 um vibratome sagittal sections and SEZ regions show tdTom expression in the sub-ependymal zone. **(D and E)** Immuno-colocalization of tdTom gene expression (red) with ependymal cells (S100β, green) and **(G and H)** primary astrocytes (GFAP, green) is indicated by yellow pseudocolor within the S100β/GFAP merged images. Quantitative assessments of the AAV4 (dark grey bars) or AAV4.18 (light grey bars) transduced cells in the dorsal and ventral SEZ are indicated by the number of tdTom+ cells **(C)** and percentage colocalization with S100β+ cells **(F)**, or GFAP+ cells **(I)**. Error bars represent standard deviation (n = 4). (n.s., not statistically significant; *p < 0.05 as determined by student t-test). Representative confocal images are shown.

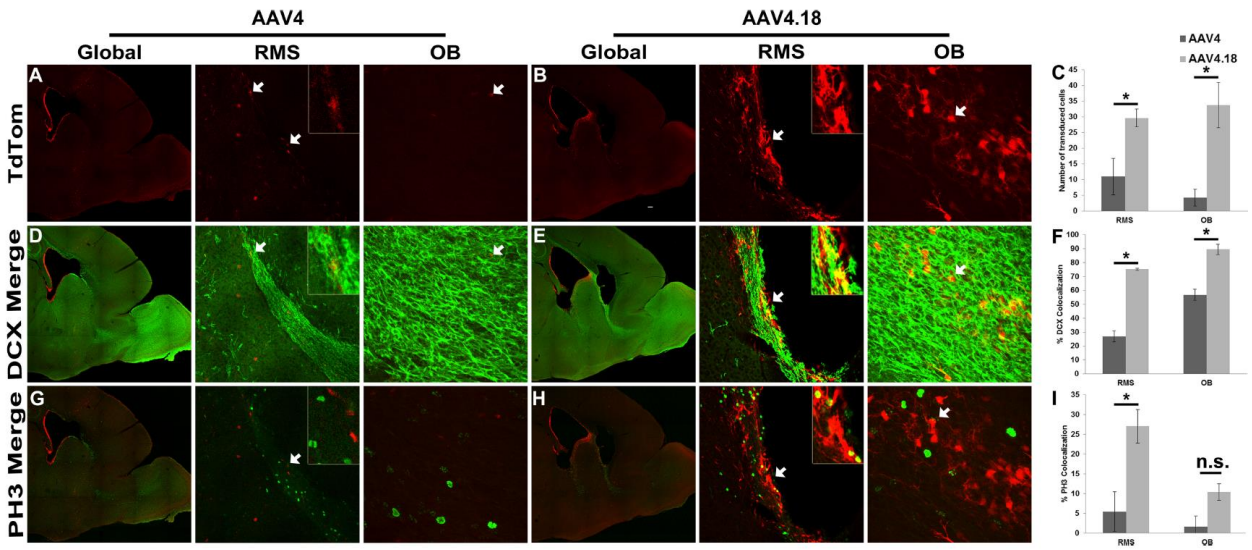

Figure 5: The AAV4.18 mutant exhibits selective tropism for migrating progenitors. P0 mice were injected with $1x10^9$ vg of AAV4 (A, D, G) or AAV4.18 (B, E, H) packaging the tdTomato reporter transgene driven by a chicken beta actin promoter into the left lateral ventricle. Comparison of tdTom expression (red) in sagittal sections of the developing mouse brain including the sub-ependymal zone (SEZ), rostral migratory stream (RMS) and olfactory bulb (OB) regions are shown. **(A, B)** Immuno-colocalization of AAV4 or AAV4.18 mediated gene expression (tdTom, red) with **(D, E)** the migrating neuroblast marker, doublecortin (Dcx+, green) and **(G, H)** the proliferative cell marker, phospho-histone H3 (PH3+, green) are shown. White arrows indicate the locations shown at higher magnification (insets) and immunocolocalized regions depicted in yellow. Quantitative analysis of the number of tdTom+ cells **(C)** and percentage colocalization with Dcx+ processes **(F)** and PH3+ cells **(I)** in the RMS and OB regions of AAV4 (dark grey bars) or 4.18 (light grey bars) treated mice are shown. Error bars represent standard deviation (n = 4). (n.s., not statistically significant; *p < 0.05 as determined by student t-test). Representative confocal images are shown.

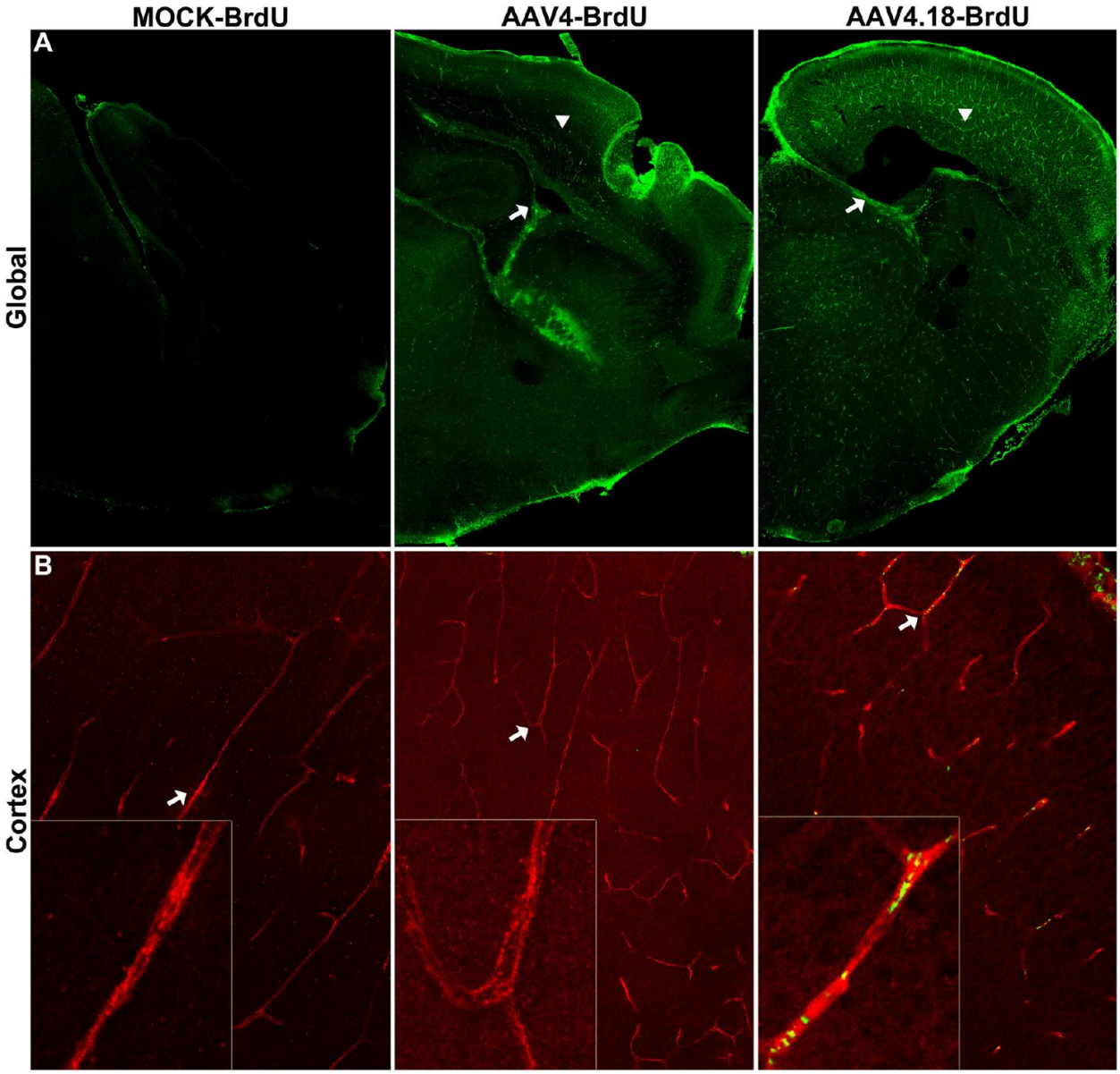

Figure 6: AAV4.18 particles show enhanced CNS spread. P0 mice were injected with $7.4x10^8$ vg of AAV4 or AAV4.18 packaging BrdU-labeled genomes into the left lateral ventricle. At 2 hours post injections, mice were sacrificed and paraformaldehyde fixed brains were sectioned, immunostained and imaged as outlined in methods. (A) Global anti-BrdU immunostaining (green) in sagittal sections of the brain obtained from mock-treated, AAV4 or AAV4.18 injected mice into the left lateral ventricle (white arrows). The positions of the cortical regions shown in higher magnification in B are indicated by white arrowheads in A. (B) Immuno-colocalization of BrdU+ viral genome-containing particles (green) and anti-CD31, endothelial cell marker immunostaining of blood vessels (red) in the cortex. All experiments were carried out in triplicate, representative images are shown.

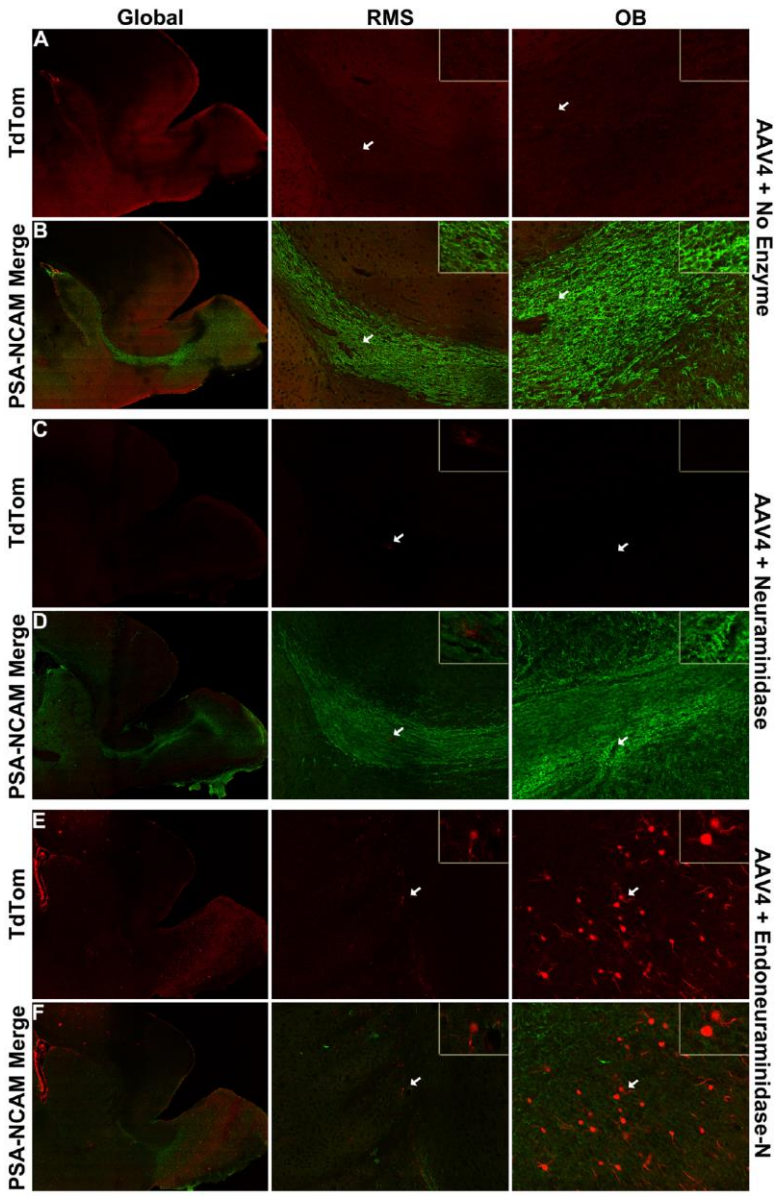

Figure 7: SA and PSA play opposing roles in AAV4 transduction within the neonatal mouse brain. (A, B) P0 mice were co-injected with mixtures of $1x10^9$ vg of AAV4 mixed with PBS (control); **(C, D)** 3.5 mU of Neuraminidase (cleaves 2,3-/2,6-linked sialic acid); or **(E, F)** 1.45 U of Endoneuraminidase-N (cleaves 2,8 linked polysialic acid) into the left lateral ventricle. At 2 weeks post-injections, mice were sacrificed and paraformaldehyde fixed brains were sectioned and immunostained. TdTom transgene expression patterns (red) and PSA-NCAM immunostaining (green) resulting from enzymatic desialylations are shown in the global context or as higher magnifications of the RMS and OB regions. White arrows indicate the locations shown at higher magnification (insets). All experiments were carried out in triplicate, representative images are shown.

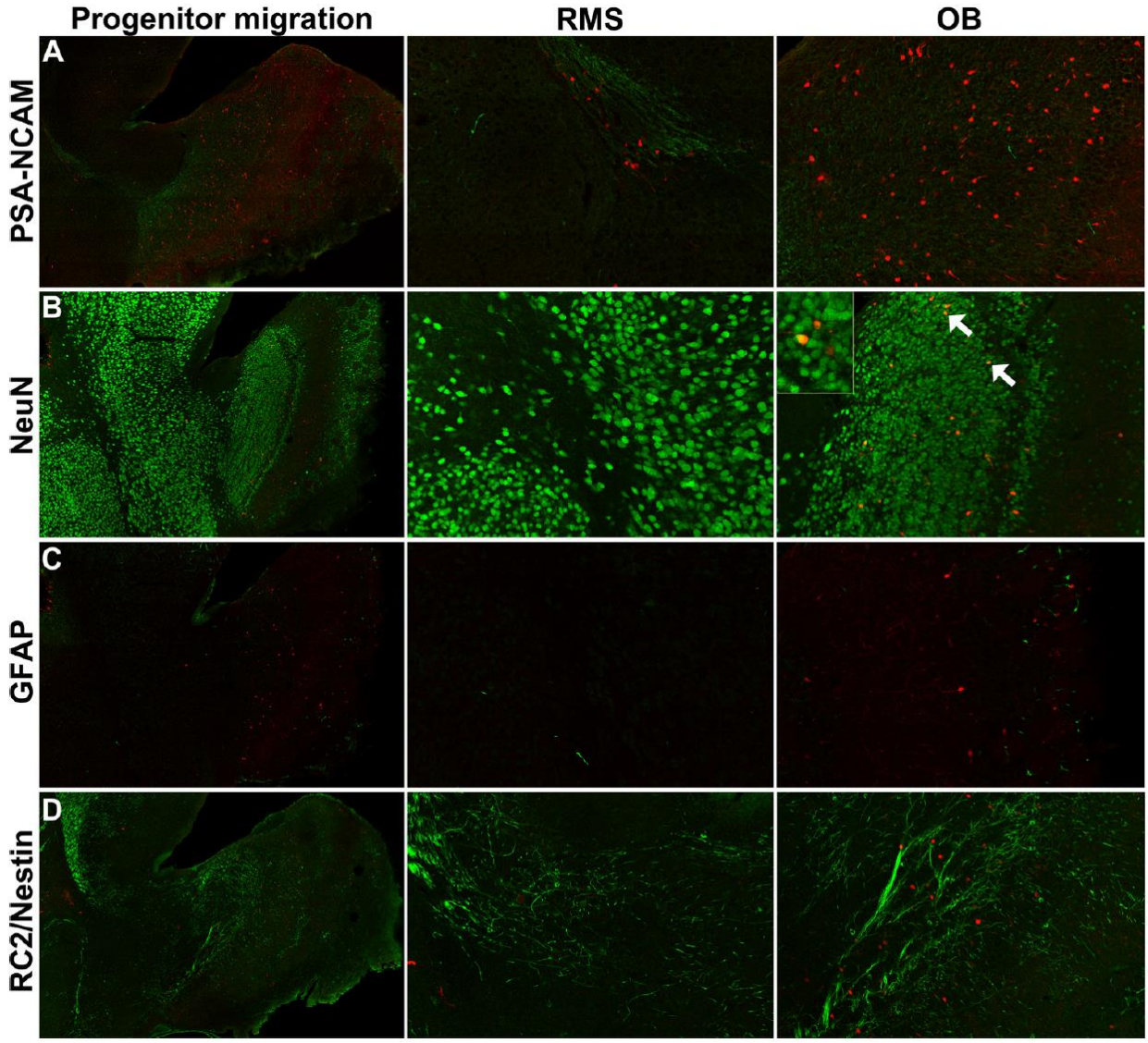

Figure 8: Removal of PSA expands AAV4 tropism to mature OB neurons. P0 mice were co-injected with $1x10^9$ vg of AAV4 mixed with 1.45 U of Endoneuraminidase-N into the left lateral ventricle. At 2 weeks post-injections, mice were sacrificed and paraformaldehyde fixed brains were sectioned and immunostained for different cellular markers, PSA-NCAM (A), NeuN (B), GFAP (C) and RC2/Nestin (D) with specific antibodies as outlined in methods. Sagittal sections of the mouse brain featuring progenitor migration in the rostral migratory stream (RMS) and olfactory bulb (OB) and immuno-colocalization of tdTom transgene expression (red) with each cellular marker (green) are shown. White arrows indicate the locations shown at higher magnification (insets) or immunocolocalized regions (shown in yellow). All experiments were carried out in triplicate, representative images are shown.

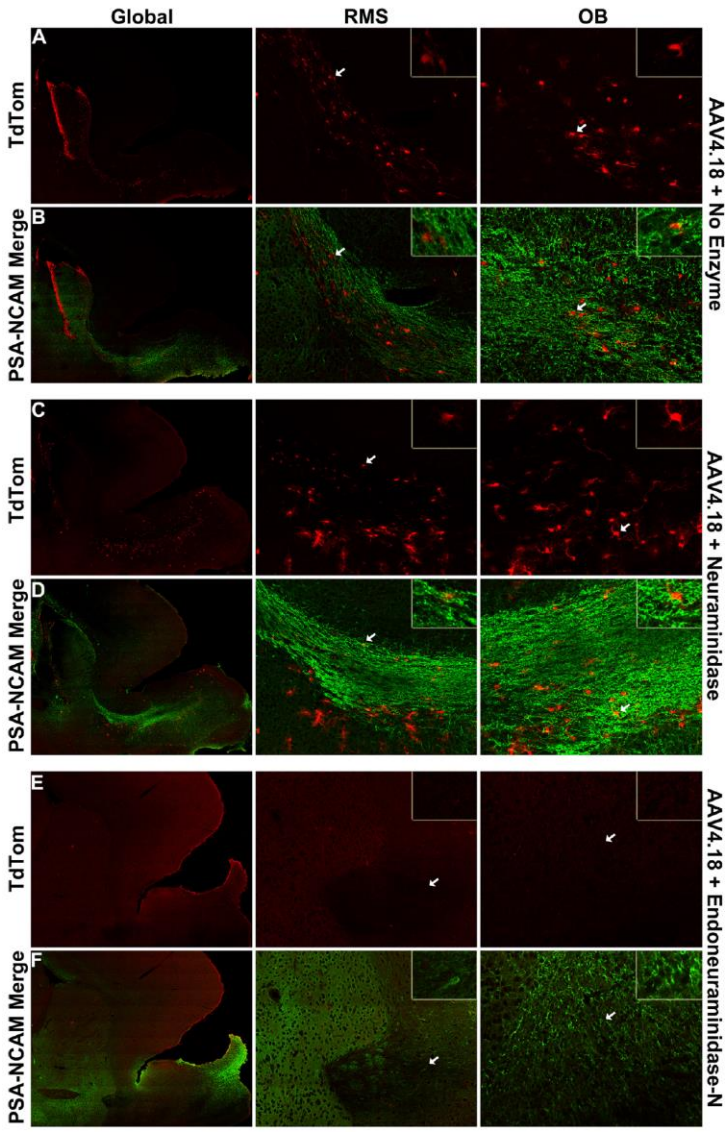

Figure 9: The AAV4.18 mutant selectively exploits polysialic acid (PSA) to transduce migrating progenitors. (A, B) P0 mice were co-injected with mixtures of $1x10^9$ vg of AAV4.18 mixed with PBS (control); **(C, D)** 5.2 mU of Neuraminidase (cleaves 2,3- and 2,6- linked sialic acid); or **(E, F)** 1.45 U of Endoneuraminidase-N (cleaves 2,8 linked sialic acid/polysialic acid) into the left lateral ventricle. Post-fixed sagittal sections of P14 mouse brains displaying tdTom transgene expression patterns resulting from enzymatic desialylation are shown in the global context or as higher magnifications of the RMS and OB regions. White arrows indicate the locations shown at higher magnification (insets) and immuno-colocalization of tdTom expression (red) with PSA-NCAM staining (green) is depicted in yellow (B, D, F). All experiments were carried out in triplicate, representative images are shown.

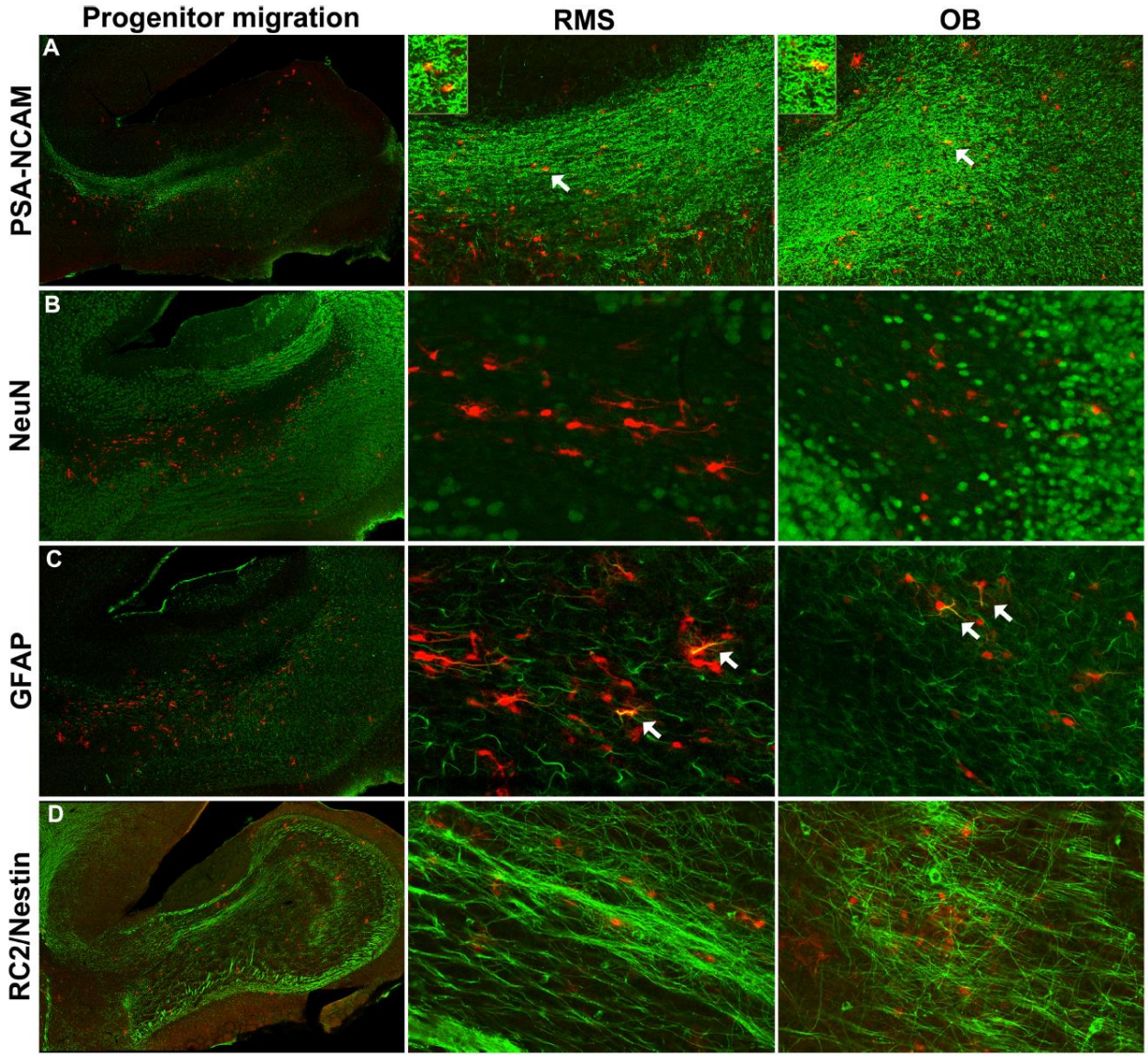

Figure 10: AAV4.18 selectively transduces migrating progenitors expressing polysialyated NCAM and GFAP. P0 mice were co-injected with $1x10^9$ vg of AAV4.18 mixed with 5.2mU of Neuraminidase into the left lateral ventricle. Postfixed P14 mouse brains were sectioned and immunostained for different cellular markers, PSA-NCAM (A), NeuN (B), GFAP (C) and RC2/Nestin (D) with specific antibodies as outlined in methods. Sagittal sections of the mouse brain featuring progenitor migration in the rostral migratory stream (RMS) and olfactory bulb (OB) and immuno-colocalization of tdTom transgene expression (red) with each cellular marker (green) are shown. White arrows indicate the locations shown at higher magnification (insets) or immunocolocalized regions (shown in yellow). All experiments were carried out in triplicate, representative images are shown.

CHAPTER 3: LIMITED SYSTEMIC BURDEN AND BRAIN-SPECIFIC GENE DELETION WITH A NOVEL AAV VECTOR

3.1 Overview

Gene therapy using recombinant adeno-associated viral (AAV) vectors is emerging as a promising approach to treat central nervous system (CNS) disorders such as Spinal muscular atrophy, Batten, Parkinson and Alzheimer disease amongst others. A critical remaining challenge for CNS-targeted gene replacement, silencing or gene editing therapies is to limit potential vector dose-related toxicity in systemic, off-target organs. Here, we address the latter concern through rational AAV vector design. Specifically, we characterize a lab-derived AAV chimeric (AAV2g9), which displays favorable CNS attributes derived from both parental counterparts, AAV2 and AAV9. This synthetic AAV strain displays preferential, robust and widespread neuronal transduction within the brain and decreased glial tropism. Importantly, we observed minimal systemic leakage of AAV2g9 compared to AAV9, when administered into the cerebral ventricles or by lumbar puncture. Correspondingly, AAV2g9 shows markedly decreased sequestration and gene transfer in off-target organs. A single intracranial injection of AAV2g9 vectors encoding guide RNAs targeting the schizophrenia risk gene MIR137 (encoding miR137) in CRISPR/Cas9 knockin mice resulted in brain-specific gene deletion with no detectable events in the liver. Dual glycan binding AAV vectors are a promising platform to potentially improve the safety of gene editing, RNAi or gene therapies for neurological disorders

3.2 Introduction

The clustered, regularly interspaced, short palindromic repeats (CRISPR)-associated endonuclease (Cas)9 technology has been utilized for targeted disruption of genomic loci in cell culture (216-219), animal studies (220-223), and recently for *in vivo* disease correction (221, 224, 225). Specifically, guide RNA (gRNA) dependent recruitment of Cas9 endonuclease (226) can be employed for generating double strand breaks in the targeted loci of the host genome (218, 227, 228). The recombinant adeno-associated viral (rAAV) vector platform offers safe, efficient and tissue specific gene transfer systems for therapeutic delivery of CRISP/Cas9 modalities, *in vivo* (224). Understandably, the integration of rAAV and CRISPR/Cas9 technologies can be instrumental for gene therapy. However, it is crucial to exercise caution and preempt potential side effects before clinical translation of such combinatorial therapeutics.

Adeno-associated viruses (AAV) are members of the *Dependoparvovirus* genus within the *Parvoviridae* family (16). These small, non-enveloped viruses package a single-stranded DNA genome within an icosahedral (T=1) capsid, approximately 25 nm in diameter (17). The topology of the AAV capsid presents a versatile surface for interaction with a wide variety of cellular ligands, carbohydrates in particular, which serve as attachment factors for viral infection (25). For instance, interactions of AAV serotype 2 with the glycosaminoglycan, heparan sulfate (hep) are well known. Other natural isolates such as AAV3b and AAV6 have also been shown to bind hep both *in vitro* and *in vivo*. Further, sialic acids with different linkage specificities and more recently, galactose (gal) have been identified as primary receptors for various AAV

strains (25, 229). Several of the aforementioned AAV strains are under active development as gene therapy vectors for different clinical indications (230, 231).

The central nervous system (CNS) is comprised of a complex architecture of neurons, astrocytes, microglia, endothelium and other cell types. Glycosaminoglycans such as hep and chondroitin sulfate as well as sialylated glycans are ubiquitously expressed in the mammalian CNS and often tightly regulated during the course of neural development (210, 232). Several viral pathogens have evolved to exploit different glycosylation patterns within the brain. For instance, hep binding has been implicated in the neurovirulence displayed by members of the *Alphavirus* genus such as sindbis virus and equine encephalitis viruses (233, 234). In case of AAV, intracranial injection of a hep binding serotype, AAV2, shows restricted, neuronal gene expression (71, 89). Controlled co-injection of safe doses of soluble heparin have been shown to enhance AAV2 spread and transduction in the CNS (47, 48). Sialic acid binding serotypes such as AAV1 or AAV5 appear superior to AAV2 in mediating spread of transgene expression in the CNS (89). Widespread transgene expression in the CNS has also been demonstrated in case of AAV9, which utilizes gal as a primary attachment receptor (37, 90). Studies involving intravascular/intrathecal administration in mouse, canine, feline and non-human primate models have provided important insight into the CNS tropism of AAV9 and Rh.10 and supported their advancement as candidate vectors for clinical trials (54, 56, 66, 94, 235).

Despite these exciting advances, several gaps exist in our understanding of AAV-glycan interactions in the CNS. Within this framework, a specific focus of the current study is to understand how glycans such as hep and gal mediate differential

AAV-mediated transduction patterns in the CNS. It is known that attachment to heparan sulfate (hep) influences the neurotropism of adeno-associated virus (AAV) serotype 2, herpes simplex virus, sindbis virus and equine encephalitis viruses amongst other examples. Although several natural AAV isolates broadly transduce neurons and glia in a hep-independent manner, glycan interactions within the central nervous system (CNS) are not well understood. We also systematically evaluated the role of galactose (gal) in determining the CNS transduction profile of AAV9 and several lab-derived strains. A hep-binding mutant (AAV2i8g9) or co-injection of soluble heparin with AAV2g9 attenuated neuronal transduction, but redirected transgene expression to glia. Another chimeric strain, AAV8g9, which binds gal, but not hep, displayed enhanced CNS transduction in both neurons and glia compared to parental AAV8 vectors. Consistent with observations that gal binding improves transduction efficiency, a gal-binding AAV9 mutant was completely attenuated in the brain. Together, these results corroborate distinct roles for hep and gal in determining neurotropism and spread of AAV vectors.

Recombinant AAV vectors have met safety endpoints in several Phase I gene therapy clinical trials for treating Hemophilia, Alpha-1 Antitrypsin (AAT) deficiency, Alzheimer disease amongst other indications (236-238). Although vector re-dosing might be essential in some indications due to loss of gene expression observed in long term follow up studies (239), preclinical studies continue to show promise and advance with cautious optimism. One concern noted in hemophilia gene therapy clinical trials is the potential for vector dose-related hepatotoxicity in patients as evidenced by a rise in transaminases (237, 240). Although resolvable by administration of anti-inflammatory steroids such as methyl prednisolone, permanent loss in gene expression has been

observed (237). The dose and composition of clinical AAV vectors has been shown to influence these outcomes in preclinical toxicity studies (241). Accordingly, scientific, regulatory and clinical communities alike have established that continued improvements in vector design, development and manufacturing are needed (242, 243).

To date, over a hundred naturally occurring strains of AAV derived from human and animal tissues have been isolated (244, 245). Multiple strains ranging from AAV serotypes 1 through 9 and Rh.10 are under active development as gene therapy vectors for different clinical indications (230, 231). Recent data from clinical gene therapy trials to treat Parkinson and Alzheimer disease have provided information that is critical towards continued AAV vector development (164, 238). In addition, preclinical studies involving intravascular/intrathecal administration in mouse, canine, feline and non-human primate models have supported the advancement of serotypes such as AAV9 as candidates for clinical trials (54, 56, 66, 94, 235). Notably, AAV9 is currently being evaluated in Phase I clinical trials for the treatment of Spinal muscular atrophy (SMA) by intravascular injection and Giant axonal neuropathy (GAN) through intrathecal injection (Clinical trial identifiers NCT02122952, NCT02362438).

A key observation from preclinical studies is that CNS administration of several naturally occurring AAV strains often results in vector sequestration within peripheral organs such as the liver and spleen via systemic leakage (94, 101, 235, 246). In the current study, we address this potential concern through vector design. Specifically, we describe the CNS transduction profile of a rationally engineered, chimeric AAV strain (AAV2g9), which harbors the ability to engage either heparan sulfate or galactose as receptors for cell entry (37, 206). We demonstrate exceptional CNS transduction

efficiency following single bolus injections of AAV2g9 as validated by two routes of administration in neonatal and adult rodents. More importantly, we establish potentially useful attributes of AAV2g9 for CNS-specific gene therapy applications, namely, preferential neuronal tropism, restricted CNS biodistribution and minimal transgene expression in off-target peripheral organs.

Lastly, systemic dissemination of CNS-directed CRISPR/Cas9 modalities can result in undesirable genome editing/disruption events in peripheral organs. The microRNA (MIR) 137 gene is ubiquitously expressed across mammalian tissue types (247). In the CNS, MIR 137 dysfunction has been strongly associated with risk of schizophrenia in patient cohorts (248-252). In addition to involvement in SZ, miR137 also plays an important role in regulation of neurogenesis and neuronal maturation in the brain (253, 254). Using AAV2g9, we demonstrate CNS-restricted gRNA mediated disruption of miR137 locus within the Cas9 transgenic mouse (222).

3.3 MATERIALS AND METHODS

Recombinant AAV vector production. An updated triple plasmid transfection protocol was used to generate recombinant AAV vectors. . The pXR plasmids 2g9, 8g9, 2i8g9 and 9W503R have been described earlier (206, 255) All other plasmids used for AAV production in this study were obtained from the UNC vector core. Briefly, the transfection mixture contained (a) the pXR9 helper plasmid or pXR2g9/2i8g9 helper plasmids; (b) the adenoviral helper plasmid pXX6-80; and (c) pTR-CBh-ScGFP, pTR-hSyn-EGFP, pTR-GFAP-EGFP or pTR-CBA-Luc plasmids encoding the green fluorescent protein (GFP) or luciferase (Luc) reporter genes driven by the chicken β

hybrid (CBh), human synapsin (hSyn), glial fibrillary acid protein (GFAP) or the chicken β actin (CBA) promoters, flanked by inverted terminal repeats (ITRs) derived from the AAV2 genome. Vector purification was carried out using iodaxinol gradient ultracentrifugation protocol, buffer exchange and concentration using vivaspin2 100 kDa molecular weight cut-off (MWCO) centrifugation columns (F-2731-100 Bioexpress, Kaysville, UT, USA). Vector genome (vg) titers were obtained by quantitative PCR (Lightcycler® 480, Roche Applied Sciences, Pleasanton, CA) using primers designed to selectively bind AAV2 ITRs (forward, 5'- AAC ATG CTA CGC AGA GAG GGA GTG G -3'; reverse, 5'- CAT GAG ACA AGG AAC CCC TAG TGA TGG AG -3') (IDT Technologies, Ames, IA).

Intracerebroventricular (ICV) administration. Animal experiments reported in this study were conducted with Balb/C or C57/Bl6 mice bred and maintained in accordance to NIH guideline as approved by the UNC Institutional Animal Care and Use Committee (IACUC). Postnatal day 0 (P0) Balb/c pups which were rapidly anesthetized on ice for 2 min followed by stereotaxic intracerebroventricular (ICV) injections. Specifically, AAV9 or AAV2g9 vectors packaging different transgenes were injected into the left lateral ventricle (total volume <3 µl) using a Hamilton 700 series syringe with a 26s gauge needle (Sigma-Aldrich, St. Louis, MO), attached to a KOPF-900 small animal stereotaxic instrument (KOPF instruments, Tujunga, CA). All neonatal injections were performed 0.5mm relative to the sagittal sinus, 2mm rostral to transverse sinus and 1.5mm deep. Following vector administration, mice were revived under a heat lamp and rubbed in the bedding before being placed back with the dam. 2 weeks post vector

administrations (P14) the mouse brains were harvested, post-fixed and immunostained as described in detail below. For co-administration of soluble heparin (generously provided by Dr. Jian Liu, School of Pharmacy, UNC), AAV vectors ($3.5x10^9$ vg) were mixed with 1 μg of heparin and a total volume of 2-3 μl administered per mouse for 30 min on ice prior to ICV injections in neonatal mice.

Intrathecal (IT) administration. AAV vectors were infused into the mouse intrathecal cerebrospinal fluid (CSF) space using Alzet mouse intrathecal catheter and pump (Alzet, 0007743, Durect corp. Cupertino, CA, USA). Briefly, the pumps were primed with 0.9% NaCl for ~12 hrs followed by AAV vectors. 8 week old C57/Bl6 males were anesthetized with intraperitoneal injection of Avertin (1.25%, 2,2,2-tribromoethanol in PBS) at 0.23 ml/10 g body weight prior to infusions. A 23 gauge needled was used to expose the L5-L6 intervertebral space and the osmotic pump was implanted and sutured under the skin. The vector was then infused at the rate of ~8 μl/hr for ~24 hours to infuse a total $1x10^{11}$ vg of AAV9 and AAV2g9 vectors packaging the CBh-ScGFP transgene. 3 weeks post administration of the vectors, the mice were sacrificed, post-fixed in paraformaldehyde, sectioned and immunostained as described below. Another cohort of 8 week old Balb/C mice was injected via IT bolus injections with AAV9 and AAV2g9 vectors as described elsewhere (256). Briefly, equal titers of vectors packaging the CBA-Luc transgene cassette (total volume 4-5 μl) was free-hand injected into the L5 and L6 intervertebral space. The injections were carried out an angle of 20-30 degrees from spinal column using the 30G disposable needle attached to 50 μl Luer-hub Hamilton syringe (Sigma-Aldrich, St. Louis, MO).

Vector genome biodistribution and pharmacokinetic analyses. Cohorts of neonatal and adult mice used for biodistribution studies were sacrificed 3 days post vector administration via the ICV or IT bolus routes. The genomic DNA was extracted from the tissue lysates and blood using the DNeasy® kit (Qiagen, Valencia, CA). To calculate viral genome copy numbers QPCR was performed with primers specific to luciferase transgene 5'-AAAAGCACTCTGATTGACAAATAC-3' and 5'-CCTTCGCTTCAAAAAATGGAAC-3'. The vector genome copy numbers were normalized to mouse lamin B2 locus as the housekeeping gene using the primers 5'-GGACCCAAGGACTACCTCAAGGG-3' and 5'- AGGGCACCTCCATCTCGGAAAC-3'. The vector biodistribution was represented as the ratio of vector genomes per cell recovered in the peripheral organs to the CNS site of injection (brain or the spinal cord). For pharmacokinetic studies, the vector genome copy numbers were calculated from total DNA isolated from 10 μl blood.

Tissue processing, immunofluorescence and confocal microscopy. Neonatal and adult mouse cohorts were sacrificed 2 weeks and 3 weeks post vector administrations respectively. The mice were overdosed with tribromoethanol (avertin) (0.2 ml/10 g of 1.25% solution) via the intraperitoneal route. This was followed by transcardial perfusions of PBS and 4% paraformaldehyde in PBS. The organs were removed and post-fixed for 24 hr prior to sectioning. Briefly, 50 μm thick sections were obtained using a Leica VT 1200S vibrating blade microtome (Leica Biosystems, IL). The spinal cords were cryo-sectioned by UNC animal histopathology core. The sections of

mouse organs from various treatments were blocked in 10% goat serum (Sigma-Aldrich, St. Louis, MO) and 1% Triton X (Sigma-Aldrich, St. Louis, MO) in PBS for 1 hr. This was followed by overnight incubation with primary monoclonal antibodies at 4˚C. The primary antibodies utilized as a part of this study are as follows: Rabbit anti-GFP (Life-Technologies- G10362, 1:750) mouse anti-GFAP (Abcam-10062, 1:1000), rabbit anti-NeuN (Abcam-104225, 1:750), chicken anti-GFP (Abcam-13970 1:750). Secondary antibodies were raised in goats and conjugated to Alexa 488 (anti-rabbit Abcam-96883, anti-chicken Abcam-96947), Alexa 594 (anti-Rabbit Abcam-96885) or Alexa 647 (anti-mouse Abcam-150115). The secondary antibodies were used at a standard dilution of 1:500. The immunohistochemical analyses of GFP expression was conducted using Vectastain ABC kit (Rabbit IgG PK-4001 kit, Vector biolabs, Burlingame, CA, USA). We used Zeiss CLSM 700 confocal laser scanning microscope for imaging sections of different organs after immunostaining (Microscopy services laboratory, UNC). The images were stitched, pseudocolored and analyzed on the Zen® Black software.

GuideRNA (gRNA) design. Two gRNAs were designed to detect 98bp Pre-miR137 flanking region and analyzed by COSMID (crispr.bme.gatech.edu) to check potential off-target sites (257). Target sequencing used to make the gRNAs are following: mir-137-g1; CGTCACCGAAGAGAGTCAG, mir-137-g3; GTAGTCGAGGAGAGTACCAG. For control gRNA, we used a 20bp sequence, which recognizes an unspecific backbone region of plasmid DNA (Con-g1; GTCGACTCTAGAGGATCCAC). Tandem repeat of U6 promoter-target sequence-

guideRNA is conjugated with EF1core promoter-tdTomato-P2A-PuroR and subcloned into the pTR vector for packaging into AAV.

Droplet digital PCR (ddPCR). PureLink Genomic DNA extraction kit (Thermo Fisher Scientific, K182002) was used to obtain DNA from brain and liver tissues. Following sequences of primers and probes were used for the ddPCR assay. Mmir137L206ddPCR; GCAGCAGTGACAGCGGTAGC, Mmir137R206ddPCR; TGGCAACCGGGAGCTTTTAG, Mmir137MTFAMddPCR; /56-FAM/TCCACCCAA/ZEN/GAATACCCGTCACCG/3IABkFQ/, Mmir137WTHEXddPCR; /5HEX/CCCTCCCAG/ZEN/CCCACCAGCTG/3IABkFQ/
For ddPCR, 2x ddPCR Supermix for Probes (No dUTP; Bio-rad, 1863023), the QX100 Droplet generator and reader (Bio-rad) were employed. 10ng genomic DNAs were subjected to PCR amplification by C1000 thermal cycler (Bio-rad) with the following condition: 95°C 10 min x1, (4°C 30 sec, 65°C 1 min)x40, 98°C 10 minx1; 2°C/sec. Obtained data was analyzed by the QuantaSoft software (Bio-rad).

3.4 RESULTS AND DISCUSSIONS

AAV2g9 and AAV9 display similar spread and transduction efficiencies in the CNS. We first carried out neonatal (P0) mouse intracerebroventricular injections (ICV) comparing AAV2g9 and AAV9 vectors packaging a self-complementary GFP (ScGFP) cassette driven by the ubiquitous chicken β actin hybrid (CBh) promoter. At 2 weeks post administration ($3.5x10^9$ vector genomes (vg)/mouse), diaminobenzidine (DAB) immunohistochemistry and confocal microscopy analysis of post-fixed mouse

brain sections revealed extensive GFP expression across multiple sections in the rostrocaudal axis of the mouse brain for both AAV strains (**Fig. 11A**). Specifically, we observed robust transduction in the olfactory bulb, striatum, hippocampus and cortical regions of the mouse brain. To further compare cellular transduction profiles of the two vectors, we generated higher magnification confocal micrographs of functionally relevant regions of the brain including the cortex, amygdala, hypothalamus and hippocampus. Mice injected with AAV9 or AAV2g9 showed comparably robust GFP expression in these regions (**Fig. 11B**). Additionally, we observed that while AAV9 treatment resulted in GFP+ cells with neuronal or glial morphology, AAV2g9 mediated GFP expression was mostly restricted to neurons. We further validated this observation using immune co-localization with the neuronal antigen marker, NeuN or glial fibrillary acid protein marker, GFAP. These results were further confirmed upon quantitation, which revealed a ~4 fold reduction in GFP+ cells with glial morphology for AAV2g9, but no significant differences between the two vectors in neuronal populations (**Fig. 13A, B**). Taken together, these results suggest that AAV2g9 spreads efficiently across the neonatal mouse brain, while demonstrating a robust and neurotropic transduction profile from a single unilateral ICV injection.

AAV2g9 and AAV9 display different cell-type specificities in the CNS. We then generated AAV9 and AAV2g9 vectors packaging single-stranded (ss) GFP cassettes driven by the neuron-specific human synapsin I (hSyn) or the glia-specific glial fibrillary acid protein (GFAP) promoter. Vectors ($3.5x10^9$ vg/mouse) were administered in postnatal day 0 (P0) mice via the ICV route and post-fixed brain tissues

analyzed at 2 weeks post administration by diaminobenzidine (DAB) immunohistochemistry, immunostaining and confocal microscopy analysis. Both AAV9 and AAV2g9 vectors packaging transgene driven by hSyn promoter displayed robust transduction across multiple sections of the mouse brain (**Fig. 12A**). Specifically, we observed GFP+ cells colocalizing with NeuN+ cells (yellow) in various regions including the striatum, cortex, hippocampus, amygdala and hypothalamus (**Fig. 12B**). As expected, no glial staining was observed for either vector supporting the potential application of such neuron-specific promoters for CNS gene therapy studies.

In contrast to hSyn promoter driven expression, we observed striking differences in the patterns of GFP expression mediated by AAV9 and AAV2g9 vectors packaging the GFAP promoter driven transgene cassette. Notably, AAV9 injections resulted in widespread GFP expression in cells with glial morphology across the entire brain parenchyma in multiple brain sections (**Fig. 12C**). In contrast, mice injected with AAV2g9 exhibit spatially restricted GFP expression within close proximity of the site of cerebrospinal fluid (CSF) injection (lateral ventricles) or along the immediate point of contact between the CSF and brain parenchyma, the inner meninges. To further confirm these observations, we co-immunostained different sections of the mouse brain for GFP expression (green) with neuronal marker-NeuN or glial marker-GFAP (red) as before. High magnification confocal micrographs generated at different brain regions show robust GFP+ expression from AAV9 injections in GFAP+ cells, but not NeuN+ cells (**Fig. 12D**). These observed patterns of transgene expression were further confirmed by quantitative analysis, which revealed ~2.5 fold reduction in glial transduced area throughout the brain with AAV2g9 vectors under GFAP promoter activity (**Fig. 13C, D**).

These results demonstrate for the first time that AAV9 vectors packaging GFAP promoter driven expression cassettes are excellent candidates for glial gene transfer applications, while AAV2g9 appears to more neurotropic and hence suitable for CNS gene transfer applications targeting neuronal populations. From the AAV biology perspective, AAV2g9 appears to preferentially transduce neurons over glia, while this is patently not the case with AAV9.

Heparan sulfate interactions are critical towards preferential neuronal transduction by AAV2g9 vectors. The interaction of AAV2 vectors with heparan sulfate (HS) proteoglycans is associated with preferential neuronal transduction in the immediate vicinity to site of CNS administration (71, 89). Co-administration of soluble heparin has been shown to block the ability of AAV2 to bind hep and alter transduction profiles *in vitro* and *in vivo* (35, 47, 48). Therefore, we compared the CNS transduction profiles of AAV2 and AAV2g9 to co-injections of AAV2g9 with 1 μg of soluble heparin in the neonatal mouse brain. Further, we generated a hep binding mutant, AAV2i8g9, as described in earlier studies by our lab (206). Specifically, we injected equal viral titers ($3.5x10^9$ vg) of AAV2, AAV2g9, AAV2g9 + soluble heparin or AAV2i8g9 packaging CBh-ScGFP transgene via the ICV route in P0 mice. As shown in **Fig. 14A**, we observed a low level of GFP+ expression as evidenced by DAB immunostaining within the hippocampal sections of AAV2 injected mouse brains. Consistent with earlier results, AAV2g9 displayed robust and widespread CNS transgene expression supporting the notion that the gal footprint enhances transduction efficiency and spread. Further, we observed a decrease in GFP+ expression across the brain parenchyma in AAV2g9 +

soluble heparin treated animals as well as AAV2i8g9 treated mouse cohorts in comparison with AAV2g9 (**Fig. 14B-D**).

High magnification confocal micrographs of multiple regions of the mouse brain, namely; the somatosensory cortex (SCT), piriform cortex (PCT), motor cortex (MCT), dentate gyrus (DG), amygdala (AMG) and hippocampal CA1, CA2 and CA3 regions were then generated. As seen in the top panel of **Fig. 14E**, we observed sporadic expression in neurons and astrocytes in case of AAV2-injected mice. On the other hand, extensive and preferential neuronal transduction was observed across these regions in case of AAV2g9 as observed earlier (**Fig. 14E**, second row panel). In contrast, loss of hep binding, either by competitive inhibition with soluble heparin or with the AAV2i8g9 mutant resulted in a decreased neuronal transduction in multiple brain regions (third row and bottom row panels, **Fig. 14E**). In addition, loss of neuronal transduction was accompanied by an increase in GFP+ cells with glial (astrocytic) morphology in these cohorts. Taken together, our observations suggest that hep binding is critical in determining the preferential neuronal tropism displayed by AAV2g9.

Galactose (gal) binding enhances CNS transduction of AAV vectors independent of heparan sulfate (hep) binding interactions. The exact mechanisms by which AAV9 exploits its primary receptor, gal (37) for CNS transduction are yet to be determined. We have previously shown that a single point mutation on the VP3 region of the AAV9 capsid (W503R) dramatically alters the systemic tropism of the virus by disrupting the gal footprint (255, 258). To this end, we compared transduction profiles of AAV9 and AAV9W503R packaging CBA-TdTomato (TdTom) fluorescent reporter

transgene ($3.5x10^9$ vg) in P0 mice via the ICV route. Two weeks post injections; mice were sacrificed, fixed and subjected to confocal analysis for TdTom expression. As shown in **Fig. 15**, AAV9-CBA-TdTom (left column) injected mouse brains exhibit robust TdTom+ transgene expression (pseudocolored white) across multiple regions of the mouse brain, namely: olfactory bulb, cortex, sub-ependymal zone, hippocampus and cerebellum. On the other hand, we observed a complete loss of TdTom+ expression in the mouse brain injected with AAV9W503R-CBA-TdTom (**Fig. 15**, right column). This result demonstrates the critical role played by gal in mediating the CNS transduction of AAV9. A single point mutation attenuating gal interactions (258, 259) on the AAV9 capsid protein results in a loss of function phenotype within the CNS.

To further demonstrate the distinct role played by hep and gal in CNS transduction by different AAV strains, we engineered the gal footprint (206) onto the primate isolate, AAV8 (244). Unlike AAV2, AAV8 does not engage hep as the cellular attachment receptor (260). Specifically, we injected equal titers ($3.5x10^9$ vg) of AAV8 or AAV8g9 packaging the CBh-ScGFP transgene in P0 mice via the ICV route. At 2 weeks post vector administration; brains and spinal cords were harvested from the mouse cohorts and subjected to immunostaining and confocal analysis. As shown in **Fig. 16A**, we observed that AAV8g9 injected mice showed enhanced spread and efficiency of GFP+ transgene expression within multiple sections of the mouse CNS. Further co-immunostaining with neuronal and glial cellular markers (i.e., NeuN and GFAP, respectively) showed that cellular tropisms were unaltered with no preferential transduction of either neurons or astrocytes by both AAV8 and AAV8g9 (**Fig. 16B**). These results indirectly support the notion that the robust CNS transduction profile is

independent of hep binding. More importantly, these results further corroborate the notion that gal binding ability can enhance both CNS transduction efficiency and spread without altering the endogenous cellular tropism displayed by a particular AAV capsid (natural or engineered).

AAV2g9 and AAV9 display similar transduction profiles in adult mice after intrathecal administration. To compare the two strains in adult mice, we carried out intrathecal (IT) infusions of AAV9 or AAV2g9 packaging CBh-ScGFP reporter transgene into the lumbar CSF space of 8 week old mice. At 3 weeks post administration of $1x10^{11}$ vg/mouse, we subjected postfixed tissues to immunohistochemical analyses and confocal imaging as outlined in online methods. As shown in **Fig. 17A**, IT infusions of both AAV9 and AAV2g9 resulted in strong transgene expression in the lumbar, thoracic and cervical spinal cord regions. Of note, we observed GFP expression in multiple gray and white matter regions of the spinal cord. Further, we compared cellular transduction profiles resulting from IT infusions of AAV9/2g9 vectors. Specifically, we focused on different regions of the adult CNS, namely: ventral horn (VH), dorsal horn (DH), intermediate gray matter region (INT), ventral funiculus (VF), lateral funiculus (LF), ventral commissure (VC), and rubrospinal tract (RT). As shown in **Fig. 17B**, both AAV2g9 and AAV9 infused mice exhibit robust GFP expression in these regions of the spinal cord. In both AAV9 and AAV2g9 injected mice, we observed that the GFP+ cells (green) in the gray matter regions of the spinal cord (VH, DH and INT) extensively colocalized with NeuN+ as well as GFAP+ cells. Within the white matter regions of spinal cord (VF, LF, VCOM and RT), the GFP+ (green) cells from either injection

extensively colocalized with GFAP+ cells (**Fig. 17B**). Importantly, these observations also underscore the potential influence of route of injection on the cellular tropism of different AAV vectors.

AAV2g9 and AAV9 display distinct systemic biodistribution and off-target transduction profiles following CNS administration. Having established the robustness of the rationally engineered AAV2g9 strain, we compared the systemic leakage, vg biodistribution and gene expression profiles in peripheral organs resulting from ICV or IT injections of AAV9 and AAV2g9 in both neonatal and adult mice. At 3 days post-administration, we extracted whole genomic DNA from different organs and determined vg copies using qPCR in different peripheral organs including the liver, heart and spleen. We observed a striking difference between the off-target biodistribution profiles of AAV9 and AAV2g9 vectors following ICV or IT injections. As seen in **Fig. 18A-C**, in the AAV9 injected neonatal mouse cohort, ~40%, 30% and 3% of the viral genomes were recovered from the liver, heart and spleen, respectively, in comparison with the brain (normalized to 100%). In contrast, AAV2g9 vg copy numbers ranged from ~1.4%. 0.7% and 0.003% in these peripheral organs. In the adult mouse cohort, AAV9 vg copies recovered in the liver, heart and spleen were 188%, 81% and 59%, respectively in comparison with vg copies recovered from the spinal cord (normalized to 100%). In contrast, only ~3%, 4.5% and 10% of vg copies were recovered from these systemic organs in the AAV2g9 treated cohort (**Fig. 18E-G**). These results suggest that unlike AAV9, AAV2g9 is sparingly sequestered in off-target, systemic organs following CNS administration.

To further corroborate the biodistribution results, we harvested different peripheral organs from the ICV and IT mouse cohorts treated with either AAV2g9 or AAV9 and subjected post-fixed tissue to immunostaining and confocal imaging analysis as outlined earlier. We observed robust GFP expression in the heart, liver and spleen of both neonatal (ICV) (**Fig. 18D**) and adult (IT) (**Fig. 18H**) mice treated with AAV9. Consistent with biodistribution data, AAV2g9 treated mice exhibit near background levels of GFP expression in both ICV and IT cohorts. Together, these results are also consistent with the reduced leakage of AAV2g9 vectors (>100 fold) into the blood circulation that was observed in comparison to AAV9 vectors (**Fig. 19**). Briefly, AAV9 vector genomes were observed in blood as early as 15 min post-administration and continued to decline over two days. These results are consistent with earlier studies reported by our lab and others (258, 261). In contrast, AAV2g9 vector genomes remained near background levels with a slight increase in copy number observed at the 24 hr and 48 hr time intervals. Together, our results confirm that unlike AAV9, AAV2g9 undergoes significantly reduced systemic leakage following CNS administration and consequently displays low levels of sequestration and transgene expression in peripheral organs.

Brain-restricted deletion of MIR 137 gene using AAV2g9 in CRISPR-Cas9 knock-in mice. We have established that CNS administration of AAV2g9 results in limited systemic exposure and efficient gene transfer within the neural tissue. To demonstrate application of this unique property, we produced AAV2g9 vectors packaging two gRNAs for targeted disruption of the MIR 137 gene in the brain.

Specifically, the gRNAs were designed to recognize both ends of the 85bp pre-miR137 region. Equal titers of AAV2g9 packaging miR137gRNA or controlgRNA were injected into Cas9 transgenic mice (222) via unilateral ICV route. 2 weeks post vector administration the mice were sacrificed and organs were harvested. The brain and liver tissues were subject to genomic DNA extraction. To evaluate gene disruption events, we utilized the droplet digital PCR technique. Briefly, primers were designed to amplify 206 bp mouse genomic region flanking the miR137 target locus. Fluorescent probes were designed to bind miR137gRNA target region (FAM, red) and an unspecific downstream locus (HEX, green). Successful disruption of miR137 locus results in exclusive excitation of HEX probe alone (green). Whereas both FAM and HEX probes are excited (orange) in case of no gene disruption events (**Fig. 20A**). First, we evaluated AAV2g9 vector genome biodistribution by performing QPCR on genomic DNA samples obtained from brain and liver tissues of the injected mice. We observed significant enrichment of AAV genomes within the brain as compared to the systemic liver tissue (**Fig. 20B**). Next, droplet digital PCR analysis revealed that the frequency of miR137 eliminated alleles was significantly higher (green dots) in mice that received AAV2g9-miR137gRNA, as compared to AAV2g9-controlgRNA cohort (**Fig. 20C, red arrow**). Correspondingly, quantitative analysis of this phenomenon demonstrated a significant increase in mutant allele frequency within the miR137gRNA injected mouse brains (**Fig. 20D**).

Next, we examined if the gene disruption events were specific to the brain. Identical ddPCR analysis conducted on liver DNA extracted from the same mouse cohorts displayed near background levels of miR137 elimination in the systemic organ

(**Fig. 20E**). Further quantitation demonstrated negligible mutant allele formation due to both AAV2g9-controlgRNA and AAV2g9-miR137gRNA injections in the liver (**Fig. 20F**). Overall, our data demonstrates CNS-restricted gene disruption within the Cas9 transgenic mouse using ICV administration of engineered AAV2g9 vector.

Micro RNAs (miRNAs) are one of the largest species of non-coding RNAs that employ post-transcriptional silencing mechanisms to control ~60% of host gene expression (262). Majority of miRNA expression occurs in the CNS where gene regulatory mechanisms within neuronal subpopulations orchestrate states of normalcy and disease (263). Large scale GWAS studies conducted across ~40,000 patients recently led to the identification of disruption in MIR 137 gene function to have a strong correlation with the SZ disease occurrence (248, 264). It is well known that establishing a CNS-specific gene delivery system is crucial for developing gene therapy strategies and generating disease models of neurological disorders. As miR137 and CAG promoter driven Cas9 are both expressed in brain and liver tissue (222, 247), it is safe to assume that the brain specific miR137 elimination relies on AAV2g9 vector design. To our knowledge, this is the first example of CNS-specific gene disruption using an engineered AAV vector.

Although we successfully demonstrate CNS-restricted gene disruption in this study, certain caveats are noteworthy and need to be addressed by future studies. For instance, we achieved a modest ~5% frequency of MIR 137 elimination within the AAV2g9-miR137gRNA injected Cas9 transgenic mouse brain. It is intriguing to speculate that the Cas9 expression within the mouse brain could be mosaic, resulting in a smaller subset of CNS cells capable of undergoing CRISPR mediated gene

disruption. Moving forward, it is important to evaluate the percentage of cells expressing Cas9 within the mouse brain. Additionally, in the current study we utilized rAAV vectors packaging single stranded DNA genomes. Packaging the gRNA constructs into a self-complementary AAV cassette can possibly enhance the gene transfer efficiency and subsequently elevate MIR 137 gene disruption frequency.

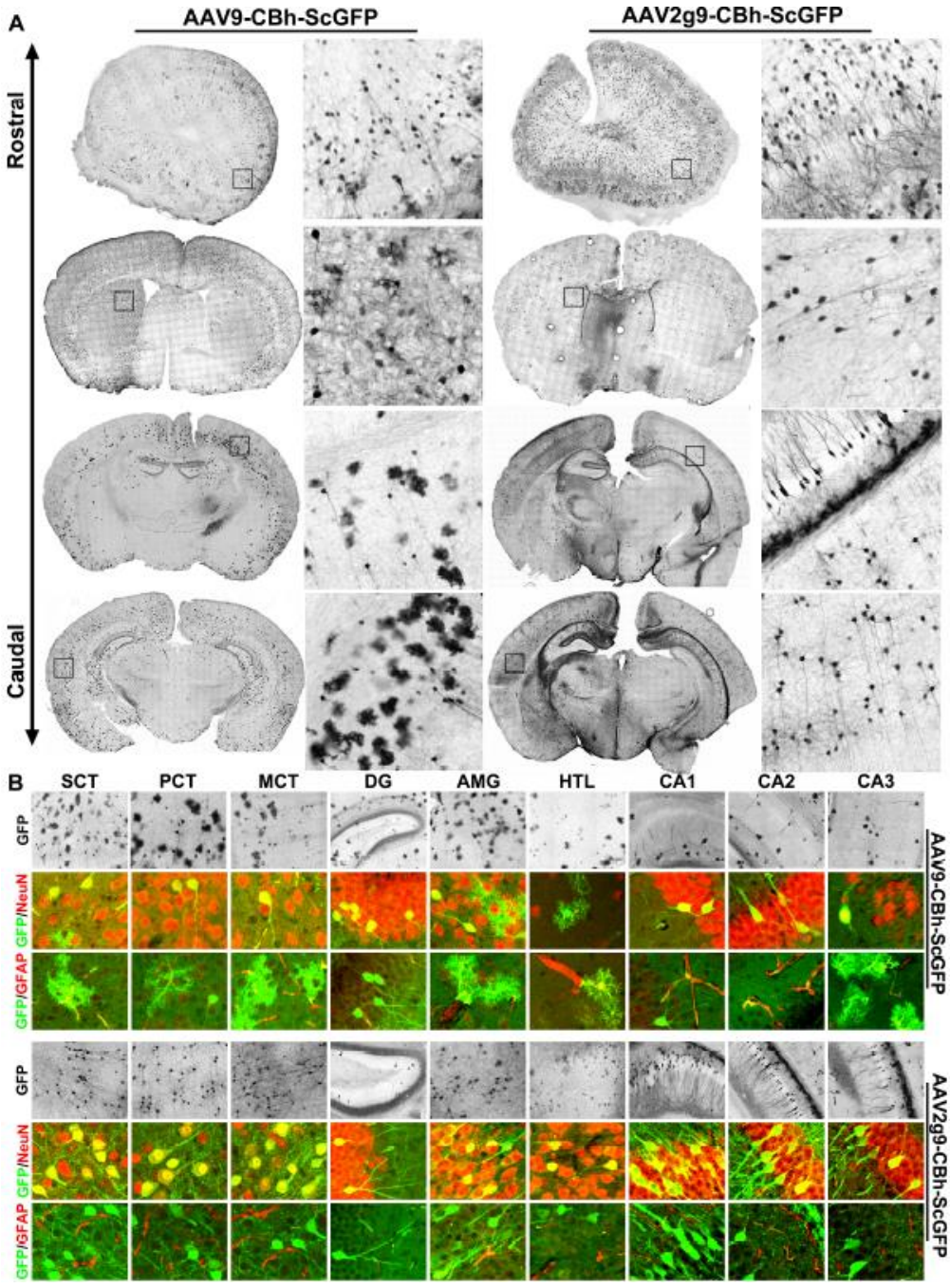

Figure 11. Comparison of transgene (GFP) expression and cellular tropisms displayed by AAV9 and AAV2g9 vectors with a ubiquitous promoter after ventricular (ICV) injection. Postnatal day 0 (P0) mice were injected with equal viral titers ($3.5x10^9$ vg) of AAV9 or AAV2g9 packaging a ScGFP transgene driven by a ubiquitous chicken β hybrid (CBh) promoter into the left lateral ventricle. At 2 weeks post vector administration, the mice were sacrificed and paraformaldehyde postfixed brains were sectioned and immunostained as described earlier. **(A)** Representative images of coronal sections obtained from olfactory bulbs, lateral ventricles and

hippocampi are shown. Inset images from whole brain sections are shown to the right of each section at higher magnification. **(B)** Top image panel shows higher magnification images of DAB staining (GFP expression) in functionally relevant regions of the mouse brain namely; somatosensory cortex (SCT), piriform (PCT), motor CT (MCT), dentate gyrus (DG), amygdala (AMG), hypothalamus (HTL) and hippocampal CA1, CA2 and CA3 are shown. Middle and bottom panels show immuno-colocalization of GFP expression (green) with neuronal marker, NeuN or glial marker, GFAP (red). All experiments were conducted in triplicate and representative images are shown.

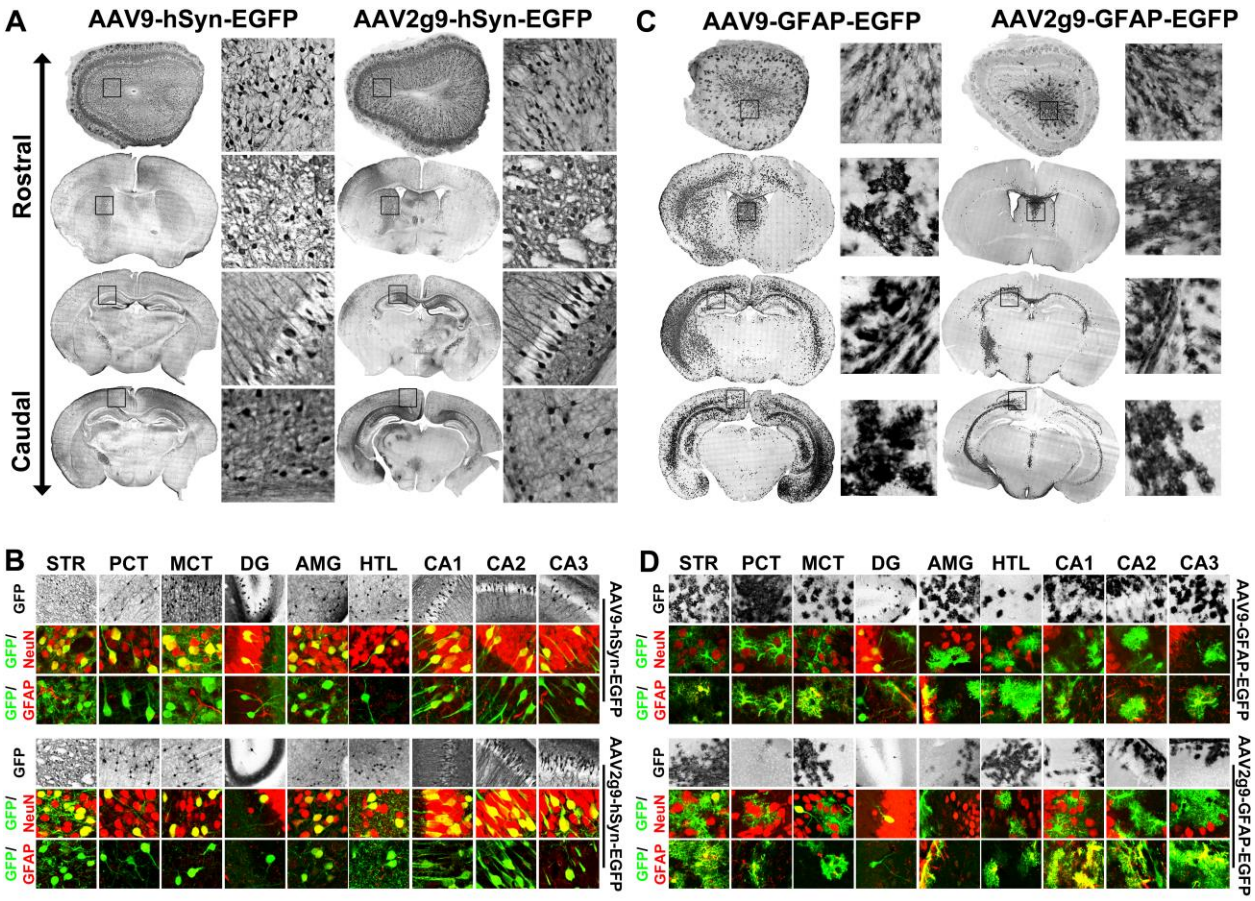

Figure 12. Comparison of transgene (GFP) expression and cellular tropisms displayed by AAV9 and AAV2g9 vectors with cell type-specific promoters after ventricular (ICV) injection. Postnatal day 0 (P0) mice were injected with equal viral titers ($3.5x10^9$ vg) of AAV9 or AAV2g9 packaging a single-stranded GFP (ssGFP) transgene driven by the **(A,B)** hSyn promoter or the **(C,D)** GFAP promoter into the left lateral ventricle. At 2 weeks post vector administration, the mice were sacrificed and paraformaldehyde postfixed brains were sectioned and immunostained. Diaminobenzidine (DAB) immunohistochemistry was used to detect GFP expression. **(A,C)** Representative images of coronal sections obtained from olfactory bulbs, lateral ventricles and hippocampi are shown. Inset images from whole brain sections are shown to the right of each section at higher magnification. **(B,D)** Representative confocal images of coronal tissue sections at higher magnification. Top image panel shows higher magnification images of DAB staining (GFP expression) in functionally relevant regions of the mouse brain namely; Striatum (STR), piriform CT, Motor CT, dentate gyrus (DG), amygdala (AMG), hypothalamus (HTL) and hippocampal CA1, CA2 and CA3 regions are shown. Middle and bottom panels show immuno-colocalization of GFP expression (green) with neuronal marker, NeuN or glial marker, GFAP (red) obtained using a Zeiss CLSM 700 confocal laser scanning microscope. Co-localized cells are pseudocolored yellow (GFP/NeuN or GFP/GFAP overlay). All experiments were conducted in triplicate and representative images are shown.

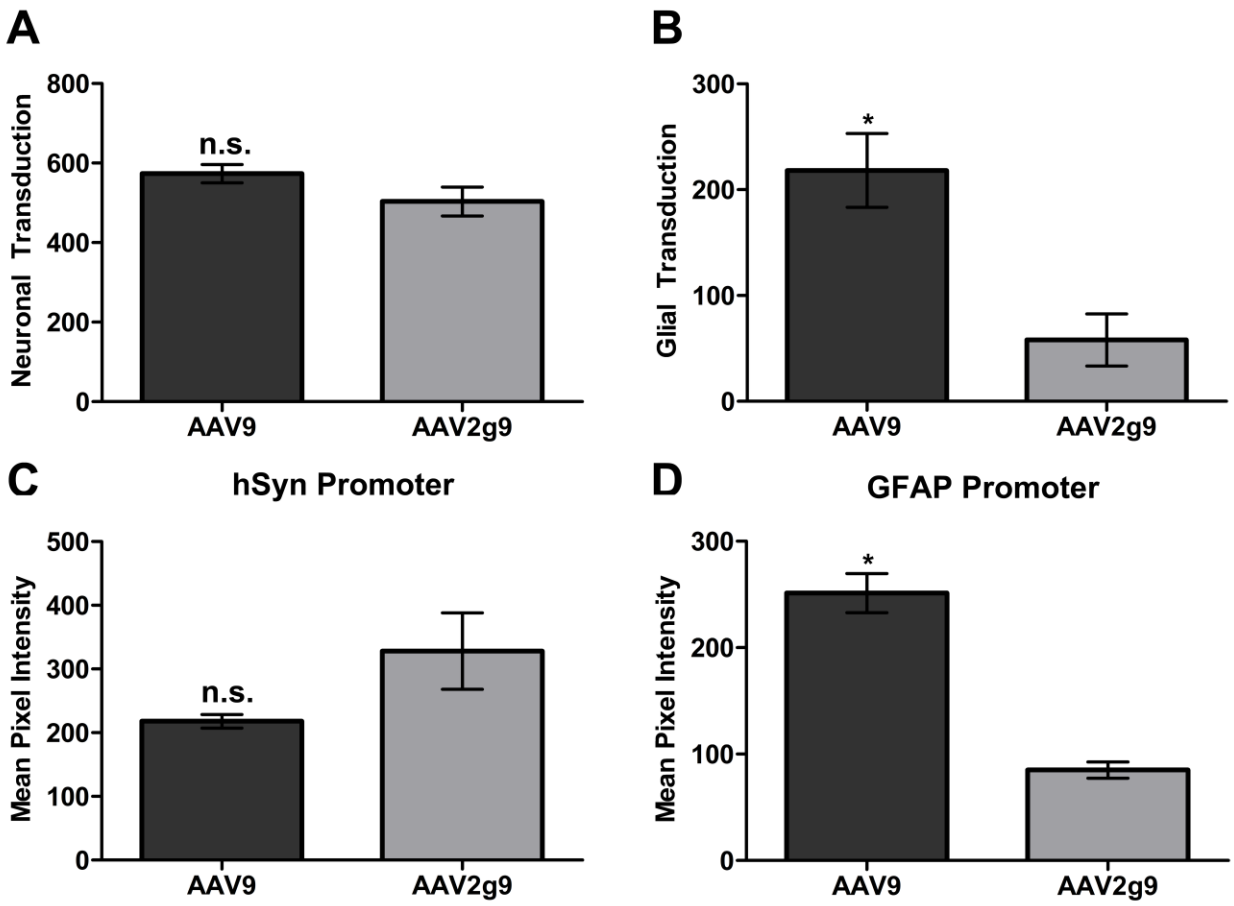

Figure 13. Quantitative assessment of transduction following ICV administration of AAV9 and AAV2g9 vectors. GFP expression was quantified in representative hippocampal sections of the mouse brains treated with AAV9 or AAV2g9 vectors. Specifically, GFP+ cells with neuronal **(A)** or glial **(B)** morphology were counted in different cortical regions including the retrosplenial, posterior parietal, somatosensory, auditory and piriform areas. Further, quantitative assessment of GFP expression following ICV administration of AAV9 and AAV2g9 vectors driven by **(C)** human synapsin (hSyn) promoter or **(D)** glial fibrillary acid protein (GFAP) promoter was carried out using ImageJ analysis software. Specifically, the mean intensity calculator function was applied across multiple sections of the mouse brain including sections of the olfactory bulbs, lateral ventricles and hippocampal regions. Data is represented as mean ± standard deviation, * represents $p<0.05$ and n.s. indicates 'not statistically significant' ($p>0.05$) as determined by student t-test. All experiments were conducted in quadruplicate.

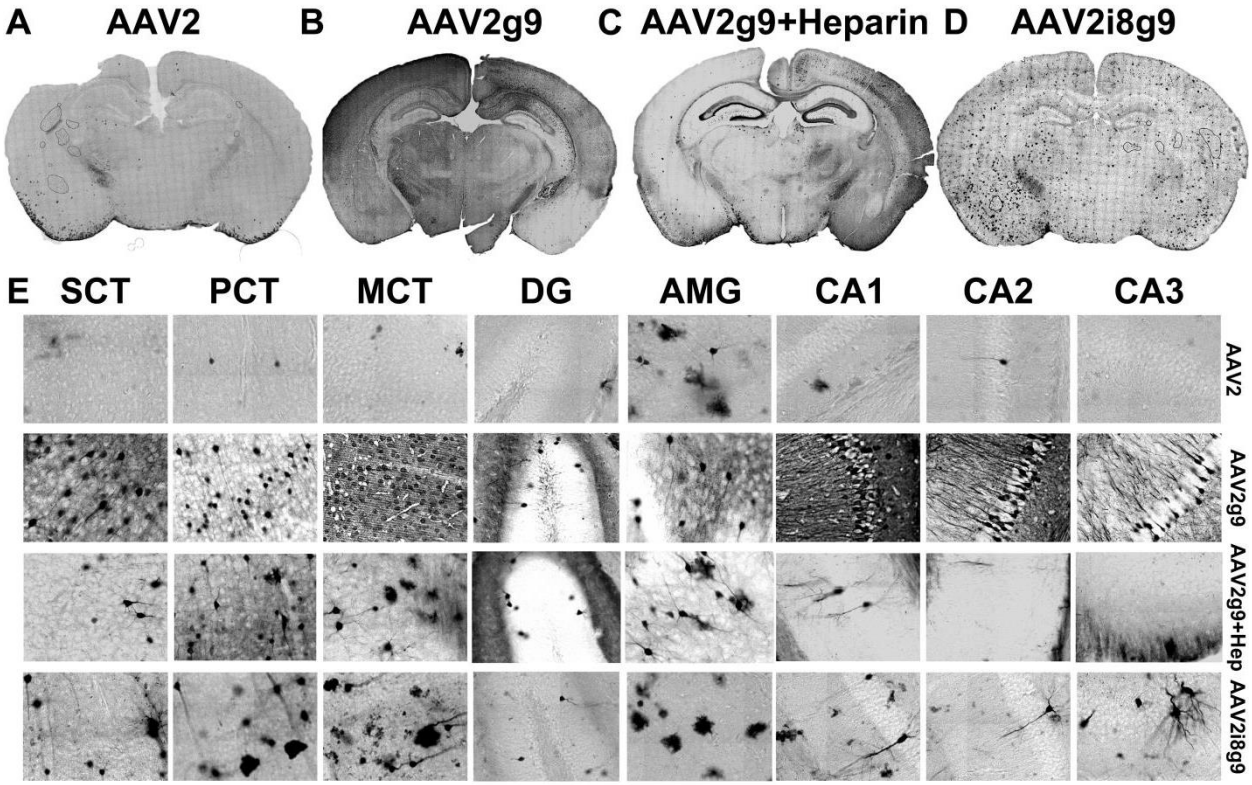

Figure 14. Heparan sulfate interactions are critical towards preferential neuronal transduction by AAV2g9 vectors. Postnatal day 0 (P0) mice were injected with equal viral titers ($3.5x10^9$ vg) of AAV2, AAV2g9 or AAV2i8g9 packaging the CBh-ScGFP transgene into the left lateral ventricle (ICV). One cohort of mice was co-injected with 1 μg soluble heparin (Hep) per mouse as indicated. 2 weeks post vector administration, the mice were sacrificed and the brains were harvested and immunostained for comparing transgene (GFP) expression (black). **(A-C)** Representative images of hippocampal sections from AAV2, AAV2g9, AAV2g9+Heparin or AAV2i8g9 injections have been shown. **(D)** Higher magnification images of GFP expression (black) in different regions of the mouse brain namely; somatosensory cortex (SCT), piriform CT, motor CT, dentate gyrus (DG), amygdala (AMG) and hippocampal CA1, CA2 and CA3 regions have been shown. The Zeiss CLSM 700 confocal laser scanning microscope was used to image stitched images of entire mouse brain and higher magnification images of individual regions. All experiments were conducted in triplicate and representative images are shown.

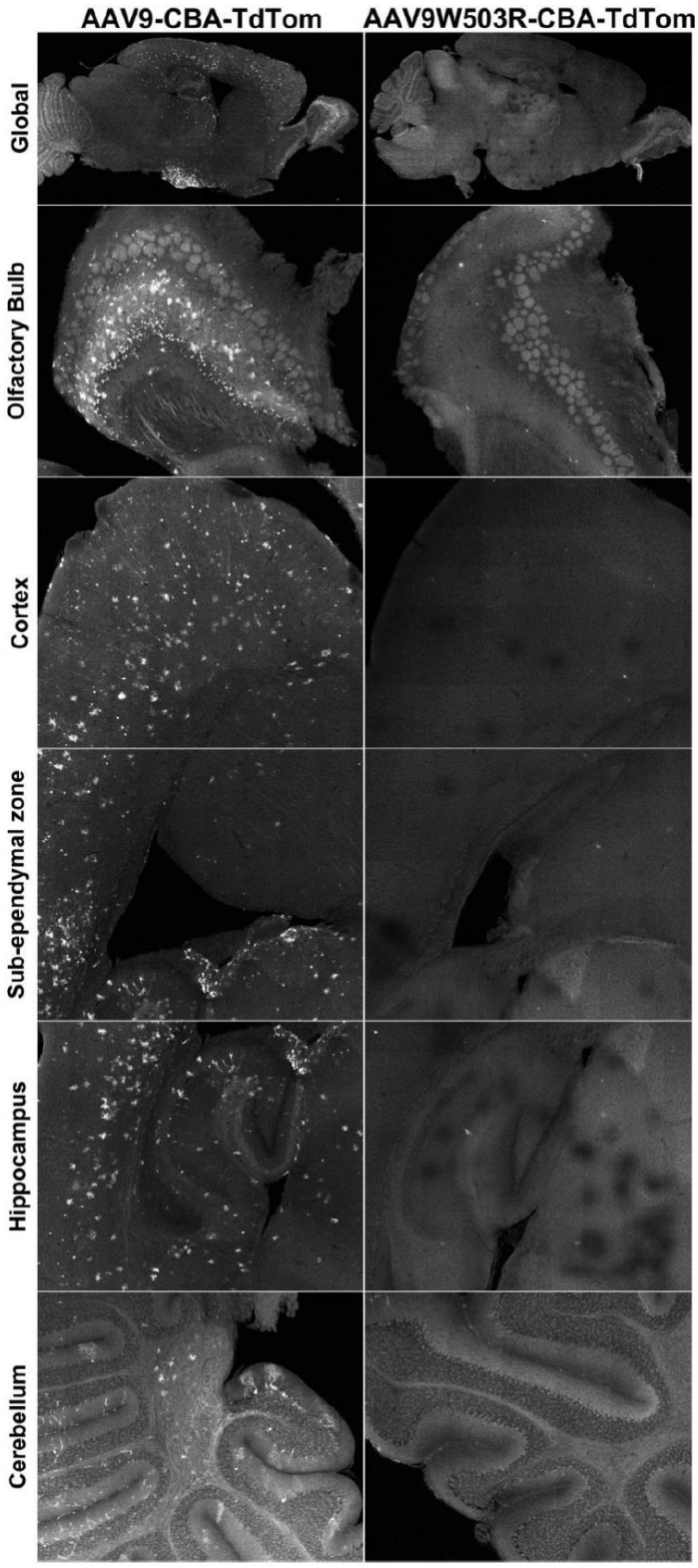

Figure 15. CNS transduction profile of a gal-binding AAV9 mutant (W503R) and AAV9 following ventricular (ICV) administration. Postnatal day 0 (P0) mice were injected with equal viral titers ($3.5x10^9$ vg) of AAV9 or AAV9W503R packaging a single-

stranded TdTomato (TdTom) fluorescent reporter transgene driven by CBA promoter into the left lateral ventricle. At 2 weeks post vector administration, the mice were sacrificed and sagittal sections were obtained from the paraformaldehyde postfixed brains. Representative confocal stitches show TdTom reporter gene expression (pseudocolored white) in the whole brain (global) and higher magnification images of individual regions (i.e. olfactory bulb, cortex, sub-ependymal zone, hippocampus and cerebellum). Zeiss CLSM 700 confocal laser scanning microscope equipped with 555nm excitation filter was used to obtain the global stitches and higher magnification images of individual regions of the mouse brain. All experiments were conducted in triplicate and representative images are shown.

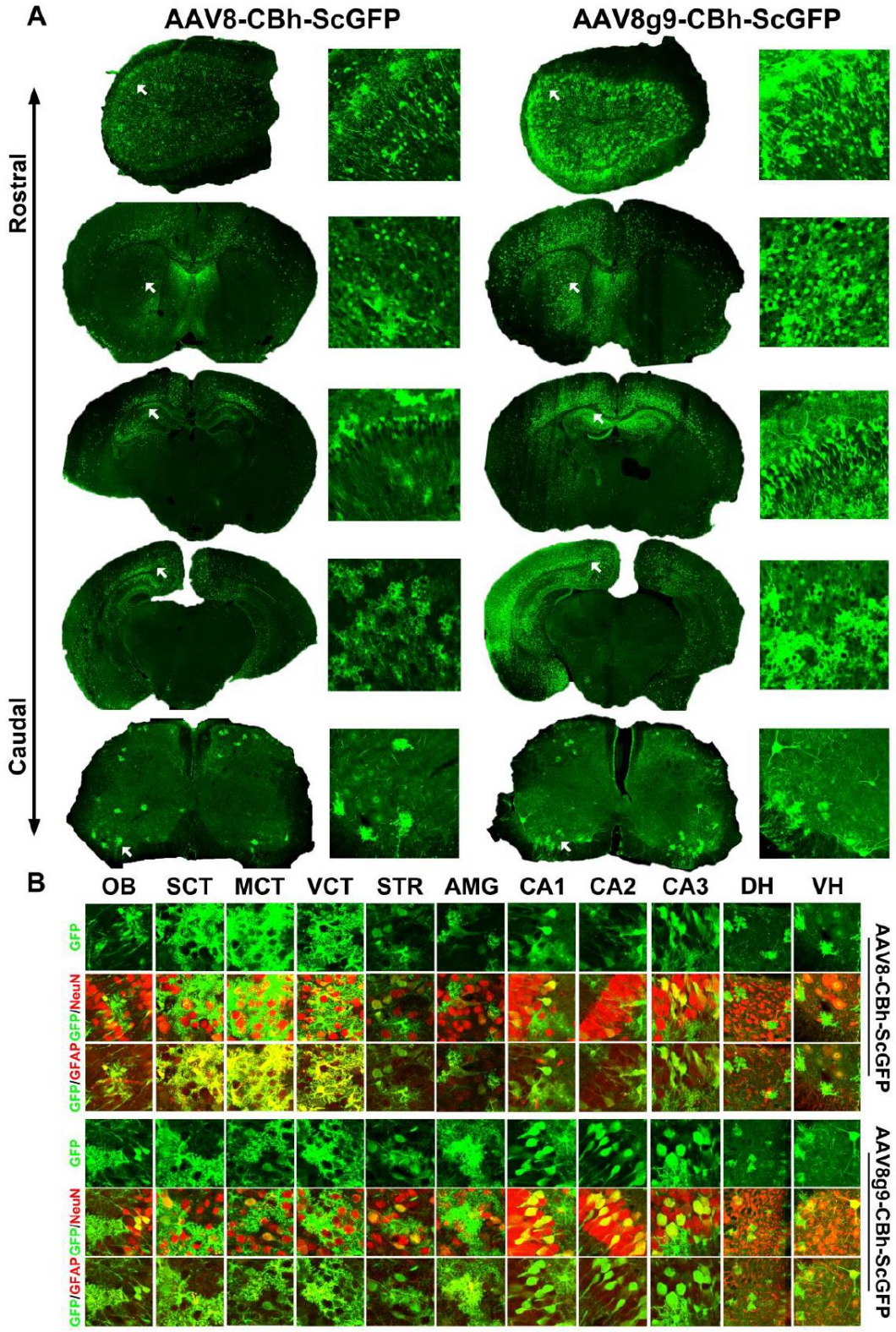

Figure 16. CNS transduction profile and cellular tropisms displayed by AAV8 and gal-binding AAV8g9 vectors following ventricular (ICV) injection. Postnatal day 0

(P0) mice were injected with equal viral titers ($3.5x10^9$ vg) of AAV8 or AAV8g9 packaging a ScGFP transgene driven by a ubiquitous chicken β hybrid (CBh) promoter into the left lateral ventricle. At 2 weeks post vector administration, the mice were sacrificed and paraformaldehyde postfixed brains were sectioned and immunostained as described earlier. **(A)** Representative images of coronal sections obtained from olfactory bulbs, lateral ventricles and hippocampi are shown. Inset images from whole brain sections (arrows) are shown to the right of each section at higher magnification. **(B)** Top image panel shows higher magnification images of GFP expression (green) in functionally relevant regions of the mouse brain namely; olfactory bulb (OB), somatosensory cortex (ss CT), motor CT (MCT), visual CT (VCT), striatum (STR), amygdala (AMG), hippocampal CA1, CA2 and CA3 of the brain and dorsal and ventral horn regions of the spinal cord are shown. Middle and bottom panels show immuno-colocalization of GFP expression (green) with neuronal marker, NeuN or glial marker, GFAP (red). All experiments were conducted in triplicate and representative images are shown.

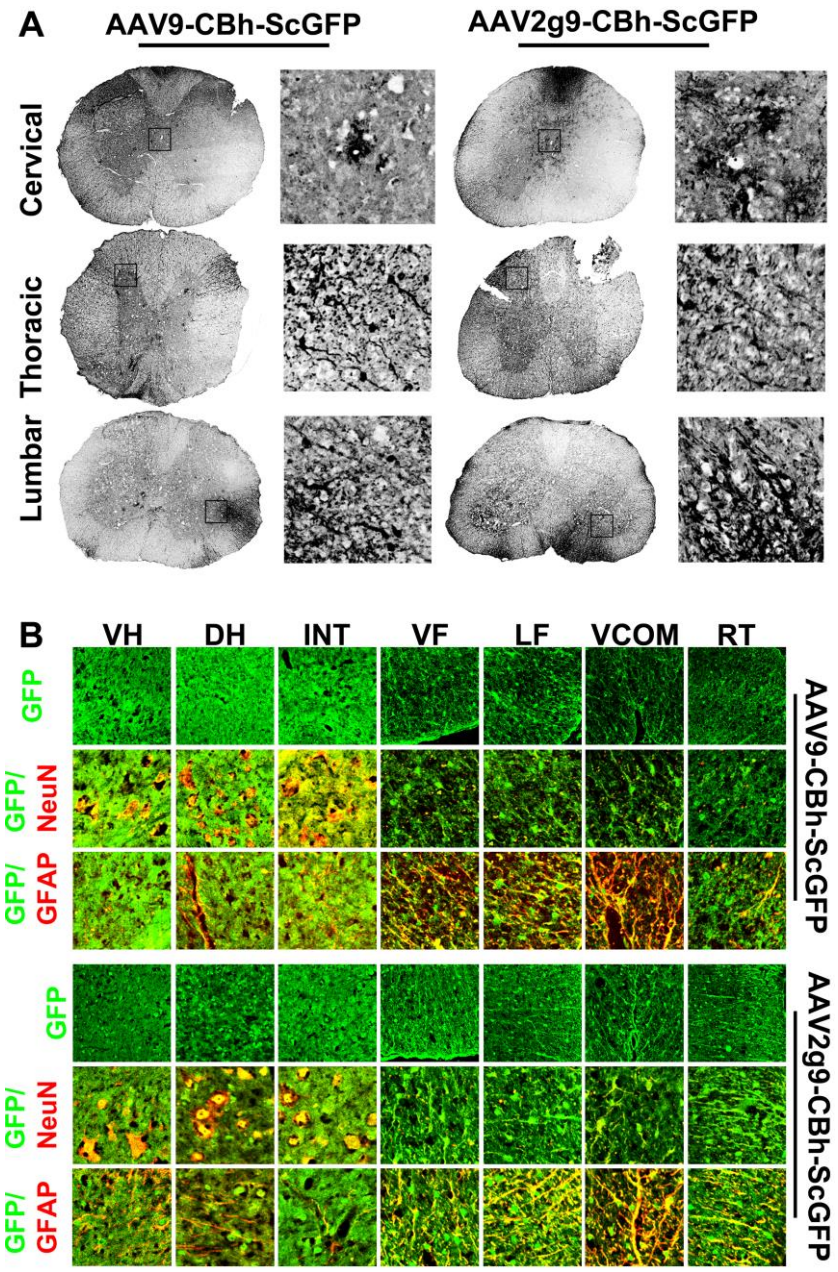

Figure 17. Comparison of transgene (GFP) expression and cellular tropism displayed by AAV9 and AAV2g9 vectors following intrathecal infusion. (A) Spinal cord sections showing cervical, thoracic and lumbar regions obtained from 8 week old adult C57/BL6 male mice infused with AAV9 or AAV2g9 packaging the CBh-ScGFP transgene ($1x10^{11}$ vg) by lumbar puncture. Mice were sacrificed and the spinal cords were postfixed in paraformaldehyde, sectioned at 3 weeks post vector administration. Diaminobenzidine (DAB) immunohistochemistry was used to detect GFP expression. Inset images from whole spinal cord cross-sections are shown to the right of each section at higher magnification**. (B)** Representative confocal images of immunostained sections at higher magnification. GFP expression (top panel, green) in the ventral horn (VH), dorsal horn (DH), intermediate zone gray matter (INT), ventral funiculus (VF),

lateral funiculus (LF), ventral commissure (VCOM) and rubrospinal tract (RT) regions is shown. Middle and bottom panels show immuno-colocalization of GFP expression (green) with neuronal marker, NeuN or glial marker, GFAP (red) obtained using a Zeiss CLSM 700 confocal laser scanning microscope equipped with 488nm, 555nm and 647nm excitation filters. Co-localized cells are pseudocolored yellow (GFP/NeuN or GFP/GFAP overlay). All experiments were conducted in triplicate and representative images are shown.

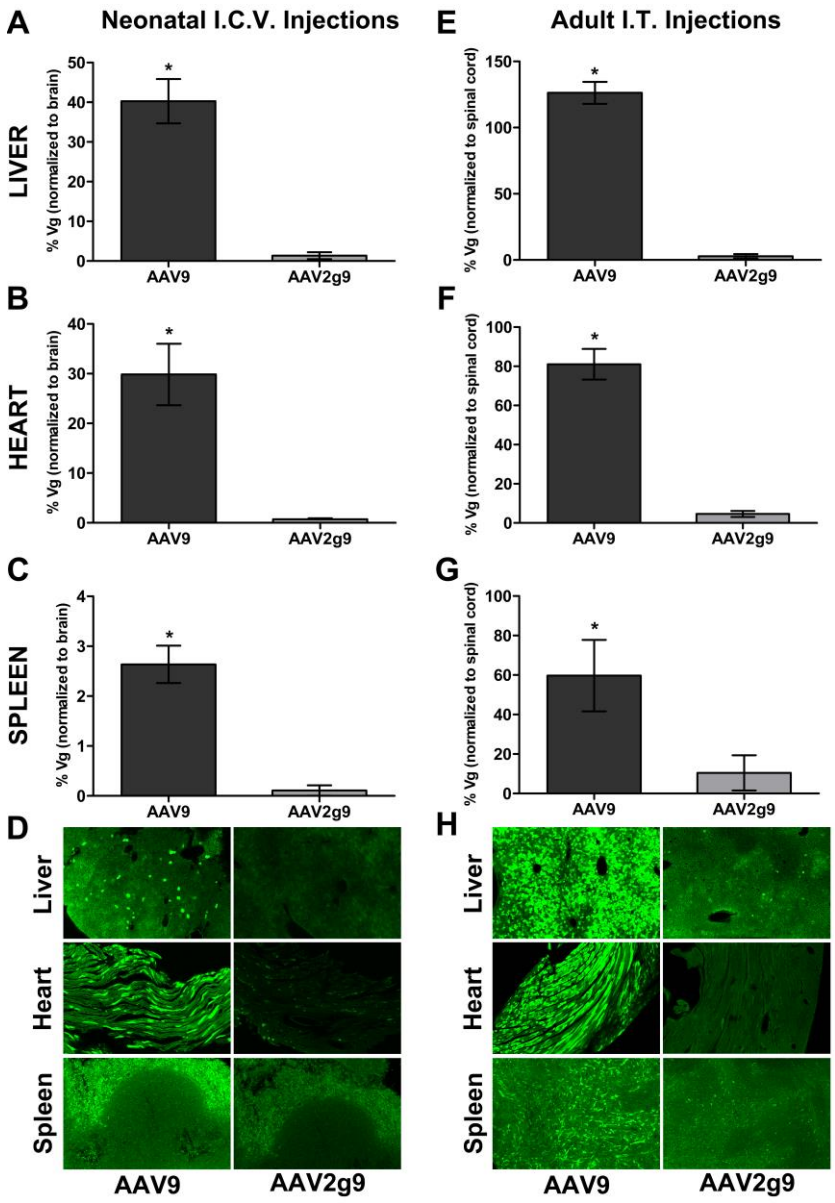

Figure 18. Comparison of systemic biodistribution and off-target transgene (GFP) expression displayed by ICV/IT injected AAV9 and AAV2g9 vectors. (A-C) Relative percentage of vector genome (vg) copy numbers for AAV9 (dark gray bars) and AAV2g9 (light gray bars) in systemic organs, i.e., liver, heart and spleen normalized to vg copy number in the brain following ICV administration in neonates. **(D)** Confocal micrographs showing GFP expression in systemic organs – liver, heart and spleen obtained from neonatal ICV cohorts. **(E-G)** Relative percentage of vector genome (vg) copy numbers for AAV9 (dark gray bars) and AAV2g9 (light gray bars) in systemic organs, i.e., liver, heart and spleen normalized to vg copy number in the spinal cord following IT administration in adult mice. **(H)** Confocal micrographs showing GFP expression in systemic organs – liver, heart and spleen obtained from adult IT cohorts. The vg copy per host genome (vg/cell) was determined by quantitative PCR of extracted DNA and normalized to the number of copies of the mouse lamin β2 gene. Data shown

is represented as mean ± standard deviation; Statistical significance (* $p<0.05$) was established using student t-test. All experiments were conducted in quadruplicate and representative images are shown.

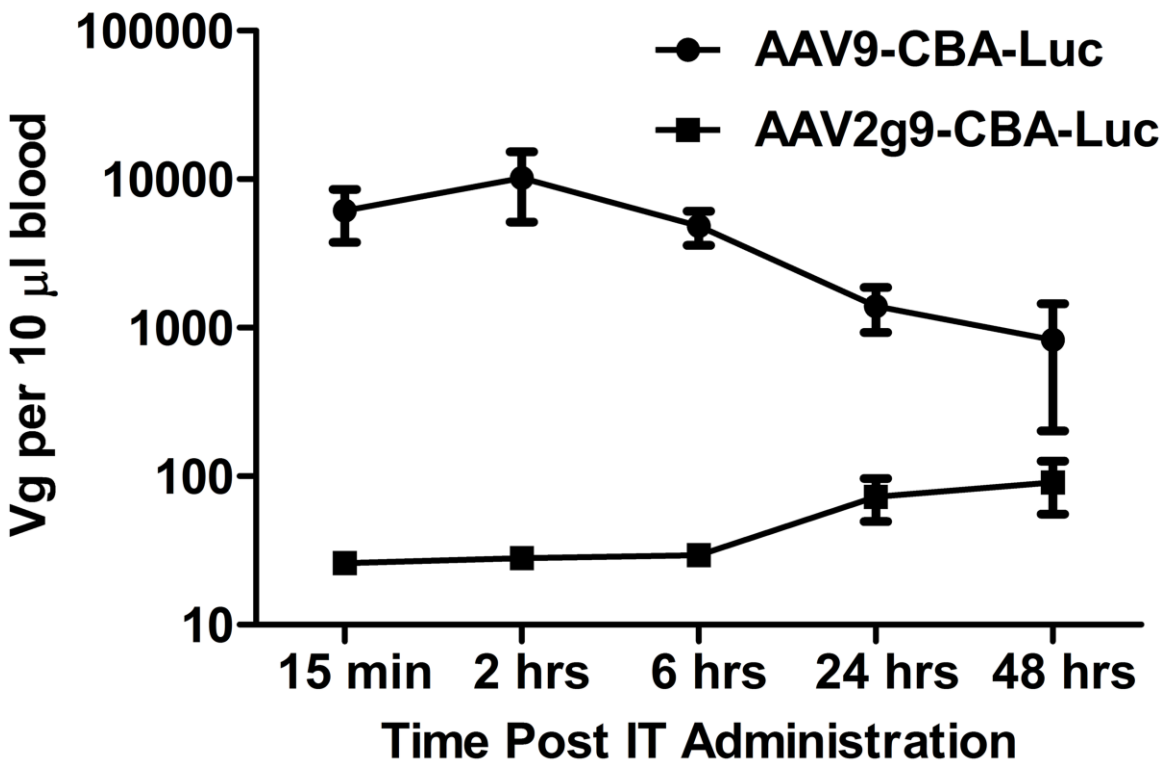

Figure 19. Comparison of blood circulation/pharmacokinetic profiles AAV9 and AAV2g9 vectors in adult mice post IT administration. 8 week old Balb/C mice were injected with equal viral titers ($7.8x10^9$vg) of AAV9 or AAV2g9 packaging CBA-Luc transgene via intrathecal injections. Approximately 10 µl blood was collected via tail vein nicks from adult mice at 15 min, 2 hrs, 6 hrs, 24 hrs and 48 hrs post IT injection. Blood samples were immediately mixed with equal volume of sodium citrate (3.8% weight/volume) to avoid coagulation. Pharmacokinetic profiles of AAV9/2g9 vectors were generated using qPCR to calculate viral genomes in the blood samples with primers specific to the luciferase transgene. Data represents mean ± standard error mean (s.e.m.) * represents $p<0.05$ as determined by student t-test. All experiments were conducted in quadruplicate.

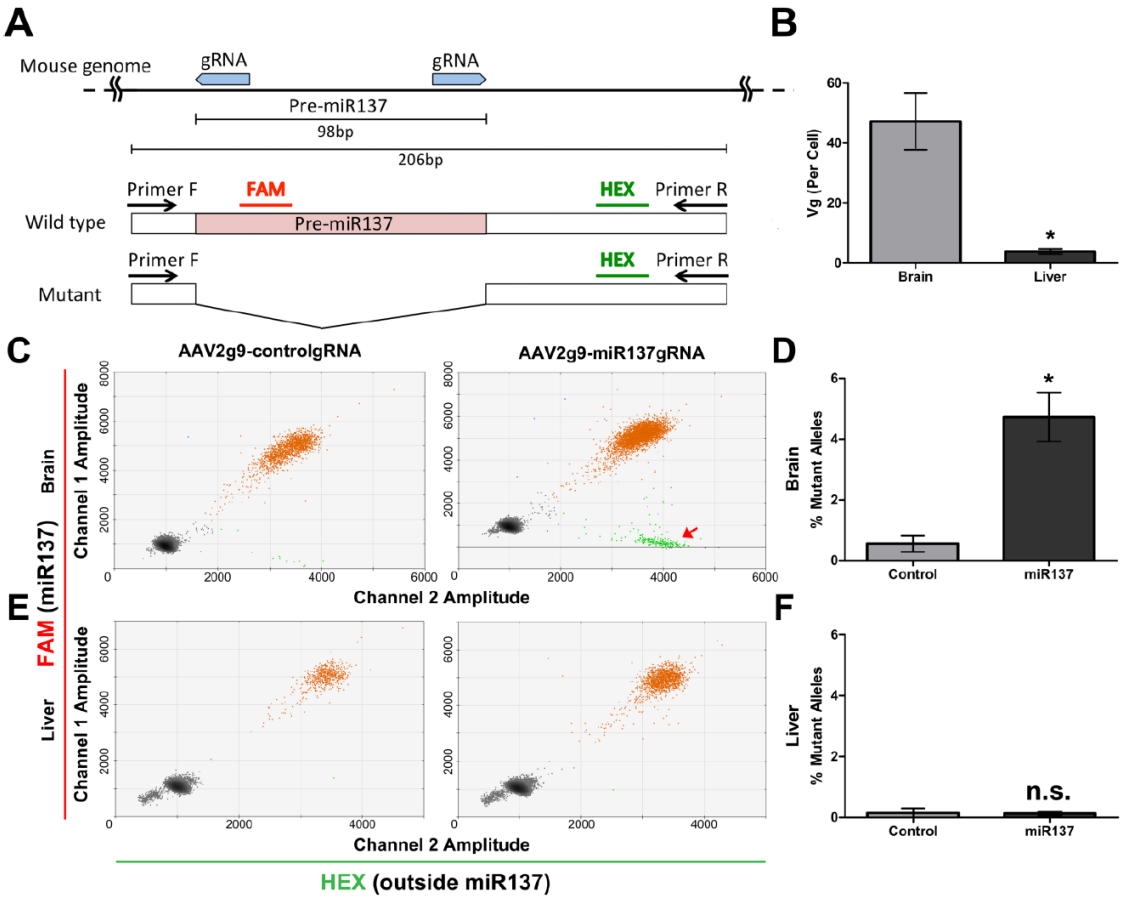

Figure 20. CNS-restricted gene disruption of MIR 137 within Cas9 transgenic mouse using AAV2g9. (**A**) Schematic representation of mouse miR137 locus (mm10, chr3:118,433,800-118,434,004). Two gRNAs were designed to generate a 98bp deletion within pre-miR137 region. Droplet digital PCR (ddPCR) primers were designed to amplify a 206bp region (wild type mir-137) and shorter mutant (mir-137 eliminated) genomic DNA. Probes detect unaltered region (HEX probe, green) and a region flanked by two miR137gRNAs (FAM probe, red). (**B**) AAV2g9 vector genome (vg) copy numbers (per cell) within the brain (light gray bars) and liver (dark gray bars) tissues, 2 weeks post ICV administration in neonatal (P0) Cas9 transgenic mice. Scatter plots showing results of ddPCR on brain (**C**) and liver (**E**) genomic DNA from AAV2g9-controlgRNA (left) or AAV2g9-miR137gRNA (right) injected mice. Specifically, HEX+/FAM+ double positive droplets (Orange) indicate wildtype alleles, while HEX+/FAM- droplets (Green; depicted by red arrow) show miR137 eliminated alleles. Results from all samples (N=3 or 4) are pooled to generate plots. (**D and F**) Quantitative analyses of ddPCR from controlgRNA (light gray bars) and miR137gRNA (dark gray bars). Wild-type or mutant allele were predicted using a 2D dot plot as shown. Graphical data represents mean ± standard error mean (s.e.m.) * represents $p<0.05$, n.s. indicates 'not statistically significant' ($p>0.05$), as determined by student t-test. All experiments were conducted in triplicate.

CHAPTER 4: AQUAPORIN 4 REGULATES THE PARAVASCULAR CLEARANCE OF AAV VECTORS FROM THE BRAIN

4.1 Overview

Adeno-associated viruses (AAV) are currently being evaluated in clinical trials for gene therapy of central nervous system (CNS) disorders. However, host factors that influence the spread, clearance and transduction efficiency of AAV vectors in the brain are not well understood. Recent studies have demonstrated that water flow mediated by aquaporin 4 (AQP4) channels located in astroglial endfeet is essential for exchange of solutes between interstitial and cerebrospinal fluid. In the current study, we demonstrate that AQP4 water transport profoundly affects various aspects of AAV gene transfer in the CNS. Mislocalization of AQP4 in aged mouse brains correlated with significantly increased retention of AAV vectors in the parenchyma following ventricular administration. Within minutes after unilateral administration into the ventricles, AQP4 knockout mice displayed highly restricted spread of fluorophore labeled AAVs compared to WT mice. We observed increased retention and transgene expression when AAV vectors were administered into the ventricles (intraCSF) of AQP4-/- mice, as compared to WT mice. These results were corroborated by markedly reduced clearance of AAV vectors from the brain as demonstrated by reduced transgene expression and vector genome accumulation in systemic organs. We postulate that deregulation of AQP4 in aged and diseased brains could markedly affect the parenchymal spread, clearance and gene transfer efficiency of AAV vectors. Assessment of biomarkers that report the

kinetics of CSF flux in prospective gene therapy patients could help understand variable treatment outcomes and guide future clinical trial design.

4.2 Introduction

Tremendous progress is being made towards building a repertoire of viral vectors for therapeutic gene transfer in the central nervous system (4, 15, 27, 229). Gene therapy approaches for treating diseases such as Spinal Muscular Atrophy (NCT02122952), Giant Axonal Neuropathy (NCT02362438), Parkinson's (NCT00229736), Alzheimer's (NCT00017940) and Lysosomal storage disorders (NCT01474343) are being tested in Phase I/II clinical trials. Almost all such therapeutic strategies currently utilize AAV biologics for delivering the corrective transgene in the disease-affected CNS (4, 266). For instance, clinical trial was conducted on 10 patients with early Alzheimer's disease by administration of AAV2 vectors packaging nerve growth factor (NGF). Post-mortem patient brains showed pathological benefits proximal to NGF expression in the form of axonal sprouting and cholinergic neuronal hypertrophy with no adverse effects for 10 years (238). However, reports from other ongoing clinical trials indicate that the efficacy of CNS gene transfer from such strategies often falls short of the therapeutic baseline in patient cohorts (164). To this end, techniques like convection-enhanced delivery (CED) of AAV vectors are being employed to target a larger brain volume from a single intracranial administration (267). Understandably, it is crucial to conduct preclinical evaluations of AAV vectors on predictive *in vivo* systems that accurately depict physiological processes and biochemical landscape of the human CNS.

Interstitial flux of biological fluids is a common mechanism employed by mammalian tissues for lymphatic waste clearance (62, 268). Due to lack of a conventional lymphatic vasculature in the brain, a combination of CSF and water moves via subarachnoid spaces and paravascular compartments to drain extracellular depositions like metabolites and proteins (104, 105, 269). Specifically, CSF engages in direct exchange of biomaterials with proximal CNS tissue via subarachnoid ducts (63, 105). Such exchange of cargo within deeper anatomical regions of neural tissue is made possible by paravascular water transport through aquaporin-4 (AQP4) channels (62, 269). Iliff and colleagues utilized fluorescent CSF tracers and AQP4 knockout (AQP4-/-) mice to visualize and elucidate mechanistic aspects of paravascular CSF flux and solute clearance in CNS (62, 270). This glial-associated lymphatic clearance of brain tissue has been termed ‘glymphatic’ clearance (269, 271).

Successful CNS spread and infection by viral biologics is a multifactorial cascade of events (193). For instance, adeno-associated viral (AAV) vectors overcome physiological barriers (e.g. blood-brain/ blood-CSF barrier) and utilize biochemical processes (e.g. receptor interactions) to achieve successful CNS gene transfer (25). Vector transduction efficiency and cell-specificity are evidently attributed to AAV capsid-cell surface receptor interactions *in vivo* (25, 31, 229). However, there is a need for better understanding the checkpoints that govern AAV vector spread, accumulation, transduction and clearance in the CNS. For this study, we hypothesized that transparenchymal CSF flux via glymphatic transport has profound implications on aforementioned properties of AAV vectors within the brain. On a molecular level, an expanding body of evidence suggests that this paravascular fluid flux is regulated by

AQP4 lining at the astrocytic endfeet (62, 269, 272, 273). We demonstrate the effects of abnormal AQP4 expression on CNS gene transfer properties of AAV vectors *in vivo*. Specifically two mouse models of dysfunctional AQP4 glymphatic transport were studied: a) age dependent mislocalization of AQP4 and; b) genetic knockout of AQP4. We show that AQP4 mediated CSF flux dictates multiple aspects of AAV-gene therapy of the CNS tissue.

4.3 Materials and Methods

Recombinant AAV vector production. An updated triple plasmid transfection protocol was used to generate recombinant AAV9 vectors (206, 255). All plasmids used for AAV production in this study were obtained from the UNC vector core. Specifically, HEK 293 cells were transfected with a mixture of (i) the pXR9 helper plasmid; (ii) the adenoviral helper plasmid pXX6-80; and (iii) pTR-CBh-ScGFP or pTR-CBA-Luc plasmids encoding the green fluorescent protein (GFP) or luciferase (Luc) reporter genes driven by the chicken β hybrid (CBh) or chicken β actin (CBA) promoter and flanked by inverted terminal repeats (ITRs) derived from the AAV2 genome. Iodaxinol gradient ultracentrifugation was used to purify AAV vectors. Fluorophore labeled AAV vectors were generated using an Alexa-647 labeling kit (Thermofisher-A20006) by following the protocol provided by the kit manufacturer. Following fluorophore labeling, the AAV vectors were dialyzed against 1X PBS for 2 overnight cycles using a 12-14 kDa MWCO dialysis column (Millipore-71505-3). Finally, quantitative PCR (QPCR) (Lightcycler® 480, Roche Applied Sciences, Pleasanton, CA) was used to calculate vector genome (vg) titers with primers designed to selectively bind AAV2 ITRs (forward,

5’- AAC ATG CTA CGC AGA GAG GGA GTG G -3’; reverse, 5’- CAT GAG ACA AGG AAC CCC TAG TGA TGG AG -3’) (IDT Technologies, Ames, IA).

Animal Experiments: The constitutive aquaporin-4 knockout (AQP4-/-) mouse model was provided by Dr. Alan Verkman in University of California in San Diego. All animal experiments reported in this study were conducted on AQP4-/- or C57/Bl6 mice bred and maintained in accordance to NIH guideline as approved by the UNC Institutional Animal Care and Use Committee (IACUC) protocol number 15-109.

Intracerebroventricular (ICV) administration. Postnatal day 0 (P0) mouse pups which were rapidly anesthetized on ice for 2 min followed by intracerebroventricular (ICV) injections using a stereotaxic apparatus. AAV vectors (< 3 µl total volume for ICV and < 1 µl total volume for ISTR) packaging the CBh-ScGFP transgene cassette were injected into the left lateral ventricle with a Hamilton 700 series syringe and 26s gauge needle (Sigma-Aldrich, St. Louis, MO), attached to a KOPF-900 small animal stereotaxic instrument (KOPF instruments, Tujunga, CA). Ventricular injections were performed at the following stereotaxic coordinates - 0.5mm relative to the sagittal sinus, 2mm rostral to transverse sinus and 1.5mm deep. Mice were revived under a heat lamp and rubbed in the bedding after AAV injections before being placed back with the dam. The mouse brains were harvested, post-fixed and immunostained 2 weeks post vector administrations (P14). The immunostaining procedure has been described in detail below. For visualizing AAV spread within the mouse brains, Alexa-647 tagged AAV vectors were mixed with 0.1% dextran (10 kDa) (5mg/ml)

(Thermofisher-D22910) reconstituted in 1XPBS prior to ICV injections. 45 min later, injected mouse pups were rapidly anesthetized using hypothermic shock, perfused with 1XPBS followed by 4% paraformaldehyde. The neonatal mouse brains were harvested and postfixed for 3 days prior to vibratome sectioning, staining and confocal microscopy.

Vector genome biodistribution. Mouse Cohorts used for biodistribution studies were sacrificed 3 days post vector administration via the ICV route. The genomic DNA was extracted from the tissue lysates and blood using the DNeasy® kit (Qiagen, Valencia, CA). Viral genome copy numbers were calculated by performing QPCR (Lightcycler® 480, Roche Applied Sciences, Pleasanton, CA) using primers specific to luciferase transgene 5'-AAAAGCACTCTGATTGACAAATAC-3' and 5'-CCTTCGCTTCAAAAAATGGAAC-3'. The vector genome copy numbers were normalized to mouse lamin B2 locus as the housekeeping gene using the primers 5'-GGACCCAAGGACTACCTCAAGGG-3' and 5'- AGGGCACCTCCATCTCGGAAAC-3'. The vector biodistribution was represented as the ratio of vector genomes per cell recovered in the peripheral organs to the CNS site of injection (brain).

Tissue processing and immunostaining. Mouse cohorts used for gene expression (GFP) studies, were sacrificed 2 weeks post vector administration via ICV route. Mouse cohorts used for visualizing viral spread were sacrificed 45 min after fluorescent AAV injections. The mice were overdosed with tribromoethanol (avertin) (0.2 ml/10 g of 1.25% solution) via the intraperitoneal route. This was followed by

transcardial perfusions of PBS and 4% paraformaldehyde in 1xPBS. The organs were removed and post-fixed for 24 hr prior to sectioning. Briefly, 50 µm thick sections were obtained using a Leica VT 1200S vibrating blade microtome (Leica Biosystems, IL). The sections of mouse organs from various treatments were blocked in 10% goat serum (Sigma-Aldrich, St. Louis, MO) and 1% Triton X (Sigma-Aldrich, St. Louis, MO) in PBS for 1 hr. This was followed by overnight incubation with primary monoclonal antibodies at 4˚C. The primary antibodies utilized as a part of this study are as follows: Rabbit anti-GFP (Life-Technologies- G10362, 1:750), rabbit anti-AQP4 (Millipore-AB3594, 1:750). Secondary antibodies were raised in goats and conjugated to Alexa 488 (anti-rabbit Abcam-96883 or Alexa 594 (anti-Rabbit Abcam-96885). The secondary antibodies were used at a standard dilution of 1:500. The immunohistochemical analyses of GFP and AQP4 expression was conducted using Vectastain ABC kit (Rabbit IgG PK-4001 kit, Vector biolabs, Burlingame, CA, USA).

Microscopy and Image processing: We used Zeiss CLSM 700 confocal laser scanning microscope (Microscopy services laboratory, UNC) or Aperio Slide scanner (Leica Biosystems, IL) (Translational pathology laboratory, UNC) for imaging immunostained mouse tissue sections. Quantitation of fluorescence intensities was carried out using the ImageJ image analysis software. For calculating AAV/dextran fluorescence, the mean pixel intensity function was applied across identical regions of interest (ROI) and threshold settings in specific anatomical regions of the mouse brain. For calculating subpial AQP4 expression profiles, individual fluorescence intensity values were recorded at 0-200 pixel positions starting from the pial surface of every

mouse brain. For calculating perivascular AQP4 polarity, fluorescence intensity values were recorded at 50 pixel positions across 4-5 major cortical blood vessels in the mouse brain. The procedure for quantitation of perivascular AQP4 polarity was adopted from a previous study (273). Confocal images were stitched, pseudocolored and analyzed on the Zen® Black software.

4.4 Results

AAV vectors readily accumulate within the aging mouse CNS. The aging brain is susceptible to increased parenchymal depositions of biomolecules such as metabolic wastes. We hypothesized that CNS administration of AAV vectors in aging mice will result in enhanced viral accumulation in the neural tissue. AAV serotype 9 (AAV9) is currently being evaluated in Phase I clinical trials for treating neurological disorders-spinal muscular atrophy and giant axonal neuropathy (Clinical trial identifiers NCT02122952, NCT02362438). To verify our hypothesis, we performed intracranial injections of AAV9 into juvenile (3 months old) and aging (>18 months old) mouse brains. In order to visualize viral particles within the brain, we generated fluorophore labeled AAV9 vectors. Additionally, prior to intracerebroventricular (ICV) injections, labeled AAVs were mixed with 10kDa fluorescent dextran tracer as an internal control for injections and microscopy. Specifically, equal mixtures of Alexa-647 labeled AAV9 vectors ($1.75x10^9$ vector genomes (vg)/mouse) and (0.1%) Alexa-488 labeled dextran were administered. 45 min post injections, the mice were rapidly anesthetized and the brains were harvested after cardiac perfusions with phosphate buffered saline (PBS) followed by 4% paraformaldehyde (PFA). Postfixed brains were sectioned on a

vibratome and Zeiss 700 confocal microscope was used to obtain whole brain stitches of the ventricular slices. We observed restricted fluorescence (red) from AAV9 vector particles at close proximity to ventricular site of administration in the juvenile mouse cohort (**Fig. 21A**, AAV9). On the other hand, identical injections performed on aging mice resulted in dramatically enhanced fluorescence (red) in deeper anatomical regions across the brain parenchyma (**Fig. 21B**, AAV9). A similar increase in fluorescence signal (green) was also observed due to dextran tracer injections in the aging mice (**Fig. 21B**, AAV9/Dex) as compared to juvenile mice (**Fig. 21A**, AAV9/Dex). This suggests that increase in parenchymal accumulation is not specific to AAV vectors. To further demonstrate AAV accumulation in the aging brain, we generated high magnification confocal micrographs of six brain regions i.e. lateral ventricles (LV), corpus callosum (CC), cortex (CT), piriform cortex (PCT), thalamus (THL) and hypothalamus (HTL). We observed fluorescence from AAV vectors and dextran tracers restricted to LV and CC regions of the juvenile mouse brain (**Fig. 21C**, AAV9 & AAV9/Dex). On the other hand, fluorescent signal was observed in all the six anatomical regions in the aging mouse brain (**Fig. 21D**, AAV9 & AAV9/Dex). Quantitation of fluorescence intensities due to AAV9 vectors shows a significant increase CC, CT, PCT, THL and HTL of the aging mice as compared to the juvenile mice (**Fig. 21E and F**, regions 2-6). It should be noted that difference in AAV fluorescence in the two groups was not-significantly different in the area surrounding the lateral ventricle site of injection (**Fig. 21E**, region 1). A similar overall enhancement in fluorescence signal was also observed due to dextran administration within different anatomical regions of the aging mouse brain (**Fig. 21G**

and H). Overall, our results show increased parenchymal accumulation of AAV vectors and dextran tracers, minutes after intracranial administration into the aging CNS.

Altered AQP4 localization correlates with AAV deposits in the aging brain. Loss of perivascular AQP4 polarity is one of the histological hallmarks that indicate impairment of CSF penetration through the brain parenchyma (273). To assess whether altered localization of AQP4 plays a role in accumulation of AAV vectors within the aged mouse brain, we analyzed AAV capsid accumulation and AQP4 expression profiles in juvenile and aging mouse brains. Fluorescently labeled AAV9 particles were injected through the intraCSF route in juvenile (3 months) and aged (18 months) mouse brains. At 45 min post-administration, animals were sacrificed and post-fixed in 4% PFA. High magnification confocal micrographs of cortical regions (**Fig. 22D and E**) revealed that the fluorescent signal from AAV9 particles (red) was strikingly elevated and appeared as deposits in the aged mouse brain (**Fig. 22B**) as compared to the juvenile cohort (**Fig. 22A**). Quantitation of this phenomenon shows a significant increase in fluorescence signal associated with AAV capsids within cortical regions of aged mouse brains compared to juvenile mice (**Fig. 22C**).

Next, to compare perivascular AQP4 polarity, we generated high magnification confocal micrographs of AQP4 expression within juvenile and aged mouse brains. Specifically, we compared AQP4 localization on penetrating large blood vessels (arterioles) within the cortex (**Fig. 22D and E,** red boxes and insets). When compared to juvenile mice (**Fig. 22D,** inset), we observed a striking increase in AQP4 expression (green) immediately surrounding the blood vessels in the aged mice (**Fig. 22E,** inset). These results are consistent with loss of AQP4 polarity as reported earlier in the

literature (273). To quantify this phenomenon, we measured fluorescence intensities in pixel positions across the blood vessel walls (**Fig. 22D and E**, insets, red dotted lines). In juvenile mice, we observed a noticeable increase in AQP4 expression within the blood vessel architecture with low, background level fluorescence signal in the surrounding tissue (**Fig. 22F**). However, AQP4 expression was mislocalized and broadly distributed in areas adjacent to the blood vessels of the aging mice (**Fig. 22F**). Taken together, these results suggest a potential correlation between altered AQP4 expression in aged mouse brains and increased parenchymal accumulation of AAV vectors.

AAV vectors exhibit significantly reduced spread within the AQP4 knockout mouse CNS. Our previous results establish a strong correlation between loss of AQP4-mediated CSF flux and increased accumulation of AAV vectors within the brain. To further delineate the role of AQP4 in other aspects of AAV mediated CNS gene transfer, we utilized the constitutive AQP4 knockout (AQP4-/-) mouse model (274). Successful knockout was ensured by detecting loss of AQP4 expression with immunohistochemistry on wildtype (WT) and AQP4-/- mouse brain sections (**Fig. 26**). First, we hypothesized that AAV vectors utilize AQP4-CSF flux to spread within the CNS. To verify, we compared spread of fluorescently labeled AAV vectors within the WT and AQP4-/- mouse brain. Specifically, we injected equal titers ($1.75x10^9$ (vg)/mouse) of Alexa-647 labeled AAV9 mixed with equimolar concentrations (0.1%) of Alexa-488 labeled 10kDa dextran-tracer into the postnatal day 0 (P0) mouse brains. The mice were sacrificed 45 min post ICV injections following which the brains were harvested and postfixed in 4% PFA.

To evaluate differences in viral spread from a global standpoint, we employed the histograph functionality (Zen Black image analysis software, Zeiss 700 confocal microscope) on whole brain confocal stitches (**Fig. 23**, top row). Briefly, white peaks on the surface of coronal brain sections indicate positions of the fluorescent AAV9 vector particles. ICV administration of AAV9 in WT mice resulted in numerous fluorescent peaks distributed across both hemispheres of the brain (**Fig. 23A**, WT, top row, AAV). Additionally, dextran tracer injection in the WT mouse resulted in similarly diffuse fluorescent peaks across the brain parenchyma (**Fig. 23B**, WT, top row, Dextran). On the other hand, ICV administration of AAV9 vectors in the AQP4-/- mice resulted in a large concentration of fluorescent peaks restricted to the immediate vicinity of the ventricular site of injection (**Fig 23A**, AQP4-/-, top row, AAV). Similarly, we observed noticeable increase in fluorescent peaks surrounding the ventricles and within the extra parenchymal CSF space due to dextran injections in AQP4-/- mice (**Fig. 23B**, AQP4-/-, top row, Dextran). In order to further demonstrate change in the spread of AAV9 vectors within the AQP4-/- brain, we generated high magnification confocal micrographs of the lateral ventricles. In comparison to WT mice (**Fig. 23A**, WT, middle row, AAV), AAV9 injections in the AQP4-/- mice resulted in increased fluorescence (red) surrounding the ventricles (**Fig. 23A**, AQP4-/-, middle row, AAV). A similar increase in the fluorescent signal (green) was also observed due to dextran injections in the AQP4-/- mice (**Fig. 23B**, AQP4-/-, middle row, Dextran) as compared to WT mice (**Fig. 23B**, WT, middle row, Dextran). Furthermore, to evaluate the numerical change in the spread of AAV and dextran particles, we quantified the fluorescence intensities in WT and AQP4-/- mouse brains after various treatments. We observed significant increase in fluorescence signal

due to AAV (~3 fold) and dextran (~6 fold) injections in the AQP4-/- mice as compared to WT mice (**Fig. 23C & D**). Our results demonstrate that during conditions of reduced transparenchymal CSF penetration, AAVs show restricted mobility within the brain. In other words, AAV vectors employ AQP4-mediated CSF flux to spread within the brain.

AAV transduction is significantly altered in the brains of AQP4-/- mice. To further delineate the role of AQP4 in other aspects of AAV mediated CNS gene transfer, we utilized the AQP4 knockout (AQP4-/-) mouse model (274). Complete loss of AQP4 expression was confirmed by immunohistochemical analysis of wildtype (WT) and AQP4-/- mouse brain sections (**Fig. 26**). We then compared transduction profiles of AAV9 vectors injected unilaterally into the ventricular CSF space (ICV injections). Specifically, we injected neonatal P0 mice with AAV9 vectors packaging a self-complementary GFP (scGFP) cassette driven by a hybrid chicken β actin (CBh) promoter. At 2 weeks post-administration, 50 μm vibratome brain sections were subject to diaminobenzidine (DAB) immunohistochemistry to visualize transgene (GFP) expression. AAV9 injections in the WT mice resulted in broad GFP expression across the brain parenchyma (**Fig. 24A**). Interestingly, ICV administration of AAV9 in AQP4-/- mice resulted in dramatically enhanced GFP expression in the CNS (**Fig 24A**). Specifically, we observed a significant increase in GFP+ cells in representative regions of the contralateral hemisphere after unilateral ICV injections in the AQP4-/- mice (**Fig. 24A**, boxes and insets). We measured pixel intensities to quantify GFP expression across different brain regions, specifically, the motor, somatosensory, auditory and piriform cortices as well as striatum and hippocampus. A significant increase in pixel intensities within the aforementioned regions in AQP4-/- mouse brain when compared to

the WT brain was observed (**Fig. 24B**). These results indicate that AAV vectors administered directly into the CSF are likely subject to rapid clearance. Reduced clearance of solutes due to lack of AQP4 function could result in retention of AAV vectors and consequently improved gene expression. Taken together, these results can possibly be explained by severely impaired parenchymal transport within the brain and CSF clearance of AAV vectors from the brain in AQP4-/- mice.

CNS-administered AAV vectors utilize AQP4 for systemic leakage and peripheral organ gene transfer. AQP4 mediated brain interstitial fluid flux shunts parenchymal cargo into CSF compartments where they drain into peripheral lymphatics or systemic blood circulation. An important safety concern raised during CNS injections of clinical vector candidates like AAV9 is systemic leakage resulting in off-target gene transfer. We hypothesized that transportation of AAV vectors from CNS tissue to peripheral organs is an AQP4 dependent process. To verify, we injected AAV9 vectors into WT and AQP4-/- mouse brains via the ICV route. 3 days post vector administrations we sacrificed one cohort of mice and carried out biodistribution studies to calculate vector genome accumulation in off-target organs. ICV injections of AAV9 results in heavy viral genome leakage (~150 fold) into peripheral organs like heart and liver (**Fig. 25B**, WT) resulting in strong off-target transgene expression (**Fig. 25A**, WT). Crucially, under identical conditions of AAV9 CNS administration, the AQP4-/- mouse cohort displayed near background levels of off-target vector genome biodistribution (**Fig. 25B**, AQP4-/-). Correspondingly, this resulted in dramatically reduced transduction (GFP expression) in the heart and liver tissue (**Fig. 25A**, AQP4-/-). Overall, for the first time,

our results indicate that AQP4 mediated CSF flux is the underlying phenomenon driving systemic leakage and off-target transduction of CNS injected AAV vectors.

4.5 Discussion

AAV vectors are being evaluated as clinical vector candidates for CNS maladies such as Alzheimer, Parkinson and Frontotemporal dementia (4, 15, 27, 229). A common hallmark of such diseases is the parenchymal accumulation of misfolded proteins and erroneous metabolic byproducts such as alpha-synuclein, hyperphosphorylated tau etc. Aging brains are more susceptible to such depositions of senile plaques (275, 276). Correspondingly, these neurocognitive disorders are more prevalent among the geriatric demographic (277). In the aging mouse brain (>18 months), both glymphatic CSF flux and transparenchymal solute clearance have been demonstrated to be severely impaired (273). In the current study, we first hypothesized that CSF flux plays a major role in retention of clinically relevant biomaterials like AAV vectors in the CNS. Our results in **Figure 21** confirm that accumulation of AAV vectors and dextran tracer increase dramatically in the aging mouse brain. As shown in **Figure 22**, AQP4 lines the major blood vessels (arteries and veins) and microvasculature (capillaries) in the brain. Furthermore, dysregulated AQP4-fluid flux is a common occurrence during conditions of ablated interstitial clearance in the CNS such as aging, Alzheimer's disease and dementia (270-273, 278). Correspondingly, **Figure 22** also confirms that increased parenchymal AAV accumulation is accompanied by indications of dysfunctional AQP4-glymphatic clearance. It is therefore tempting to speculate that the older patient demographic offers a CNS landscape that allows for increased retention of AAV vectors

within the brain. Future gene expression studies done on aging animals might uncover the effect of dysfunctional AQP4 on other aspects of therapeutic AAV gene transfer such as dosage and efficacy.

To directly investigate if the absence of AQP4 water channel protein affects AAV vector functioning in the brain, we compared WT mice with constitutive AQP4 knockout mouse model (AQP4-/-) generated by Verkman and colleagues (274). AQP4-/- mice have reduced glymphatic water transport resulting in slower clearance of parenchymal accumulations such as Amyloid-β in the CNS (269). Accordingly, intraventricular administration of fluorophore labeled AAV vectors in the AQP4-/- mice resulted in restricted spread and increased fluorescence from accumulating AAV vector particles (**Fig. 23**). Intriguingly, we observed differences in spread and accumulation of AAV vectors depending upon the level and functional status of AQP4 in the brain. Specifically, while **Figure 21 and 22** depict the dysregulated status of the AQP4 channel protein in the aging brain, in **Figure 23** AAV particles were exposed to a CNS environment lacking AQP4 altogether. Both conditions resulted in enhanced retention of AAV particles in the brain. Interestingly however, while AAV vectors successfully spread within the aging brain (**Fig. 21**), knocking out AQP4 restricts the viral mobility (**Fig. 23**). These results demonstrate that fluid flux via AQP4 channels is crucial for AAV vector spread in the parenchyma.

In addition to the implications on AAV vector retention and spread within the CNS, the AQP4 glymphatic flux also has a significant effect on AAV transduction and systemic leakage. Interestingly, intraCSF administration of AAV9 resulted in a significant increase in transduction efficiency within the AQP4-/- mice (**Fig. 24**). Similarly

dramatic effects were also observed with respect to the systemic leakage of AAV9 particles from the CNS. Specifically, AQP4-/- mice injected with equal concentrations of AAV9 underwent a significantly reduced systemic leakage. Thus resulting in diminished biodistribution and gene expression in peripheral organs such as heart and liver (**Fig. 25**).

Overall, our study suggests that AQP4-glymphatic flux has critical implications on determining parameters of AAV-mediated CNS gene transfer. Moving forward, kinetic-biomarkers of CSF flux can be used to devise the right combination of AAV capsid, dosage and injection strategies to ensure therapeutic gene transfer for treating CNS dysfunctions (279).

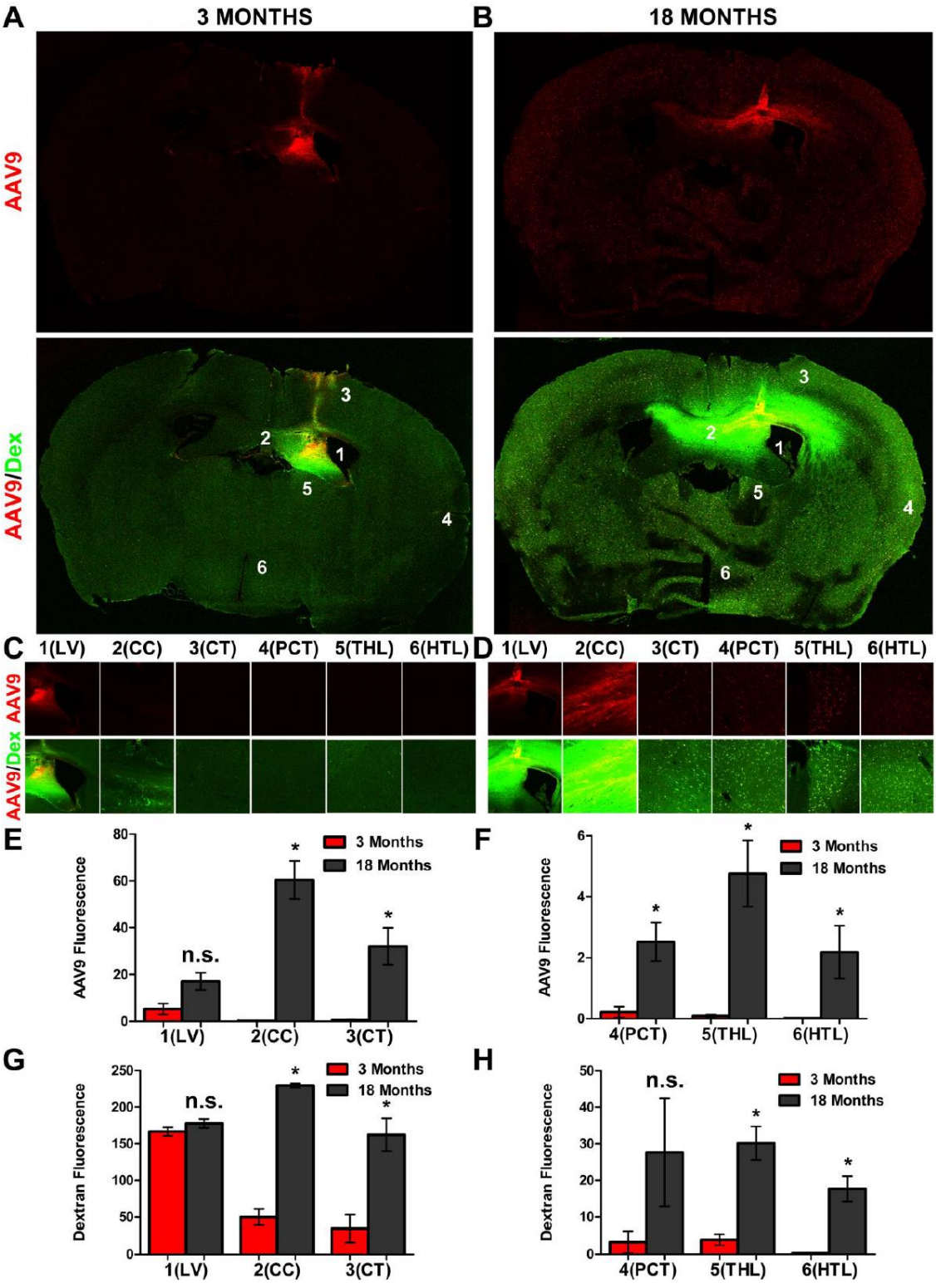

Figure 21. Comparison of AAV vector accumulation within juvenile and aging mouse brains. 3 month and 18 month old mice were injected with equal viral titers ($1.75x10^9$ vg per animal) of Alexa-647 tagged fluorescent AAV9 vectors mixed with

0.5% Alexa-488 tagged fluorescent 10 kDa dextran tracer (5 mg/ml) into the left lateral ventricle. 45 min post injections, the mice were anesthetized and sacrificed for organ harvests. Paraformaldehyde fixed brains were sectioned on a vibratome and Zeiss 700 confocal microscopy was used to generate fluorescence images of the mouse brains. (A and B) Representative confocal stitches of coronal sections containing the lateral ventricular site of injection. Top row shows accumulation of fluorophore labeled AAV9 (red). Bottom row shows merge of AAV (red) and dextran (green) fluorescent signals. Additionally, 6 brain regions: i.e. lateral ventricles (LV), corpus callosum (CC), cortex (CT), piriform cortex (PCT), thalamus (THL) and hypothalamus (HTL) have been numbered 1-6 as positional cues to higher magnification images below. (C and D) Higher magnification confocal micrographs show regions of interest in juvenile (C); and aging (D) mouse cohorts. Images show differences in fluorescence signal due to AAV (top row, red) and AAV/dextran merge (bottom row, red/green). Quantitation of fluorescence intensities from AAV (E and F) and dextran (G and H) channels within regions 1-6 have been shown. Graphical data shown is represented as mean + standard deviation. P values were calculated by unpaired, 2 tailed student t-test. ‘n.s.’ indicates not statistically significant; ‘*’ indicates statistically significant ($p<0.05$). All experiments were conducted in triplicate, representative images are being shown.

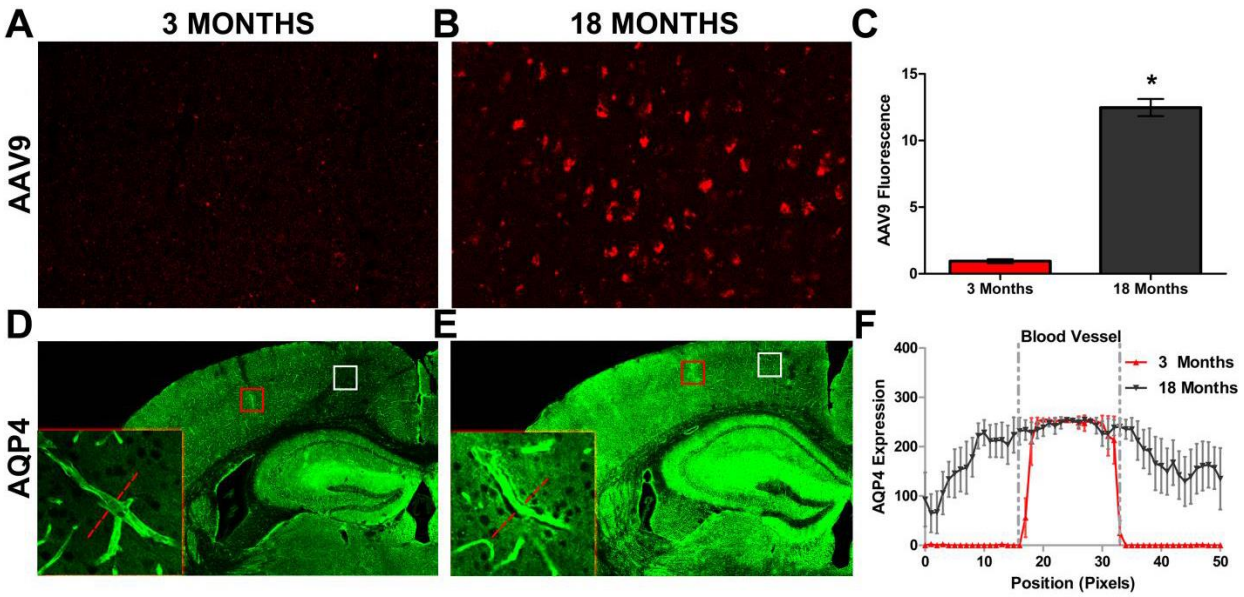

Figure 22. Aged mice display abnormal AAV accumulation and altered AQP4 localization in the brain. (A and B) Comparison of accumulation of fluorophore labeled AAV9 vector particles (red) 45 min after ICV injections in the 3 month and 18 month old mouse brain. **(C)** Quantitation of fluorescence intensities from AAV9 accumulation within cortical regions of 3 month and 18 month old mice. Graphical data shown is represented as mean ± standard deviation. P values were calculated by unpaired, 2 tailed student t-test. '*' indicates statistically significant ($p<0.05$). **(D and E)** 3 month and 18 month old mouse brains injected with fluorescent AAV9 vectors (Fig. 1) were immunostained for AQP4 expression (green). Red boxes indicate positions of large blood vessels (arterioles) shown in higher magnification within the insets on the left. White boxes indicate cortical regions where AAV accumulation was compared **(F)** Fluorescence intensity (green) of AQP4 expression was measured as a function of distance (in pixels) across 4-5 large blood vessels (red boxes, D and E) per mouse (red dotted line, insets within D and E). Error bars on the graphs represent 95% confidence interval of fluorescence intensity calculated at every pixel position across the blood vessel (F). All experiments were conducted in triplicate, representative images are being shown.

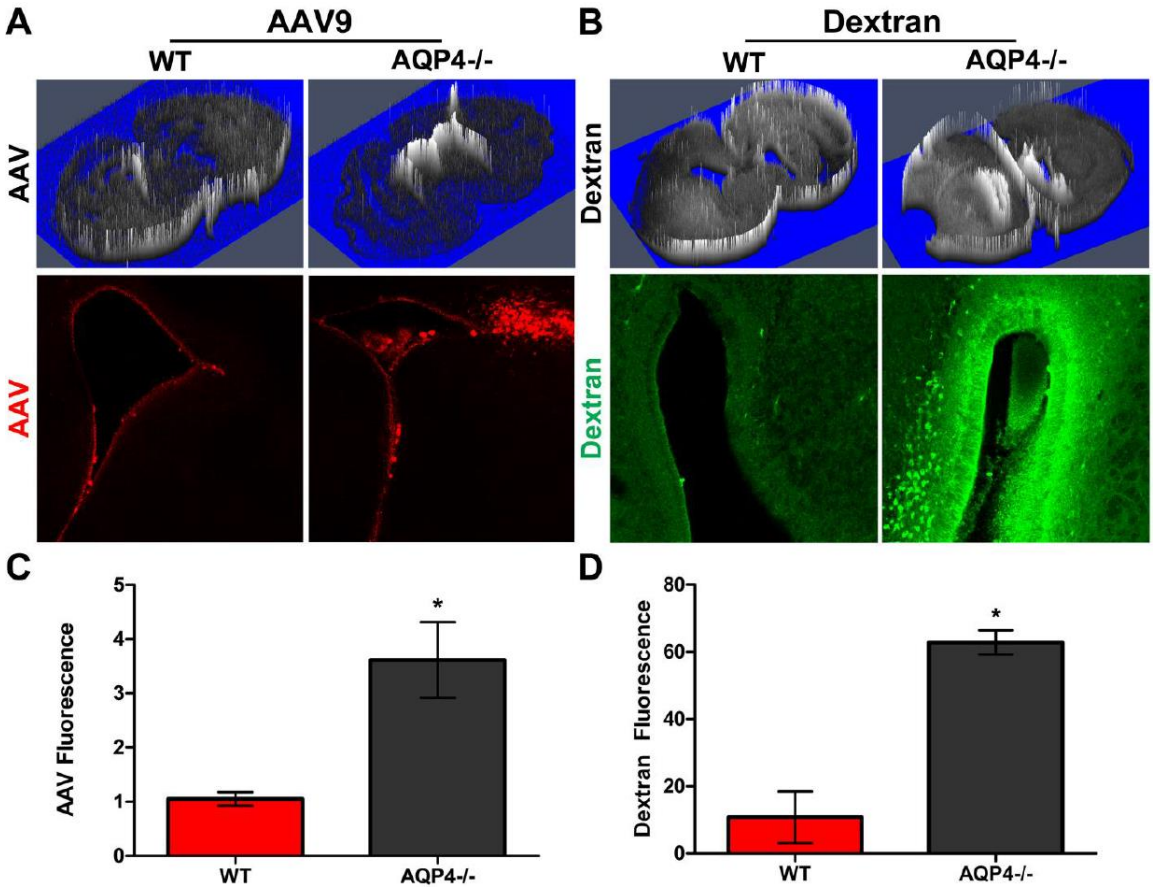

Figure 23. Comparison of AAV vector spread within wildtype and aquaporin-4 knockout mouse CNS. Postnatal day 0 (P0) wildtype (WT) and aquaporin-4 knockout (AQP4-/-) mice were injected with equal viral titers ($1.75x10^9$ vg per animal) of Alexa-647 tagged fluorescent AAV9 vectors mixed with 0.1% Alexa-488 tagged fluorescent 10 kDa dextran tracer (5 mg/ml) into the left lateral ventricle. 45 min post injections, the mouse pups were anesthetized and sacrificed for organ harvests. Paraformaldehyde fixed brains were sectioned on a vibratome and Zeiss 700 confocal microscopy was used to generate fluorescence images of the mouse brains. **(A and B)** Top row- Histograph functionality (ZEN black image analysis software for Zeiss 700 laser scanning microscope) was applied across whole brain confocal stitches of AAV+dextran injected mouse brains. White peaks within the histographs represent positions of fluorescent AAV or dextran particles within mouse brains. Bottom row- higher magnification fluorescence images of the lateral ventricles show differential accumulation of AAV vectors (red) and dextran tracers (green) at the site of injection in WT and AQP4-/- mice. (**C and D)** Quantitation of fluorescence intensities due to AAV9 (C) and dextran (D) administration into WT and AQP4-/- mouse brains. Graphical data shown is represented as mean $\pm$ standard deviation. P values were calculated by unpaired, 2 tailed student t-test. 'n.s.' indicates not statistically significant; '*' indicates statistically significant ($p<0.05$). All experiments were conducted in triplicate, representative images are being shown.

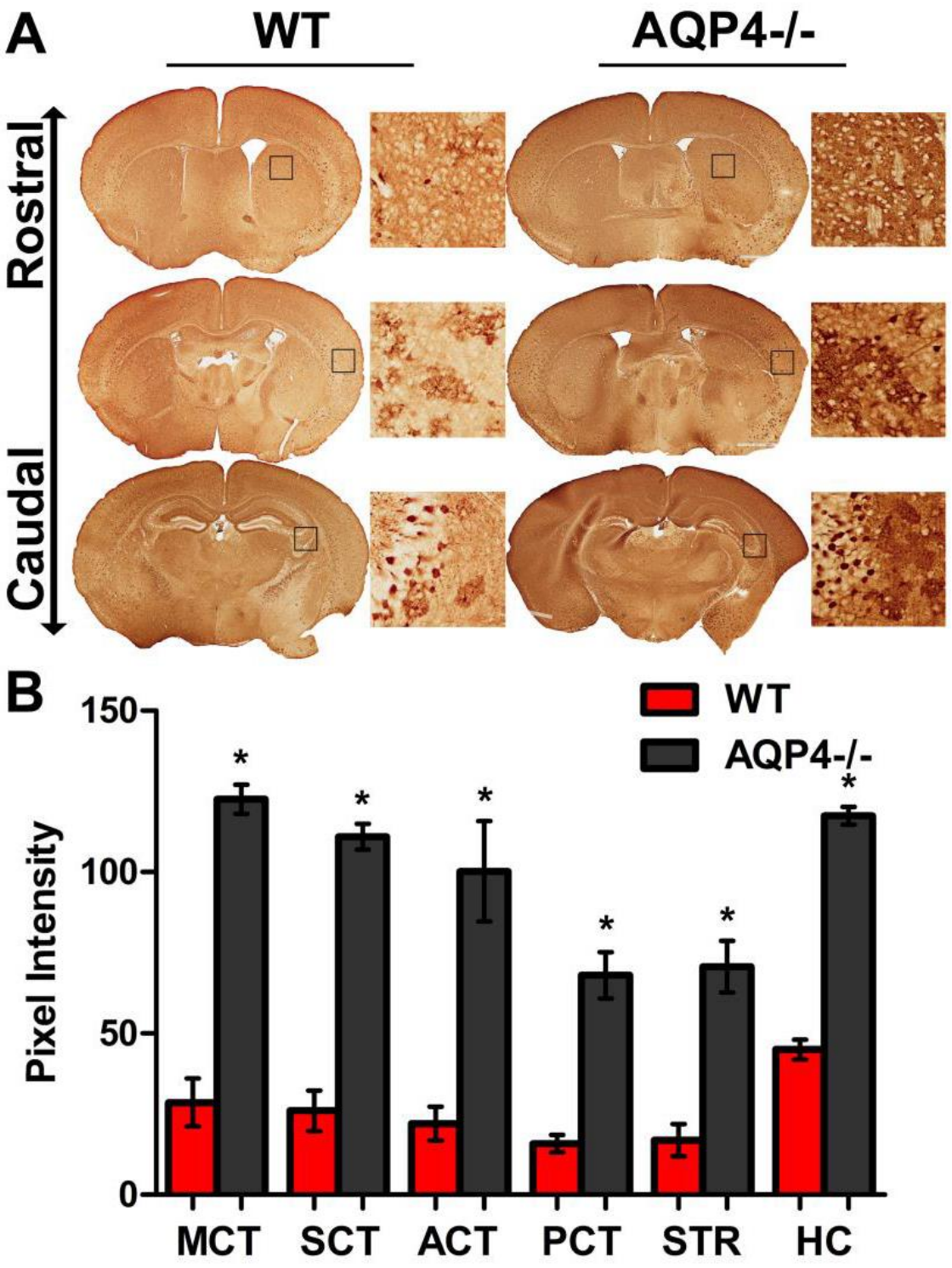

Figure 24. Comparison of AAV transduction efficiency following intraCSF administration in WT and AQP4-/- mouse brains. Postnatal day 0 (P0) mice were injected with equal viral titers ($3.5x10^9$ vg per animal) of AAV9 packaging the self-complementary GFP transgene driven by hybrid chicken β actin promoter (CBh) into the left lateral ventricle. 2 weeks post vector administration the mice were sacrificed and the

brains were harvested, postfixed and vibratome sectioned. **(A)** Diaminobenzidine (DAB) immunohistochemistry was used to visualize GFP expression (brown) within the WT and AQP4-/- mouse brains. Boxes indicate the positions of higher magnification insets adjacent to the whole brain coronal stitches. **(B)** Quantitation of pixel intensities from GFP expression within motor cortex (MCT), somatosensory cortex (SCT), auditory cortex (ACT), piriform cortex (PCT), striatum (STR) and hippocampal (HC) regions of WT (red) and AQP4-/- (grey) mice injected with AAV9 vectors. Graphical data shown is represented as mean $\pm$ standard deviation. P values were calculated by unpaired, 2 tailed student t-test. 'n.s.' indicates not statistically significant; '*' indicates statistically significant ($p<0.05$). All experiments were conducted in triplicate, representative images are being shown.

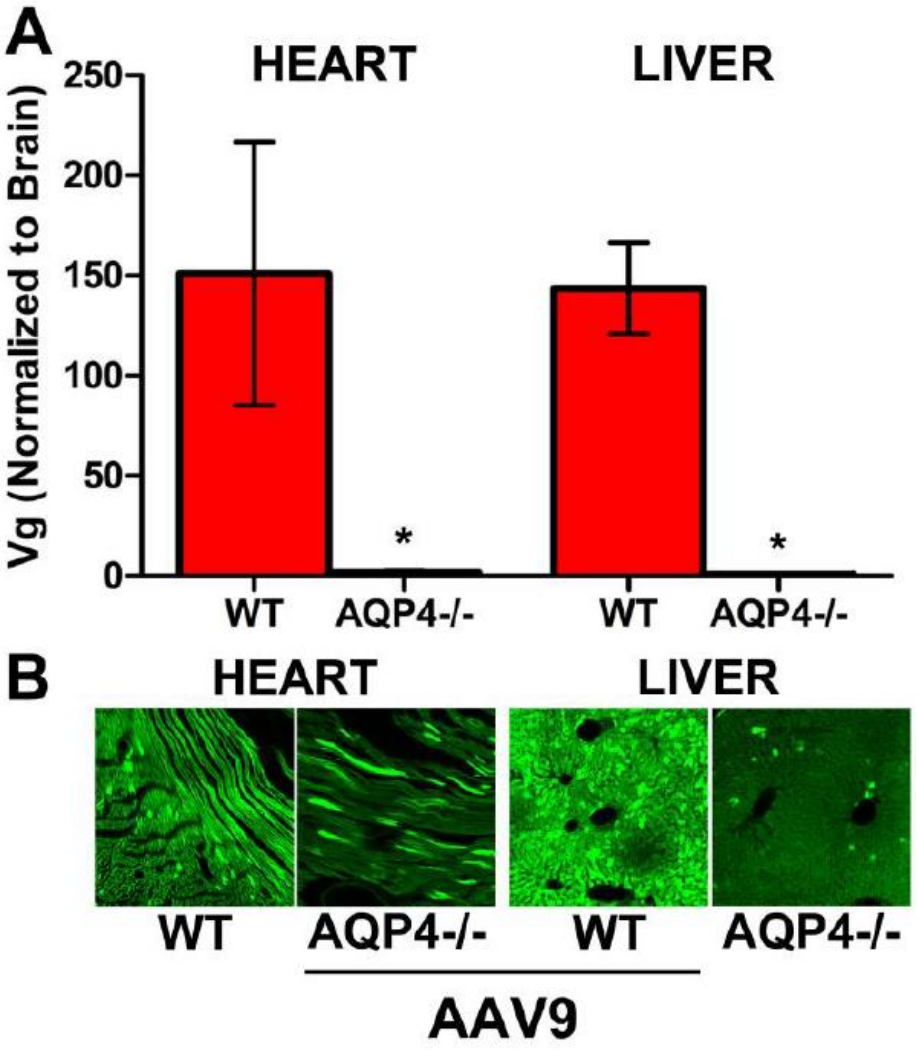

Figure 25. Comparison of off-target transduction and biodistribution of AAV vectors following intracranial administrations in WT and AQP4-/- mice. Postnatal day 0 (P0) WT or AQP4-/- mice were injected with equal viral titers ($3.5x10^9$ vg per animal) of AAV9 packaging the self-complementary GFP transgene driven by hybrid chicken β actin promoter (CBh) into the left lateral ventricle. 2 weeks post vector administration the mice were sacrificed and peripheral organs were harvested, postfixed and vibratome sectioned. **(A)** Vector genome (vg) copy numbers within the heart and liver of WT and AQP4-/- mice injected with AAV9 vectors (normalized to vg in the brain) via ICV injections. The vg copy per host genome (vg/cell) was determined by QPCR of extracted genomic DNA and normalized to the number of copies of the mouse lamin β gene. **(B)** Confocal micrographs showing GFP expression (green) in heart and liver, following brain injections of AAV9. Graphical data shown is represented as mean ± standard deviation. P values were calculated by unpaired, 2 tailed student t-test. 'n.s.' indicates not statistically significant; '*' indicates statistically significant ($p<0.05$). All experiments were conducted in quadruplicate, representative images are being shown.

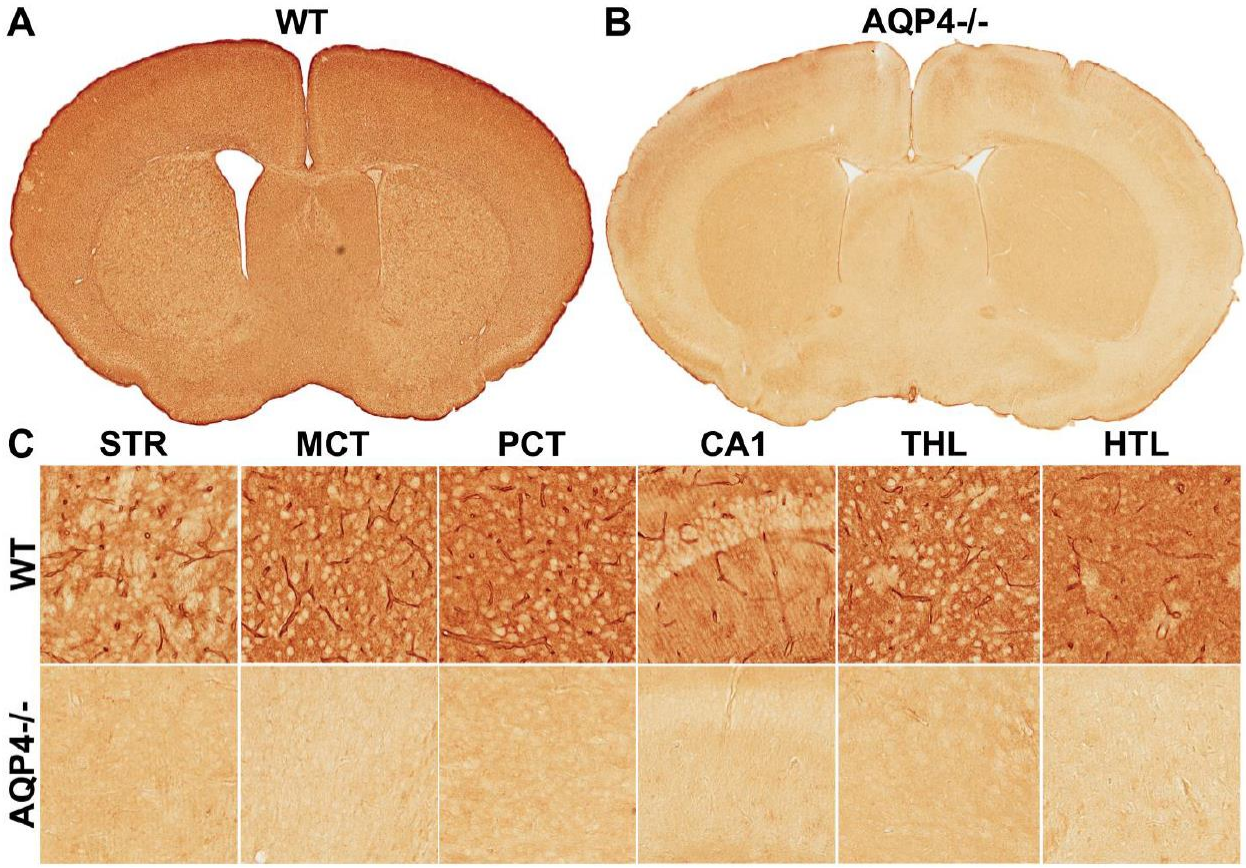

Figure 26. Comparison of AQP4 expression in WT and AQP4-/- mouse brain. 2 week old WT and AQP4-/- mice were harvested, postfixed and vibratome sectioned. **(A & B)** Diaminobenzidine (DAB) immunohistochemistry was used to compare AQP4 expression (brown) in the whole brain stitches of WT and AQP4-/- mice. **(C & D)** Comparison of AQP4 expression in functionally relevant anatomical regions of the mouse brains. Specifically, high magnification images of six anatomical regions- striatum, motor cortex, piriform cortex, hippocampal CA1, thalamus and hypothalamus have been shown. All experiments were conducted in quadruplicate, representative images are being shown.

Chapter 5: SYNOPSIS AND FUTURE DIRECTIONS

5.1: The Big Picture

AAV gene therapy has come a long way since the initial discovery of the wildtype virus as a contaminant in adenoviral stocks. The combination of comprehensive understanding of AAV biology and some significant achievements in AAV vector engineering has equipped us with technology to generate recombinant AAVs (rAAVs) (24, 172, 280). Using rAAV vector technology, any ssDNA within the packaging capacity (~4.7kb between AAV ITRs) can be encapsidated as an AAV serotype of choice. Such flexibility has enabled scientists to characterize an arsenal of natural and engineered AAVs as gene transfer vectors towards research and therapeutic applications.

From the vantage point of CNS gene therapy, AAV vectors offer the following attractive features - (a) there is no conceivable evidence correlating AAV serotypes with pathogenicity/disease in animal models or human patients; (b) unlike many other viruses, AAV is not highly immunogenic, with the immune response being usually restricted to generation of anti-capsid neutralizing antibodies (281); (c) upon host nuclear entry, the genomic contents of AAV predominantly exist in an episomal form and utilize the cellular machinery for gene expression (16, 188, 189). It is important to mention that a small percentage of AAV genomes have been reported to undergo highly specific insertion at the AAVS1 locus of human chromosome 19 (186). In contrast, host genome integration is an integral part of the life cycles of other viral vectors like

lentiviruses, adenoviruses and herpes viruses (187). Such events are often associated with insertional and frame shift mutageneses, sometimes resulting in carcinogenic outcomes for the host cells. (d) AAVs transduce both dividing and non-dividing mammalian cells. This is especially important for CNS transduction where a majority of cells stop dividing once complete maturity is attained. (e) Lastly, direct brain administrations of different AAV serotypes result in distinctive patterns of cellular and regional gene expression in the CNS (53, 71, 72, 89-91, 114, 267, 282). Such variations in AAV transduction profiles have been attributed to capsid-receptor interactions in different hosts (172). For instance, AAV serotype 9 (AAV9) binds N-terminal galactose residues on the mammalian cell surfaces and shows extensive neuronal as well as glial transduction in animal models (37, 94). On the other hand, AAV2, which utilizes Heparan sulfate as the primary receptor demonstrates neuronal tropism and minimal spread from the injection site in the mammalian brain parenchyma (71, 182). Another unique example is AAV4, which binds sialic acid and displays exclusive tropism for astrocytes at the injection site of the mammalian brain (34, 77).

Numerous genetic disorders exhibit distinct manifestations in the CNS. Viral vectors, especially Adeno-associated viruses (AAV) have emerged as the vehicle of choice for supplying healthy cargo of therapeutic genes for such CNS indications (4, 15, 27). The past few decades have witnessed consistent progress towards characterization and preclinical evaluations of AAV vectors in small/large animals and non-human primates (NHPs) (283). Such efforts enable us to make informed decisions regarding parameters like viral serotype, route of administration, immune response,

dosage and biosafety; and employ AAV vectors for therapeutic gene transfer in the clinic.

Continuous efforts in vector design have resulted in an ever increasing toolkit of novel AAV vectors. The key areas requiring vector design and improvement include- transduction efficiency, cell/tissue specificity, packaging capacity and antibody evasion. My doctoral thesis in Asokan Lab in part was focused on developing a deeper understanding of the physiological and biochemical checkpoints that control AAV biologics in the CNS. The interesting phenotypes were often uncovered during screening of multiple AAV variants *in vivo*. The findings showcased in this thesis were the consummation of a systematic sequence of tests conducted on *in vitro* and *in vivo* platforms to unravel the underlying biology of specific phenomena pertaining to AAV vectors in the CNS. To this end, I was fortunate to be working in a laboratory that offered the bandwidth to produce an extensive portfolio of natural and engineered AAV vectors to be tested within the mammalian CNS landscape.

Given the bench-to-bedside nature of the field, it is absolutely crucial that preclinical evaluation of AAV biologics be carried out in predictive *in vivo* systems that mimic the patient CNS. To this end, my research work spanned the use of mouse models in neonatal, juvenile and geriatric demographics displaying varying physio-chemical statuses. In the following chapter, I have proposed follow up studies that have the potential to answer questions pertinent to the theme of my PhD work.

5.2: Future Directions

In the first project, we focused on the African green monkey isolate, AAV serotype 4. AAV4 utilizes *O*-linked sialic acid for cellular attachment. Systemically administered AAV4 results in highly targeted gene transfer in heart and lung tissue. In the CNS, cerebral ventricular system constitutes the ductal connectivity of CSF deep within the brain parenchyma. In addition to the ventricular system, the CSF maintains contact with the CNS tissue via subarachnoid ducts, foramena in the cerebellum and spinal cavity. The key advantage of administering AAV biologics into the CSF space is the ability to target maximal CNS tissue from a single injection. In the context of ventricular administration, AAV4 shows highly specific transduction of the ependymal cells. Although, the underlying glycan receptor interaction of AAV4 is well known, we discovered the biochemical requirement for the virus to traverse the brain parenchyma further. We focused on AAV spread, transduction and cellular tropism for this study.

The formation of functional neurons and glia from the initial pool of neural stem cells (NSCs) is thought to be due to expression of time-sensitive molecular signatures that trigger migration and differentiation (284, 285). For instance, olfactory neurogenesis in mammals is characterized by the migration of a subset of ependyma-derived neuronal progenitors from the sub-ependymal zone (SEZ) via the rostral migratory stream (RMS). These neuroblasts radially differentiate into interneurons of the granular and periglomerular layers in the olfactory bulb (OB), while cells of radial glial lineage differentiate to form glial tubes that guide these migratory processes (284). In addition to rostral migration, a subpopulation of the subependymal progenitors migrate in the caudal direction towards the hippocampal boundary (286). This migration is almost

exclusively gliogenic and gives rise to astrocytes and oligodendrocytes in the neocortex and white matter regions of the brain (287, 288). The ability of such precursor cells to continuously migrate, differentiate and replenish neuronal subpopulations makes them attractive candidates for therapeutic gene delivery in treating neurodegenerative diseases.

Currently available techniques to label or manipulate various aspects of progenitor cell migration during postnatal neurodevelopment include injection of equine infectious anemia viruses or retroviruses packaging fluorescent transgenes directly into adult sub-ventricular zone; DNA analog mediated cell lineage tracking; cell type-specific promoters; transgenic mouse models; or immunohistological analyses (211, 289-292). In addition to these tools, different viral vectors derived from rabies virus, herpes simplex virus and lentiviruses have enabled efficient gene transfer to the mammalian central and peripheral nervous systems (110, 293, 294). Despite this broad spectrum of tools and reagents, targeted genetic manipulation of specific subsets of neuronal progenitors *in vivo* remains a daunting challenge.

Migration and differentiation of neuronal precursors in the developing brain is a carefully orchestrated event. The cell surface biomarker, polysialic acid (PSA) is known to regulate neural plasticity and plays an indispensable role in embryonic and adult neurogenesis (210). In my first project, we reported a novel, engineered AAV4.18 that displays a switch in glycan receptor specificity from sialic acid (SA) to PSA and consequently, acquires the ability to target migrating progenitors in the developing brain. The new AAV strain spreads throughout the brain parenchyma following intracerebroventricular administration, but selectively transduces a subset of ependyma-

derived neuroblasts in the subventricular zone, rostral migratory stream and olfactory bulb (295). Engineering viral tools to exploit molecular signatures could enable selective reprogramming of progenitors to understand and repair damaged CNS tissue.

The engineered AAV4.18 strain has several possible applications. Packaging genome editing tools such as the CRISPR/Cas9 nucleases (296) within AAV4.18 can facilitate targeted ablation of genetic factors that drive neural stem cell recruitment and differentiation during development or trauma (288, 297, 298). For instance, ependymal cells lining the spinal canal have been shown to give rise to neuroblasts and astrocytes in response to stroke (298). Manipulating different mechanisms to maintain an undifferentiated quiescent state or activate normally quiescent cells in order to promote the expansion and migration of progenitors might enable lineage tracing (299). In addition, the highly selective tropism for migrating neuroblasts also make the engineered AAV4.18 strain a promising vector for manipulating the stem cell niche by overexpressing dominant negative transgene cassettes to model neurodevelopmental disorders (300) or deliver neural stem cell reprogramming factors (301, 302).

For my second project, we evaluated a dual glycan binding AAV2g9 vector that harbors the ability to bind both HS and Gal on mammalian cell-surfaces. From the AAV biology perspective, our study provides new insights into the role of capsid-glycan interactions in determining CNS spread and systemic leakage. Earlier studies in our lab and others have demonstrated that the diverse cellular tropisms and biodistribution profiles of different AAV strains are intricately linked to their glycan receptor binding profiles (38, 172). For instance, intracranial injection of the heparan sulfate binding strain, AAV2 shows restricted, neuronal gene expression (71). This preferential

neuronal tropism of AAV2 appears to correlate with the higher concentration of heparan sulfate proteoglycans (HSPGs) on the surface of neurons compared to glia (42).

However, as a caveat to this neurotropic bias, the ability of AAV2 to bind HS with high affinity also restricts vector spread and the effective volume of CNS tissue transduced (89). In contrast, the galactose binding strain, AAV9, shows both neuronal and glial transduction as well as efficient CNS spread (55, 56). Consistent with the latter attributes, AAV9 capsids also appear to be prone to systemic leakage and transduction in the liver and other organs following CNS administration (94, 235, 246). In our current study, we demonstrated that the dual glycan binding AAV2g9 strain inherited traits from both parental AAV serotypes, i.e., neurotropism from AAV2 and robust CNS spread and transduction from AAV9.

Our study demonstrates that the interplay between capsids and cell surface glycans can determine CNS spread and transduction efficiency of AAV vectors administered into the cerebrospinal fluid. However, it is also known that viruses can travel large anatomical distances within the CNS using synaptic connections or axonal transport (303, 304). Viral entry into the neuronal cell body (soma) leading to dissemination at the axonal projections represents anterograde transport, while the opposite scenario is termed retrograde transport. In this regard, AAV strains have been shown to employ axonal transport to undergo single or bidirectional movement within the brain parenchyma (112, 118, 120, 305). In particular, hep binding AAV2 particles have been shown to exclusively move in the anterograde direction (115), whereas sialic acid binding AAV1 or gal binding AAV9 particles appear to shuttle in both directions (117, 118, 120). Exactly how each glycan receptor influences the axonal transport of

different natural AAV isolates as well as engineered strains, such as the dual glycan binding strain AAV2g9 reported here remains to be determined.

From the vector development perspective, our studies have important implications for gene therapy, silencing and editing. First, it should be noted that the CNS transduction efficiency and systemic gene expression from a single ICV/IT dose of AAV9 is particularly striking. Although, not ideal for CNS-specific indications due to the systemic leakage profile, AAV9 could serve as an optimal vector candidate for treatment of lysosomal storage disorders and other such diseases, which are characterized by multi-organ involvement in addition to the CNS. On the other hand, AAV2g9 displays favorable attributes for therapeutic applications targeting neuronal populations within the CNS. Further, the features displayed by the engineered AAV2g9 strain exemplify the feasibility of making rational improvements to AAV vector design with the goal of imparting favorable biodistribution profiles. When combined with cell-specific elements such as the hSyn promoter, as established in the current study or miRNA targeting elements (235, 246), such approaches can help to efficiently restrict transgene expression to neuronal populations within the CNS and reduce systemic exposure. Crucially, we demonstrate that therapeutic delivery of gene editing nucleases using AAV2g9 helps mitigate the risk for off-target effects at the organ level.

Conventional treatments for mental illnesses like attention deficit hyperactivity disorder (ADHD), bipolar disorder (BD) and schizophrenia (SZ) are exclusively designed to ameliorate psychosomatic symptoms. Interestingly, diseases like SZ and BD display strong genetic predispositions in patient cohorts (306). Understandably, devising the next generation of therapeutic interventions for such disorders requires development of

animal models with underpinning disease genetic signature. The AAV2g9 vector offers the unprecedented advantage of CNS contained CRISPR/Cas9 gene disruption using capsid engineering. As shown in Fig. 20, chapter 3, we demonstrate ~5% mutant allele formation in the brain using this approach. Understandably, future studies can be designed to achieve improvement of gene editing efficiency. The availability of smaller Cas9 species e.g. from *Staphylococcus aureus* offers the unique possibility of packaging both CRISPR endonuclease and the targeting gRNAs within the single AAV cassette. Such a strategy also offers the ability to perform targeted gene editing in any animal model and circumvents the need for using transgenic Cas9 mice. Nevertheless, optimization of the site(s) of CNS administration, AAV dosage and promoter usage; and use of self-complementary AAV cassettes are all viable targets to pursue for improving the gene editing efficiency with AAV2g9 in the CNS.

In the third study, we studied glymphatic flux mediated by AQP4-water transport as an important parameter that governs various aspects of AAV gene transfer within the CNS. More importantly, animal testing of clinical conditions like traumatic brain injury (TBI) have revealed significant loss (~60%) in AQP4-mediated glymphatic water transport (270). Correspondingly, the risk of developing neurodegenerative disorders stemming from parenchymal aggregations of neurofibrillary tangles such as Alzheimer's and dementia are significantly higher in the post-TBI demographic (278, 307-310). It is intriguing to speculate with our data that CSF administration of AAV vectors in post-TBI patient cohort, will display inherently reduced vector spread within the CNS.

As shown in Figure 24, in chapter 4, the increase in viral residence within CNS also translated to enhanced gene transfer efficiency from CSF injections of AAV vectors

in AQP4-/- mice. Interestingly, a reverse phenotype was observed in case of transduction efficiency from parenchymal administration of AAV vectors (data not shown). Specifically, AAV9 administration into the neonatal mouse striatum transduces significantly smaller area within the AQP4-/- mouse. It is known that AAV9 successfully employs axonal transport in both retrograde and anterograde directions to travel long distances within the brain (118-120, 311). We speculate that under conditions of ablated CSF flux in the AQP4-/- brain, AAV vectors are unable to “hit” all the neuronal projections with the same efficiency, from a single parenchymal injection. Conversely, AAV2 is only able to travel in the anterograde direction in the CNS (114, 115). Supporting our hypothesis regarding the role of axonal transport, we do not see reduction in transduced area from intrastriatal injections of AAV2 within the AQP4-/- mouse cohort (data not shown). Taken together, ablation of AQP4 fluid flux negatively affects transduction of bidirectional axonal transporters like AAV9 possibly due to diminished levels of axonal transport. In future, studies with unidirectional transporters like AAV2 (anterograde) and AAV6 (retrograde), can further juxtapose the roles of CSF flux and axonal transport on AAV transduction within the CNS.

In addition to viral spread, retention and transduction, we also proposed that AQP4 fluid flux plays a major role in systemic leakage of interstitial deposits such as AAV vectors. Accordingly, we saw a significant reduction of off-target biodistribution and gene expression in peripheral organs from intracranial administration of AAV9 vectors in the AQP4-/- mice (Fig. 25). To our knowledge, this is the first demonstration of AQP4 fluid flux as the biological flushing mechanism that clears AAV vectors into the systemic

circulation/organs. Accordingly, in the absence of AQP4, AAV vectors are effectively contained within the CNS.

Events like aging, neurological storage disorders and traumatic brain injuries can have direct implications on AQP4 function and therefore glymphatic solute clearance (270-273, 278). We believe that future preclinical evaluations of CNS gene therapy strategies can benefit from results obtained from predictive *in vivo* systems like AQP4-/- condition and aged mice. Additionally, biomarkers of CSF flux can be made an integral part in the recruitment process of patient candidates with neurological disorders towards therapeutic AAV gene transfer (279).

The success of CNS gene therapy hinges on a thorough understanding of successes achieved and challenges faced during experimental, preclinical and clinical administrations of therapeutic gene transfer strategies. In this regard, although AAV vector mediated gene transfer in the CNS has demonstrated safe and successful replenishment of proteins, the efficacy of gene therapy reported in the last decade of clinical trials has not met the expectations of researchers and clinicians. There remains a critical need for predictive *in vivo* models of neurodegenerative disorders; establishing correlation between preclinical studies conducted in rodent and primate animal models, and recruitment of representative patient cohorts for clinical trials. Moving forward, it is particularly important to invest time and effort towards various aspects of AAV vector design, development of biomarkers and animal models to overcome the existing roadblocks.

REFERENCES

1. Purves D*., et al* (2001) Neuroscience, 2nd edition

2. Wenger DA, Coppola S & Liu SL (2002) Lysosomal storage disorders: Diagnostic dilemmas and prospects for therapy*. Genet Med* 4(6): 412-419.

3. Lin D*, et al* (2005) AAV2/5 vector expressing galactocerebrosidase ameliorates CNS disease in the murine model of globoid-cell leukodystrophy more efficiently than AAV2*. Mol Ther* 12(3): 422-430.

4. Simonato M*, et al* (2013) Progress in gene therapy for neurological disorders*. Nat Rev Neurol* 9(5): 277-291.

5. Boustany RM (2013) Lysosomal storage diseases--the horizon expands*. Nat Rev Neurol* 9(10): 583-598.

6. Irwin DJ, Lee VM & Trojanowski JQ (2013) Parkinson's disease dementia: Convergence of alpha-synuclein, tau and amyloid-beta pathologies*. Nat Rev Neurosci* 14(9): 626-636.

7. Orr HT & Zoghbi HY (2007) Trinucleotide repeat disorders*. Annu Rev Neurosci* 30: 575-621.

8. Kullmann DM, Schorge S, Walker MC & Wykes RC (2014) Gene therapy in epilepsy-is it time for clinical trials?*. Nat Rev Neurol* 10(5): 300-304.

9. Obeso JA, Rodriguez-Oroz MC, Stamelou M, Bhatia KP & Burn DJ (2014) The expanding universe of disorders of the basal ganglia*. Lancet* 384(9942): 523-531.

10. Singer HS & Minzer K (2003) Neurobiology of tourette's syndrome: Concepts of neuroanatomic localization and neurochemical abnormalities*. Brain Dev* 25 Suppl 1: S70-84.

11. Ravits J (2014) Focality, stochasticity and neuroanatomic propagation in ALS pathogenesis*. Exp Neurol*

12. Sinha P*, et al* (2014) Autism as a disorder of prediction*. Proc Natl Acad Sci U S A* 111(42): 15220-15225.

13. Moffett JR, Ross B, Arun P, Madhavarao CN & Namboodiri AM (2007) N-acetylaspartate in the CNS: From neurodiagnostics to neurobiology*. Prog Neurobiol* 81(2): 89-131.

14. Moult PR (2009) Neuronal glutamate and GABAA receptor function in health and disease*. Biochem Soc Trans* 37(Pt 6): 1317-1322.

15. Gray SJ (2013) Gene therapy and neurodevelopmental disorders. *Neuropharmacology* 68: 136-142.

16. Bowles DE, Rabinowitz JE & Samulski RJ (2006) in *Parvoviruses,* eds Kerr JR, Cotmore SF, Bloom ME, Linden RM & Parrish CR (Edward Arnold Ltd., New York), pp 15-24.

17. Agbandje-McKenna M & Kleinschmidt J (2011) AAV capsid structure and cell interactions. *Methods Mol Biol* 807: 47-92.

18. Rabinowitz JE, *et al* (2002) Cross-packaging of a single adeno-associated virus (AAV) type 2 vector genome into multiple AAV serotypes enables transduction with broad specificity. *J Virol* 76(2): 791-801.

19. Vandenberghe LH, Wilson JM & Gao G (2009) Tailoring the AAV vector capsid for gene therapy. *Gene Ther* 16(3): 311-319.

20. Gao G, *et al* (2004) Clades of adeno-associated viruses are widely disseminated in human tissues. *J Virol* 78(12): 6381-6388.

21. Gao GP, *et al* (2002) Novel adeno-associated viruses from rhesus monkeys as vectors for human gene therapy. *Proc Natl Acad Sci U S A* 99(18): 11854-11859.

22. Xiao X, Li J & Samulski RJ (1998) Production of high-titer recombinant adeno-associated virus vectors in the absence of helper adenovirus. *J Virol* 72(3): 2224-2232.

23. Xiao X, Xiao W, Li J & Samulski RJ (1997) A novel 165-base-pair terminal repeat sequence is the sole cis requirement for the adeno-associated virus life cycle. *J Virol* 71(2): 941-948.

24. Grieger JC, Choi VW & Samulski RJ (2006) Production and characterization of adeno-associated viral vectors. *Nat Protoc* 1(3): 1412-1428.

25. Huang LY, Halder S & Agbandje-McKenna M (2014) Parvovirus glycan interactions. *Curr Opin Virol* 7C: 108-118.

26. Pillay S, *et al* (2016) An essential receptor for adeno-associated virus infection. *Nature* 530(7588): 108-112.

27. Lentz TB, Gray SJ & Samulski RJ (2012) Viral vectors for gene delivery to the central nervous system. *Neurobiol Dis* 48(2): 179-188.

28. Maguire CA, *et al* (2010) Directed evolution of adeno-associated virus for glioma cell transduction. *J Neurooncol* 96(3): 337-347.

29. Jang JH, *et al* (2011) An evolved adeno-associated viral variant enhances gene delivery and gene targeting in neural stem cells. *Mol Ther* 19(4): 667-675.

30. Gray SJ*, et al* (2010) Directed evolution of a novel adeno-associated virus (AAV) vector that crosses the seizure-compromised blood-brain barrier (BBB)*. Mol Ther* 18(3): 570-578.

31. Asokan A, Schaffer DV & Jude Samulski R (2012) The AAV vector toolkit: Poised at the clinical crossroads*. Mol Ther* 20(4): 699-708.

32. Walters RW*, et al* (2001) Binding of adeno-associated virus type 5 to 2,3-linked sialic acid is required for gene transfer*. J Biol Chem* 276(23): 20610-20616.

33. Wu Z, Miller E, Agbandje-McKenna M & Samulski RJ (2006) Alpha2,3 and alpha2,6 N-linked sialic acids facilitate efficient binding and transduction by adeno-associated virus types 1 and 6*. J Virol* 80(18): 9093-9103.

34. Kaludov N, Brown KE, Walters RW, Zabner J & Chiorini JA (2001) Adeno-associated virus serotype 4 (AAV4) and AAV5 both require sialic acid binding for hemagglutination and efficient transduction but differ in sialic acid linkage specificity*. J Virol* 75(15): 6884-6893.

35. Summerford C & Samulski RJ (1998) Membrane-associated heparan sulfate proteoglycan is a receptor for adeno-associated virus type 2 virions*. J Virol* 72(2): 1438-1445.

36. Handa A, Muramatsu S, Qiu J, Mizukami H & Brown KE (2000) Adeno-associated virus (AAV)-3-based vectors transduce haematopoietic cells not susceptible to transduction with AAV-2-based vectors*. J Gen Virol* 81(Pt 8): 2077-2084.

37. Shen S, Bryant KD, Brown SM, Randell SH & Asokan A (2011) Terminal N-linked galactose is the primary receptor for adeno-associated virus 9*. J Biol Chem* 286(15): 13532-13540.

38. Bell CL*, et al* (2011) The AAV9 receptor and its modification to improve in vivo lung gene transfer in mice*. J Clin Invest* 121(6): 2427-2435.

39. Bartlett JS, Samulski RJ & McCown TJ (1998) Selective and rapid uptake of adeno-associated virus type 2 in brain*. Hum Gene Ther* 9(8): 1181-1186.

40. Davidson BL*, et al* (2000) Recombinant adeno-associated virus type 2, 4, and 5 vectors: Transduction of variant cell types and regions in the mammalian central nervous system*. Proc Natl Acad Sci U S A* 97(7): 3428-3432.

41. Mandel RJ & Burger C (2004) Clinical trials in neurological disorders using AAV vectors: Promises and challenges*. Curr Opin Mol Ther* 6(5): 482-490.

42. Hsueh YP & Sheng M (1999) Regulated expression and subcellular localization of syndecan heparan sulfate proteoglycans and the syndecan-binding protein CASK/LIN-2 during rat brain development*. J Neurosci* 19(17): 7415-7425.

43. Hsueh YP*, et al* (1998) Direct interaction of CASK/LIN-2 and syndecan heparan sulfate proteoglycan and their overlapping distribution in neuronal synapses*. J Cell Biol* 142(1): 139-151.

44. Kawamoto S, Shi Q, Nitta Y, Miyazaki J & Allen MD (2005) Widespread and early myocardial gene expression by adeno-associated virus vector type 6 with a beta-actin hybrid promoter*. Mol Ther* 11(6): 980-985.

45. Wu Z*, et al* (2006) Single amino acid changes can influence titer, heparin binding, and tissue tropism in different adeno-associated virus serotypes*. J Virol* 80(22): 11393-11397.

46. Arnett AL*, et al* (2013) Heparin-binding correlates with increased efficiency of AAV1- and AAV6-mediated transduction of striated muscle, but negatively impacts CNS transduction*. Gene Ther* 20(5): 497-503.

47. Nguyen JB, Sanchez-Pernaute R, Cunningham J & Bankiewicz KS (2001) Convection-enhanced delivery of AAV-2 combined with heparin increases TK gene transfer in the rat brain*. Neuroreport* 12(9): 1961-1964.

48. Mastakov MY, Baer K, Kotin RM & During MJ (2002) Recombinant adeno-associated virus serotypes 2- and 5-mediated gene transfer in the mammalian brain: Quantitative analysis of heparin co-infusion*. Mol Ther* 5(4): 371-380.

49. Ahmed SS*, et al* (2013) A single intravenous rAAV injection as late as P20 achieves efficacious and sustained CNS gene therapy in canavan mice*. Mol Ther* 21(12): 2136-2147.

50. Yamashita T*, et al* (2013) Rescue of amyotrophic lateral sclerosis phenotype in a mouse model by intravenous AAV9-ADAR2 delivery to motor neurons*. EMBO Mol Med* 5(11): 1710-1719.

51. Benkhelifa-Ziyyat S*, et al* (2013) Intramuscular scAAV9-SMN injection mediates widespread gene delivery to the spinal cord and decreases disease severity in SMA mice*. Mol Ther* 21(2): 282-290.

52. Iwata N*, et al* (2013) Global brain delivery of neprilysin gene by intravascular administration of AAV vector in mice*. Sci Rep* 3: 1472.

53. Dayton RD, Wang DB & Klein RL (2012) The advent of AAV9 expands applications for brain and spinal cord gene delivery*. Expert Opin Biol Ther* 12(6): 757-766.

54. Bevan AK*, et al* (2011) Systemic gene delivery in large species for targeting spinal cord, brain, and peripheral tissues for pediatric disorders*. Mol Ther* 19(11): 1971-1980.

55. Cearley CN & Wolfe JH (2007) A single injection of an adeno-associated virus vector into nuclei with divergent connections results in widespread vector distribution in

the brain and global correction of a neurogenetic disease. *J Neurosci* 27(37): 9928-9940.

56. Foust KD, *et al* (2009) Intravascular AAV9 preferentially targets neonatal neurons and adult astrocytes. *Nat Biotechnol* 27(1): 59-65.

57. Chamberlin NL, Du B, de Lacalle S & Saper CB (1998) Recombinant adeno-associated virus vector: Use for transgene expression and anterograde tract tracing in the CNS. *Brain Res* 793(1-2): 169-175.

58. McCown TJ, Xiao X, Li J, Breese GR & Samulski RJ (1996) Differential and persistent expression patterns of CNS gene transfer by an adeno-associated virus (AAV) vector. *Brain Res* 713(1-2): 99-107.

59. Bockstael O, *et al* (2012) Rapid transgene expression in multiple precursor cell types of adult rat subventricular zone mediated by adeno-associated type 1 vectors. *Hum Gene Ther* 23(7): 742-753.

60. Tenenbaum L, *et al* (2004) Recombinant AAV-mediated gene delivery to the central nervous system. *J Gene Med* 6 Suppl 1: S212-22.

61. Sawamoto K, *et al* (2006) New neurons follow the flow of cerebrospinal fluid in the adult brain. *Science* 311(5761): 629-632.

62. Iliff JJ, *et al* (2012) A paravascular pathway facilitates CSF flow through the brain parenchyma and the clearance of interstitial solutes, including amyloid beta. *Sci Transl Med* 4(147): 147ra111.

63. Koh L, Zakharov A & Johnston M (2005) Integration of the subarachnoid space and lymphatics: Is it time to embrace a new concept of cerebrospinal fluid absorption? *Cerebrospinal Fluid Res* 2: 6.

64. Lehtinen MK, *et al* (2013) The choroid plexus and cerebrospinal fluid: Emerging roles in development, disease, and therapy. *J Neurosci* 33(45): 17553-17559.

65. Samaranch L, *et al* (2013) Strong cortical and spinal cord transduction after AAV7 and AAV9 delivery into the cerebrospinal fluid of nonhuman primates. *Hum Gene Ther* 24(5): 526-532.

66. Samaranch L, *et al* (2012) Adeno-associated virus serotype 9 transduction in the central nervous system of nonhuman primates. *Hum Gene Ther* 23(4): 382-389.

67. Fu H, *et al* (2003) Self-complementary adeno-associated virus serotype 2 vector: Global distribution and broad dispersion of AAV-mediated transgene expression in mouse brain. *Mol Ther* 8(6): 911-917.

68. Fu H*, et al* (2007) Significantly increased lifespan and improved behavioral performances by rAAV gene delivery in adult mucopolysaccharidosis IIIB mice*. Gene Ther* 14(14): 1065-1077.

69. Liu G, Martins I, Wemmie JA, Chiorini JA & Davidson BL (2005) Functional correction of CNS phenotypes in a lysosomal storage disease model using adeno-associated virus type 4 vectors*. J Neurosci* 25(41): 9321-9327.

70. Passini MA & Wolfe JH (2001) Widespread gene delivery and structure-specific patterns of expression in the brain after intraventricular injections of neonatal mice with an adeno-associated virus vector*. J Virol* 75(24): 12382-12392.

71. Davidson BL*, et al* (2000) Recombinant adeno-associated virus type 2, 4, and 5 vectors: Transduction of variant cell types and regions in the mammalian central nervous system*. Proc Natl Acad Sci U S A* 97(7): 3428-3432.

72. Chakrabarty P*, et al* (2013) Capsid serotype and timing of injection determines AAV transduction in the neonatal mice brain*. PLoS One* 8(6): e67680.

73. Glascock JJ*, et al* (2012) Decreasing disease severity in symptomatic, smn(-/-);SMN2(+/+), spinal muscular atrophy mice following scAAV9-SMN delivery*. Hum Gene Ther* 23(3): 330-335.

74. Rafi MA, Rao HZ, Luzi P, Curtis MT & Wenger DA (2012) Extended normal life after AAVrh10-mediated gene therapy in the mouse model of krabbe disease*. Mol Ther* 20(11): 2031-2042.

75. Cabrera-Salazar MA*, et al* (2010) Intracerebroventricular delivery of glucocerebrosidase reduces substrates and increases lifespan in a mouse model of neuronopathic gaucher disease*. Exp Neurol* 225(2): 436-444.

76. Liu G, Martins I, Wemmie JA, Chiorini JA & Davidson BL (2005) Functional correction of CNS phenotypes in a lysosomal storage disease model using adeno-associated virus type 4 vectors*. J Neurosci* 25(41): 9321-9327.

77. Liu G, Martins IH, Chiorini JA & Davidson BL (2005) Adeno-associated virus type 4 (AAV4) targets ependyma and astrocytes in the subventricular zone and RMS*. Gene Ther* 12(20): 1503-1508.

78. Alvarez-Buylla A & Lim DA (2004) For the long run: Maintaining germinal niches in the adult brain*. Neuron* 41(5): 683-686.

79. Benraiss A*, et al* (2012) Sustained induction of neuronal addition to the adult rat neostriatum by AAV4-delivered noggin and BDNF*. Gene Ther* 19(5): 483-493.

80. Govindasamy L*, et al* (2006) Structurally mapping the diverse phenotype of adeno-associated virus serotype 4*. J Virol* 80(23): 11556-11570.

81. Padron E*, et al* (2005) Structure of adeno-associated virus type 4*. J Virol* 79(8): 5047-5058.

82. Jacques SJ*, et al* (2012) AAV8(gfp) preferentially targets large diameter dorsal root ganglion neurones after both intra-dorsal root ganglion and intrathecal injection*. Mol Cell Neurosci* 49(4): 464-474.

83. Vulchanova L*, et al* (2010) Differential adeno-associated virus mediated gene transfer to sensory neurons following intrathecal delivery by direct lumbar puncture*. Mol Pain* 6: 31-8069-6-31.

84. Hirai T*, et al* (2012) Intrathecal shRNA-AAV9 inhibits target protein expression in the spinal cord and dorsal root ganglia of adult mice*. Hum Gene Ther Methods* 23(2): 119-127.

85. Snyder BR*, et al* (2011) Comparison of adeno-associated viral vector serotypes for spinal cord and motor neuron gene delivery*. Hum Gene Ther* 22(9): 1129-1135.

86. Federici T*, et al* (2012) Robust spinal motor neuron transduction following intrathecal delivery of AAV9 in pigs*. Gene Ther* 19(8): 852-859.

87. Gray SJ, Nagabhushan Kalburgi S, McCown TJ & Jude Samulski R (2013) Global CNS gene delivery and evasion of anti-AAV-neutralizing antibodies by intrathecal AAV administration in non-human primates*. Gene Ther* 20(4): 450-459.

88. Lin D*, et al* (2005) AAV2/5 vector expressing galactocerebrosidase ameliorates CNS disease in the murine model of globoid-cell leukodystrophy more efficiently than AAV2*. Mol Ther* 12(3): 422-430.

89. Burger C*, et al* (2004) Recombinant AAV viral vectors pseudotyped with viral capsids from serotypes 1, 2, and 5 display differential efficiency and cell tropism after delivery to different regions of the central nervous system*. Mol Ther* 10(2): 302-317.

90. Cearley CN & Wolfe JH (2006) Transduction characteristics of adeno-associated virus vectors expressing cap serotypes 7, 8, 9, and Rh10 in the mouse brain*. Mol Ther* 13(3): 528-537.

91. Broekman ML, Comer LA, Hyman BT & Sena-Esteves M (2006) Adeno-associated virus vectors serotyped with AAV8 capsid are more efficient than AAV-1 or -2 serotypes for widespread gene delivery to the neonatal mouse brain*. Neuroscience* 138(2): 501-510.

92. Cearley CN*, et al* (2008) Expanded repertoire of AAV vector serotypes mediate unique patterns of transduction in mouse brain*. Mol Ther* 16(10): 1710-1718.

93. Sondhi D*, et al* (2007) Enhanced survival of the LINCL mouse following CLN2 gene transfer using the rh.10 rhesus macaque-derived adeno-associated virus vector*. Mol Ther* 15(3): 481-491.

94. Gray SJ*, et al* (2011) Preclinical differences of intravascular AAV9 delivery to neurons and glia: A comparative study of adult mice and nonhuman primates*. Mol Ther* 19(6): 1058-1069.

95. Bevan AK*, et al* (2011) Systemic gene delivery in large species for targeting spinal cord, brain, and peripheral tissues for pediatric disorders*. Mol Ther* 19(11): 1971-1980.

96. Zhang H*, et al* (2011) Several rAAV vectors efficiently cross the blood-brain barrier and transduce neurons and astrocytes in the neonatal mouse central nervous system*. Mol Ther* 19(8): 1440-1448.

97. Yang B*, et al* (2014) Global CNS transduction of adult mice by intravenously delivered rAAVrh.8 and rAAVrh.10 and nonhuman primates by rAAVrh.10*. Mol Ther*

98. McCarty DM, DiRosario J, Gulaid K, Muenzer J & Fu H (2009) Mannitol-facilitated CNS entry of rAAV2 vector significantly delayed the neurological disease progression in MPS IIIB mice*. Gene Ther* 16(11): 1340-1352.

99. Shen F*, et al* (2013) Intravenous delivery of adeno-associated viral vector serotype 9 mediates effective gene expression in ischemic stroke lesion and brain angiogenic foci*. Stroke* 44(1): 252-254.

100. Chen YH, Claflin K, Geoghegan JC & Davidson BL (2012) Sialic acid deposition impairs the utility of AAV9, but not peptide-modified AAVs for brain gene therapy in a mouse model of lysosomal storage disease*. Mol Ther* 20(7): 1393-1399.

101. Rosenberg JB*, et al* (2014) Comparative efficacy and safety of multiple routes of direct CNS administration of adeno-associated virus gene transfer vector serotype rh.10 expressing the human arylsulfatase A cDNA to nonhuman primates*. Hum Gene Ther Clin Dev*

102. Rennels ML, Gregory TF, Blaumanis OR, Fujimoto K & Grady PA (1985) Evidence for a 'paravascular' fluid circulation in the mammalian central nervous system, provided by the rapid distribution of tracer protein throughout the brain from the subarachnoid space*. Brain Res* 326(1): 47-63.

103. Hadaczek P*, et al* (2006) The "perivascular pump" driven by arterial pulsation is a powerful mechanism for the distribution of therapeutic molecules within the brain*. Mol Ther* 14(1): 69-78.

104. Cserr HF, Harling-Berg CJ & Knopf PM (1992) Drainage of brain extracellular fluid into blood and deep cervical lymph and its immunological significance*. Brain Pathol* 2(4): 269-276.

105. Abbott NJ (2004) Evidence for bulk flow of brain interstitial fluid: Significance for physiology and pathology*. Neurochem Int* 45(4): 545-552.

106. Beier KT*, et al* (2011) Anterograde or retrograde transsynaptic labeling of CNS neurons with vesicular stomatitis virus vectors*. Proc Natl Acad Sci U S A* 108(37): 15414-15419.

107. Taylor MP, Kobiler O & Enquist LW (2012) Alphaherpesvirus axon-to-cell spread involves limited virion transmission*. Proc Natl Acad Sci U S A* 109(42): 17046-17051.

108. Granstedt AE, Brunton BW & Enquist LW (2013) Imaging the transport dynamics of single alphaherpesvirus particles in intact peripheral nervous system explants from infected mice*. Mbio* 4(3): e00358-13.

109. Rothermel M, Brunert D, Zabawa C, Diaz-Quesada M & Wachowiak M (2013) Transgene expression in target-defined neuron populations mediated by retrograde infection with adeno-associated viral vectors*. J Neurosci* 33(38): 15195-15206.

110. Wickersham IR, Finke S, Conzelmann KK & Callaway EM (2007) Retrograde neuronal tracing with a deletion-mutant rabies virus*. Nat Methods* 4(1): 47-49.

111. Osakada F*, et al* (2011) New rabies virus variants for monitoring and manipulating activity and gene expression in defined neural circuits*. Neuron* 71(4): 617-631.

112. Salegio EA*, et al* (2013) Axonal transport of adeno-associated viral vectors is serotype-dependent*. Gene Ther* 20(3): 348-352.

113. Hollis ER,2nd, Kadoya K, Hirsch M, Samulski RJ & Tuszynski MH (2008) Efficient retrograde neuronal transduction utilizing self-complementary AAV1*. Mol Ther* 16(2): 296-301.

114. Kells AP*, et al* (2009) Efficient gene therapy-based method for the delivery of therapeutics to primate cortex*. Proc Natl Acad Sci U S A* 106(7): 2407-2411.

115. Ciesielska A*, et al* (2011) Anterograde axonal transport of AAV2-GDNF in rat basal ganglia*. Mol Ther* 19(5): 922-927.

116. San Sebastian W*, et al* (2013) Adeno-associated virus type 6 is retrogradely transported in the non-human primate brain*. Gene Ther* 20(12): 1178-1183.

117. Low K, Aebischer P & Schneider BL (2013) Direct and retrograde transduction of nigral neurons with AAV6, 8, and 9 and intraneuronal persistence of viral particles*. Hum Gene Ther* 24(6): 613-629.

118. Castle MJ, Perlson E, Holzbaur EL & Wolfe JH (2014) Long-distance axonal transport of AAV9 is driven by dynein and kinesin-2 and is trafficked in a highly motile Rab7-positive compartment*. Mol Ther* 22(3): 554-566.

119. Masamizu Y*, et al* (2011) Local and retrograde gene transfer into primate neuronal pathways via adeno-associated virus serotype 8 and 9*. Neuroscience* 193: 249-258.

120. Castle MJ, Gershenson ZT, Giles AR, Holzbaur EL & Wolfe JH (2014) Adeno-associated virus serotypes 1, 8, and 9 share conserved mechanisms for anterograde and retrograde axonal transport. *Hum Gene Ther*

121. Shepherd GM (2013) Corticostriatal connectivity and its role in disease. *Nat Rev Neurosci* 14(4): 278-291.

122. Eslamboli A, *et al* (2007) Long-term consequences of human alpha-synuclein overexpression in the primate ventral midbrain. *Brain* 130(Pt 3): 799-815.

123. Periquet M, Fulga T, Myllykangas L, Schlossmacher MG & Feany MB (2007) Aggregated alpha-synuclein mediates dopaminergic neurotoxicity in vivo. *J Neurosci* 27(12): 3338-3346.

124. Giacobini E & Gold G (2013) Alzheimer disease therapy--moving from amyloid-beta to tau. *Nat Rev Neurol* 9(12): 677-686.

125. Pronin AN, Morris AJ, Surguchov A & Benovic JL (2000) Synucleins are a novel class of substrates for G protein-coupled receptor kinases. *J Biol Chem* 275(34): 26515-26522.

126. Chen L & Feany MB (2005) Alpha-synuclein phosphorylation controls neurotoxicity and inclusion formation in a drosophila model of parkinson disease. *Nat Neurosci* 8(5): 657-663.

127. Fujiwara H, *et al* (2002) Alpha-synuclein is phosphorylated in synucleinopathy lesions. *Nat Cell Biol* 4(2): 160-164.

128. Anderson JP, *et al* (2006) Phosphorylation of ser-129 is the dominant pathological modification of alpha-synuclein in familial and sporadic lewy body disease. *J Biol Chem* 281(40): 29739-29752.

129. Gorbatyuk OS, *et al* (2008) The phosphorylation state of ser-129 in human alpha-synuclein determines neurodegeneration in a rat model of parkinson disease. *Proc Natl Acad Sci U S A* 105(2): 763-768.

130. Nagatsu T & Sawada M (2007) Biochemistry of postmortem brains in parkinson's disease: Historical overview and future prospects. *J Neural Transm Suppl* (72)(72): 113-120.

131. Li XG, *et al* (2006) Viral-mediated temporally controlled dopamine production in a rat model of parkinson disease. *Mol Ther* 13(1): 160-166.

132. Branda CS & Dymecki SM (2004) Talking about a revolution: The impact of site-specific recombinases on genetic analyses in mice. *Dev Cell* 6(1): 7-28.

133. Muramatsu S, *et al* (2010) A phase I study of aromatic L-amino acid decarboxylase gene therapy for parkinson's disease. *Mol Ther* 18(9): 1731-1735.

134. Lang AE & Lozano AM (1998) Parkinson's disease. second of two parts. *N Engl J Med* 339(16): 1130-1143.

135. Olanow CW, Obeso JA & Stocchi F (2006) Continuous dopamine-receptor treatment of parkinson's disease: Scientific rationale and clinical implications. *Lancet Neurol* 5(8): 677-687.

136. Obeso JA, *et al* (2000) Pathophysiology of the basal ganglia in parkinson's disease. *Trends Neurosci* 23(10 Suppl): S8-19.

137. Cederfjall E, Sahin G, Kirik D & Bjorklund T (2012) Design of a single AAV vector for coexpression of TH and GCH1 to establish continuous DOPA synthesis in a rat model of parkinson's disease. *Mol Ther* 20(7): 1315-1326.

138. Cederfjall E, *et al* (2013) Continuous DOPA synthesis from a single AAV: Dosing and efficacy in models of parkinson's disease. *Sci Rep* 3: 2157.

139. Gasmi M, *et al* (2007) Striatal delivery of neurturin by CERE-120, an AAV2 vector for the treatment of dopaminergic neuron degeneration in parkinson's disease. *Mol Ther* 15(1): 62-68.

140. Hida H, *et al* (2003) Pleiotrophin exhibits a trophic effect on survival of dopaminergic neurons in vitro. *Eur J Neurosci* 17(10): 2127-2134.

141. Marchionini DM, *et al* (2007) Role of heparin binding growth factors in nigrostriatal dopamine system development and parkinson's disease. *Brain Res* 1147: 77-88.

142. Gombash SE, *et al* (2012) Striatal pleiotrophin overexpression provides functional and morphological neuroprotection in the 6-hydroxydopamine model. *Mol Ther* 20(3): 544-554.

143. Georgievska B, Kirik D & Bjorklund A (2002) Aberrant sprouting and downregulation of tyrosine hydroxylase in lesioned nigrostriatal dopamine neurons induced by long-lasting overexpression of glial cell line derived neurotrophic factor in the striatum by lentiviral gene transfer. *Exp Neurol* 177(2): 461-474.

144. Kirik D, Rosenblad C, Bjorklund A & Mandel RJ (2000) Long-term rAAV-mediated gene transfer of GDNF in the rat parkinson's model: Intrastriatal but not intranigral transduction promotes functional regeneration in the lesioned nigrostriatal system. *J Neurosci* 20(12): 4686-4700.

145. Mendez I, *et al* (2005) Cell type analysis of functional fetal dopamine cell suspension transplants in the striatum and substantia nigra of patients with parkinson's disease. *Brain* 128(Pt 7): 1498-1510.

146. Rosenstein JM (1995) Why do neural transplants survive? an examination of some metabolic and pathophysiological considerations in neural transplantation. *Exp Neurol* 133(1): 1-6.

147. Kordower JH, Liu YT, Winn S & Emerich DF (1995) Encapsulated PC12 cell transplants into hemiparkinsonian monkeys: A behavioral, neuroanatomical, and neurochemical analysis. *Cell Transplant* 4(2): 155-171.

148. Redmond DE,Jr, *et al* (2013) Comparison of fetal mesencephalic grafts, AAV-delivered GDNF, and both combined in an MPTP-induced nonhuman primate parkinson's model. *Mol Ther* 21(12): 2160-2168.

149. Csete M, Rodriguez L, Wilcox M & Chadalavada S (2004) Erythropoietin receptor is expressed on adult rat dopaminergic neurons and erythropoietin is neurotrophic in cultured dopaminergic neuroblasts. *Neurosci Lett* 359(1-2): 124-126.

150. Demers EJ, McPherson RJ & Juul SE (2005) Erythropoietin protects dopaminergic neurons and improves neurobehavioral outcomes in juvenile rats after neonatal hypoxia-ischemia. *Pediatr Res* 58(2): 297-301.

151. Genc S, *et al* (2001) Erythropoietin exerts neuroprotection in 1-methyl-4-phenyl-1,2,3,6-tetrahydropyridine-treated C57/BL mice via increasing nitric oxide production. *Neurosci Lett* 298(2): 139-141.

152. Zhang F, *et al* (2006) Erythropoietin protects CA1 neurons against global cerebral ischemia in rat: Potential signaling mechanisms. *J Neurosci Res* 83(7): 1241-1251.

153. Xue YQ, *et al* (2010) AAV9-mediated erythropoietin gene delivery into the brain protects nigral dopaminergic neurons in a rat model of parkinson's disease. *Gene Ther* 17(1): 83-94.

154. Bankiewicz KS, *et al* (2000) Convection-enhanced delivery of AAV vector in parkinsonian monkeys; in vivo detection of gene expression and restoration of dopaminergic function using pro-drug approach. *Exp Neurol* 164(1): 2-14.

155. Peterson AL & Nutt JG (2008) Treatment of parkinson's disease with trophic factors. *Neurotherapeutics* 5(2): 270-280.

156. Aron L & Klein R (2011) Repairing the parkinsonian brain with neurotrophic factors. *Trends Neurosci* 34(2): 88-100.

157. Emborg ME, *et al* (2007) Subthalamic glutamic acid decarboxylase gene therapy: Changes in motor function and cortical metabolism. *J Cereb Blood Flow Metab* 27(3): 501-509.

158. Luo J, *et al* (2002) Subthalamic GAD gene therapy in a parkinson's disease rat model. *Science* 298(5592): 425-429.

159. Bartus RT (2012) Translating the therapeutic potential of neurotrophic factors to clinical 'proof of concept': A personal saga achieving a career-long quest. *Neurobiol Dis* 48(2): 153-178.

160. Nauta HJ, Wehman JC, Koliatsos VE, Terrell MA & Chung K (1999) Intraventricular infusion of nerve growth factor as the cause of sympathetic fiber sprouting in sensory ganglia. *J Neurosurg* 91(3): 447-453.

161. Nutt JG, *et al* (2003) Randomized, double-blind trial of glial cell line-derived neurotrophic factor (GDNF) in PD. *Neurology* 60(1): 69-73.

162. Lang AE, *et al* (2006) Randomized controlled trial of intraputamenal glial cell line-derived neurotrophic factor infusion in parkinson disease. *Ann Neurol* 59(3): 459-466.

163. Hovland DN,Jr, *et al* (2007) Six-month continuous intraputamenal infusion toxicity study of recombinant methionyl human glial cell line-derived neurotrophic factor (r-metHuGDNF in rhesus monkeys. *Toxicol Pathol* 35(7): 1013-1029.

164. Bartus RT, Weinberg MS & Samulski RJ (2014) Parkinson's disease gene therapy: Success by design meets failure by efficacy. *Mol Ther* 22(3): 487-497.

165. HERS HG (1965) Inborn lysosomal diseases. *Gastroenterology* 48: 625-633.

166. Haltia M & Goebel HH (2013) The neuronal ceroid-lipofuscinoses: A historical introduction. *Biochim Biophys Acta* 1832(11): 1795-1800.

167. Parenti G (2009) Treating lysosomal storage diseases with pharmacological chaperones: From concept to clinics. *EMBO Mol Med* 1(5): 268-279.

168. Sly WS, Quinton BA, McAlister WH & Rimoin DL (1973) Beta glucuronidase deficiency: Report of clinical, radiologic, and biochemical features of a new mucopolysaccharidosis. *J Pediatr* 82(2): 249-257.

169. Daly TM, Ohlemiller KK, Roberts MS, Vogler CA & Sands MS (2001) Prevention of systemic clinical disease in MPS VII mice following AAV-mediated neonatal gene transfer. *Gene Ther* 8(17): 1291-1298.

170. Daly TM, Vogler C, Levy B, Haskins ME & Sands MS (1999) Neonatal gene transfer leads to widespread correction of pathology in a murine model of lysosomal storage disease. *Proc Natl Acad Sci U S A* 96(5): 2296-2300.

171. Elliger SS, Elliger CA, Aguilar CP, Raju NR & Watson GL (1999) Elimination of lysosomal storage in brains of MPS VII mice treated by intrathecal administration of an adeno-associated virus vector. *Gene Ther* 6(6): 1175-1178.

172. Murlidharan G, Samulski RJ & Asokan A (2014) Biology of adeno-associated viral vectors in the central nervous system. *Front Mol Neurosci* 7: 0076.

173. Skorupa AF, Fisher KJ, Wilson JM, Parente MK & Wolfe JH (1999) Sustained production of beta-glucuronidase from localized sites after AAV vector gene transfer results in widespread distribution of enzyme and reversal of lysosomal storage lesions in a large volume of brain in mucopolysaccharidosis VII mice. *Exp Neurol* 160(1): 17-27.

174. Bosch A, Perret E, Desmaris N & Heard JM (2000) Long-term and significant correction of brain lesions in adult mucopolysaccharidosis type VII mice using recombinant AAV vectors. *Mol Ther* 1(1): 63-70.

175. Sferra TJ, *et al* (2000) Recombinant adeno-associated virus-mediated correction of lysosomal storage within the central nervous system of the adult mucopolysaccharidosis type VII mouse. *Hum Gene Ther* 11(4): 507-519.

176. Hennig AK, *et al* (2003) Intravitreal gene therapy reduces lysosomal storage in specific areas of the CNS in mucopolysaccharidosis VII mice. *J Neurosci* 23(8): 3302-3307.

177. Karolewski BA & Wolfe JH (2006) Genetic correction of the fetal brain increases the lifespan of mice with the severe multisystemic disease mucopolysaccharidosis type VII. *Mol Ther* 14(1): 14-24.

178. Frisella WA, *et al* (2001) Intracranial injection of recombinant adeno-associated virus improves cognitive function in a murine model of mucopolysaccharidosis type VII. *Mol Ther* 3(3): 351-358.

179. Liu G, *et al* (2007) Adeno-associated virus type 5 reduces learning deficits and restores glutamate receptor subunit levels in MPS VII mice CNS. *Mol Ther* 15(2): 242-247.

180. Fu H, *et al* (2002) Neurological correction of lysosomal storage in a mucopolysaccharidosis IIIB mouse model by adeno-associated virus-mediated gene delivery. *Mol Ther* 5(1): 42-49.

181. Cressant A, *et al* (2004) Improved behavior and neuropathology in the mouse model of sanfilippo type IIIB disease after adeno-associated virus-mediated gene transfer in the striatum. *J Neurosci* 24(45): 10229-10239.

182. Summerford C & Samulski RJ (1998) Membrane-associated heparan sulfate proteoglycan is a receptor for adeno-associated virus type 2 virions. *J Virol* 72(2): 1438-1445.

183. Fu H, *et al* (2007) Significantly increased lifespan and improved behavioral performances by rAAV gene delivery in adult mucopolysaccharidosis IIIB mice. *Gene Ther* 14(14): 1065-1077.

184. Fu H, *et al* (2003) Self-complementary adeno-associated virus serotype 2 vector: Global distribution and broad dispersion of AAV-mediated transgene expression in mouse brain. *Mol Ther* 8(6): 911-917.

185. Heldermon CD, *et al* (2010) Therapeutic efficacy of bone marrow transplant, intracranial AAV-mediated gene therapy, or both in the mouse model of MPS IIIB. *Mol Ther* 18(5): 873-880.

186. McCarty DM, Young SM,Jr & Samulski RJ (2004) Integration of adeno-associated virus (AAV) and recombinant AAV vectors. *Annu Rev Genet* 38: 819-845.

187. Bokhoven M, *et al* (2009) Insertional gene activation by lentiviral and gammaretroviral vectors. *J Virol* 83(1): 283-294.

188. Nash K, Chen W & Muzyczka N (2008) Complete in vitro reconstitution of adeno-associated virus DNA replication requires the minichromosome maintenance complex proteins. *J Virol* 82(3): 1458-1464.

189. Duan D, *et al* (1998) Circular intermediates of recombinant adeno-associated virus have defined structural characteristics responsible for long-term episomal persistence in muscle tissue. *J Virol* 72(11): 8568-8577.

190. Dismuke DJ, Tenenbaum L & Samulski RJ (2013) Biosafety of recombinant adeno-associated virus vectors. *Curr Gene Ther* 13(6): 434-452.

191. Hadaczek P, *et al* (2009) Transduction of nonhuman primate brain with adeno-associated virus serotype 1: Vector trafficking and immune response. *Hum Gene Ther* 20(3): 225-237.

192. Ciesielska A, *et al* (2013) Cerebral infusion of AAV9 vector-encoding non-self proteins can elicit cell-mediated immune responses. *Mol Ther* 21(1): 158-166.

193. Koyuncu OO, Hogue IB & Enquist LW (2013) Virus infections in the nervous system. *Cell Host Microbe* 13(4): 379-393.

194. Racaniello VR (2006) One hundred years of poliovirus pathogenesis. *Virology* 344(1): 9-16.

195. Kopp SJ, *et al* (2009) Infection of neurons and encephalitis after intracranial inoculation of herpes simplex virus requires the entry receptor nectin-1. *Proc Natl Acad Sci U S A* 106(42): 17916-17920.

196. Lafon M (2005) Rabies virus receptors. *J Neurovirol* 11(1): 82-87.

197. Varki A & Schauer R (2009) in *Essentials of Glycobiology,* eds Varki A, et al (The Consortium of Glycobiology Editors, La Jolla, California, Cold Spring Harbor (NY)),

198. Cohen M & Varki A (2010) The sialome--far more than the sum of its parts. *Omics* 14(4): 455-464.

199. Neu U, Bauer J & Stehle T (2011) Viruses and sialic acids: Rules of engagement. *Curr Opin Struct Biol* 21(5): 610-618.

200. Frierson JM, *et al* (2012) Utilization of sialylated glycans as coreceptors enhances the neurovirulence of serotype 3 reovirus. *J Virol* 86(24): 13164-13173.

201. Maginnis MS, Nelson CD & Atwood WJ (2014) JC polyomavirus attachment, entry, and trafficking: Unlocking the keys to a fatal infection. *J Neurovirol*

202. Shen S, *et al* (2012) Glycan binding avidity determines the systemic fate of adeno-associated virus type 9. *J Virol* 86(19): 10408-10417.

203. Shen S, Troupes AN, Pulicherla N & Asokan A (2013) Multiple roles for sialylated glycans in determining the cardiopulmonary tropism of adeno-associated virus 4. *J Virol* 87(24): 13206-13213.

204. Walters RW, Pilewski JM, Chiorini JA & Zabner J (2002) Secreted and transmembrane mucins inhibit gene transfer with AAV4 more efficiently than AAV5. *J Biol Chem* 277(26): 23709-23713.

205. Shen S, Troupes AN, Pulicherla N & Asokan A (2013) Multiple roles for sialylated glycans in determining the cardiopulmonary tropism of adeno-associated virus 4. *J Virol* 87(24): 13206-13213.

206. Shen S, *et al* (2013) Engraftment of a galactose receptor footprint onto adeno-associated viral capsids improves transduction efficiency. *J Biol Chem*

207. Hauck B, Zhao W, High K & Xiao W (2004) Intracellular viral processing, not single-stranded DNA accumulation, is crucial for recombinant adeno-associated virus transduction. *J Virol* 78(24): 13678-13686.

208. Berns KI & Adler S (1972) Separation of two types of adeno-associated virus particles containing complementary polynucleotide chains. *J Virol* 9(2): 394-396.

209. Schnaar RL, Gerardy-Schahn R & Hildebrandt H (2014) Sialic acids in the brain: Gangliosides and polysialic acid in nervous system development, stability, disease, and regeneration. *Physiol Rev* 94(2): 461-518.

210. Rutishauser U (2008) Polysialic acid in the plasticity of the developing and adult vertebrate nervous system. *Nat Rev Neurosci* 9(1): 26-35.

211. Battista D & Rutishauser U (2010) Removal of polysialic acid triggers dispersion of subventricularly derived neuroblasts into surrounding CNS tissues. *J Neurosci* 30(11): 3995-4003.

212. Ono K, Tomasiewicz H, Magnuson T & Rutishauser U (1994) N-CAM mutation inhibits tangential neuronal migration and is phenocopied by enzymatic removal of polysialic acid. *Neuron* 13(3): 595-609.

213. Gage FH (2000) Mammalian neural stem cells. *Science* 287(5457): 1433-1438.

214. Ponti G, Peretto P & Bonfanti L (2006) A subpial, transitory germinal zone forms chains of neuronal precursors in the rabbit cerebellum. *Dev Biol* 294(1): 168-180.

215. Bonfanti L (2006) PSA-NCAM in mammalian structural plasticity and neurogenesis. *Prog Neurobiol* 80(3): 129-164.

216. Mali P, *et al* (2013) RNA-guided human genome engineering via Cas9. *Science* 339(6121): 823-826.

217. Cong L, *et al* (2013) Multiplex genome engineering using CRISPR/Cas systems. *Science* 339(6121): 819-823.

218. Cho SW, Kim S, Kim JM & Kim JS (2013) Targeted genome engineering in human cells with the Cas9 RNA-guided endonuclease. *Nat Biotechnol* 31(3): 230-232.

219. Jinek M, *et al* (2013) RNA-programmed genome editing in human cells. *Elife* 2: e00471.

220. Yin H, *et al* (2016) Therapeutic genome editing by combined viral and non-viral delivery of CRISPR system components in vivo. *Nat Biotechnol* 34(3): 328-333.

221. Swiech L, *et al* (2015) In vivo interrogation of gene function in the mammalian brain using CRISPR-Cas9. *Nat Biotechnol* 33(1): 102-106.

222. Platt RJ, *et al* (2014) CRISPR-Cas9 knockin mice for genome editing and cancer modeling. *Cell* 159(2): 440-455.

223. Ran FA, *et al* (2015) In vivo genome editing using staphylococcus aureus Cas9. *Nature* 520(7546): 186-191.

224. Nelson CE, *et al* (2016) In vivo genome editing improves muscle function in a mouse model of duchenne muscular dystrophy. *Science* 351(6271): 403-407.

225. Tabebordbar M, *et al* (2016) In vivo gene editing in dystrophic mouse muscle and muscle stem cells. *Science* 351(6271): 407-411.

226. Jinek M, *et al* (2012) A programmable dual-RNA-guided DNA endonuclease in adaptive bacterial immunity. *Science* 337(6096): 816-821.

227. Kabadi AM, Ousterout DG, Hilton IB & Gersbach CA (2014) Multiplex CRISPR/Cas9-based genome engineering from a single lentiviral vector. *Nucleic Acids Res* 42(19): e147.

228. Sander JD & Joung JK (2014) CRISPR-cas systems for editing, regulating and targeting genomes. *Nat Biotechnol* 32(4): 347-355.

229. Murlidharan G, Samulski RJ & Asokan A (2014) Biology of adeno-associated viral vectors in the central nervous system. *Front Mol Neurosci* 7: 76.

230. Hastie E & Samulski RJ (2015) Adeno-associated virus at 50: A golden anniversary of discovery, research, and gene therapy success--a personal perspective. *Hum Gene Ther* 26(5): 257-265.

231. Ojala DS, Amara DP & Schaffer DV (2015) Adeno-associated virus vectors and neurological gene therapy. *Neuroscientist* 21(1): 84-98.

232. Smith PD, Coulson-Thomas VJ, Foscarin S, Kwok JC & Fawcett JW (2015) "GAG-ing with the neuron": The role of glycosaminoglycan patterning in the central nervous system. *Exp Neurol*

233. Gardner CL, Ebel GD, Ryman KD & Klimstra WB (2011) Heparan sulfate binding by natural eastern equine encephalitis viruses promotes neurovirulence. *Proc Natl Acad Sci U S A* 108(38): 16026-16031.

234. Ryman KD, *et al* (2007) Heparan sulfate binding can contribute to the neurovirulence of neuroadapted and nonneuroadapted sindbis viruses. *J Virol* 81(7): 3563-3573.

235. Yang B, *et al* (2014) Global CNS transduction of adult mice by intravenously delivered rAAVrh.8 and rAAVrh.10 and nonhuman primates by rAAVrh.10. *Mol Ther* 22(7): 1299-1309.

236. Flotte TR (2013) Birth of a new therapeutic platform: 47 years of adeno-associated virus biology from virus discovery to licensed gene therapy. *Mol Ther* 21(11): 1976-1981.

237. Nathwani AC, *et al* (2014) Long-term safety and efficacy of factor IX gene therapy in hemophilia B. *N Engl J Med* 371(21): 1994-2004.

238. Tuszynski MH, *et al* (2015) Nerve growth factor gene therapy: Activation of neuronal responses in alzheimer disease. *JAMA Neurol*

239. Jacobson SG, *et al* (2015) Improvement and decline in vision with gene therapy in childhood blindness. *N Engl J Med* 372(20): 1920-1926.

240. Mingozzi F & High KA (2013) Immune responses to AAV vectors: Overcoming barriers to successful gene therapy. *Blood* 122(1): 23-36.

241. Gao K, *et al* (2014) Empty virions in AAV8 vector preparations reduce transduction efficiency and may cause total viral particle dose-limiting side-effects. *Mol Ther Methods Clin Dev* 1(9): 20139.

242. O'Reilly M, *et al* (2014) Gene therapy: Charting a future course--summary of a national institutes of health workshop, april 12, 2013. *Hum Gene Ther* 25(6): 488-497.

243. Kiem HP, *et al* (2014) Charting a clear path: The ASGCT standardized pathways conference. *Mol Ther* 22(7): 1235-1238.

244. Gao G*, et al* (2003) Adeno-associated viruses undergo substantial evolution in primates during natural infections*. Proc Natl Acad Sci U S A* 100(10): 6081-6086.

245. Gao G*, et al* (2004) Clades of adeno-associated viruses are widely disseminated in human tissues*. J Virol* 78(12): 6381-6388.

246. Xie J*, et al* (2011) MicroRNA-regulated, systemically delivered rAAV9: A step closer to CNS-restricted transgene expression*. Mol Ther* 19(3): 526-535.

247. Chen S*, et al* (2014) Post-transcriptional regulation by miR-137 underlies the low abundance of CAR and low rate of bilirubin clearance in neonatal mice*. Life Sci* 107(1-2): 8-13.

248. Schizophrenia Psychiatric Genome-Wide Association Study (GWAS) Consortium (2011) Genome-wide association study identifies five new schizophrenia loci*. Nat Genet* 43(10): 969-976.

249. Crowley JJ*, et al* (2015) Disruption of the microRNA 137 primary transcript results in early embryonic lethality in mice*. Biol Psychiatry* 77(2): e5-7.

250. Olde Loohuis NF*, et al* (2015) MicroRNA-137 controls AMPA-receptor-mediated transmission and mGluR-dependent LTD*. Cell Rep* 11(12): 1876-1884.

251. Siegert S*, et al* (2015) The schizophrenia risk gene product miR-137 alters presynaptic plasticity*. Nat Neurosci* 18(7): 1008-1016.

252. Verma P, Augustine GJ, Ammar MR, Tashiro A & Cohen SM (2015) A neuroprotective role for microRNA miR-1000 mediated by limiting glutamate excitotoxicity*. Nat Neurosci* 18(3): 379-385.

253. Smrt RD*, et al* (2010) MicroRNA miR-137 regulates neuronal maturation by targeting ubiquitin ligase mind bomb-1*. Stem Cells* 28(6): 1060-1070.

254. Szulwach KE*, et al* (2010) Cross talk between microRNA and epigenetic regulation in adult neurogenesis*. J Cell Biol* 189(1): 127-141.

255. Pulicherla N*, et al* (2011) Engineering liver-detargeted AAV9 vectors for cardiac and musculoskeletal gene transfer*. Mol Ther* 19(6): 1070-1078.

256. Fairbanks CA (2003) Spinal delivery of analgesics in experimental models of pain and analgesia*. Adv Drug Deliv Rev* 55(8): 1007-1041.

257. Cradick TJ, Qiu P, Lee CM, Fine EJ & Bao G (2014) COSMID: A web-based tool for identifying and validating CRISPR/Cas off-target sites*. Mol Ther Nucleic Acids* 3: e214.

258. Shen S*, et al* (2012) Glycan binding avidity determines the systemic fate of adeno-associated virus 9*. J Virol*

259. Bell CL, Gurda BL, Van Vliet K, Agbandje-McKenna M & Wilson JM (2012) Identification of the galactose binding domain of the AAV9 capsid. *J Virol* 86: 7326-7333.

260. Akache B*, et al* (2006) The 37/67-kilodalton laminin receptor is a receptor for adeno-associated virus serotypes 8, 2, 3, and 9. *J Virol* 80(19): 9831-9836.

261. Kotchey NM*, et al* (2011) A potential role of distinctively delayed blood clearance of recombinant adeno-associated virus serotype 9 in robust cardiac transduction. *Mol Ther* 19(6): 1079-1089.

262. Friedman RC, Farh KK, Burge CB & Bartel DP (2009) Most mammalian mRNAs are conserved targets of microRNAs. *Genome Res* 19(1): 92-105.

263. Coolen M & Bally-Cuif L (2009) MicroRNAs in brain development and physiology. *Curr Opin Neurobiol* 19(5): 461-470.

264. Kwon E, Wang W & Tsai LH (2013) Validation of schizophrenia-associated genes CSMD1, C10orf26, CACNA1C and TCF4 as miR-137 targets. *Mol Psychiatry* 18(1): 11-12.

265. Hindson BJ*, et al* (2011) High-throughput droplet digital PCR system for absolute quantitation of DNA copy number. *Anal Chem* 83(22): 8604-8610.

266. Murlidharan G & Samulski,R.J., Asokan,A. (2016) in *Translational Neuroscience-Fundamental Approaches for Neurological Disorders-*
"Gene Therapy of CNS Disorders Using Recombinant AAV Vectors"
, ed Tuszynski MH (Springer, pp 9-32.

267. Hadaczek P*, et al* (2006) Convection-enhanced delivery of adeno-associated virus type 2 (AAV2) into the striatum and transport of AAV2 within monkey brain. *Hum Gene Ther* 17(3): 291-302.

268. Aukland K & Reed RK (1993) Interstitial-lymphatic mechanisms in the control of extracellular fluid volume. *Physiol Rev* 73(1): 1-78.

269. Iliff JJ & Nedergaard M (2013) Is there a cerebral lymphatic system?. *Stroke* 44(6 Suppl 1): S93-5.

270. Iliff JJ*, et al* (2014) Impairment of glymphatic pathway function promotes tau pathology after traumatic brain injury. *J Neurosci* 34(49): 16180-16193.

271. Iliff JJ, Goldman SA & Nedergaard M (2015) Implications of the discovery of brain lymphatic pathways. *Lancet Neurol* 14(10): 977-979.

272. Hoshi A*, et al* (2012) Characteristics of aquaporin expression surrounding senile plaques and cerebral amyloid angiopathy in alzheimer disease. *J Neuropathol Exp Neurol* 71(8): 750-759.

273. Kress BT*, et al* (2014) Impairment of paravascular clearance pathways in the aging brain*. Ann Neurol* 76(6): 845-861.

274. Ma T*, et al* (1997) Generation and phenotype of a transgenic knockout mouse lacking the mercurial-insensitive water channel aquaporin-4*. J Clin Invest* 100(5): 957-962.

275. Mawuenyega KG*, et al* (2010) Decreased clearance of CNS beta-amyloid in alzheimer's disease*. Science* 330(6012): 1774.

276. Ross CA & Poirier MA (2004) Protein aggregation and neurodegenerative disease*. Nat Med* 10 Suppl: S10-7.

277. Lindsay J*, et al* (2002) Risk factors for alzheimer's disease: A prospective analysis from the canadian study of health and aging*. Am J Epidemiol* 156(5): 445-453.

278. Smith DH, Johnson VE & Stewart W (2013) Chronic neuropathologies of single and repetitive TBI: Substrates of dementia?*. Nat Rev Neurol* 9(4): 211-221.

279. Fanara P*, et al* (2012) Cerebrospinal fluid-based kinetic biomarkers of axonal transport in monitoring neurodegeneration*. J Clin Invest* 122(9): 3159-3169.

280. Grieger JC & Samulski RJ (2012) Adeno-associated virus vectorology, manufacturing, and clinical applications*. Methods Enzymol* 507: 229-254.

281. Martino AT, Herzog RW, Anegon I & Adjali O (2011) Measuring immune responses to recombinant AAV gene transfer*. Methods Mol Biol* 807: 259-272.

282. Klein RL, Dayton RD, Tatom JB, Henderson KM & Henning PP (2008) AAV8, 9, Rh10, Rh43 vector gene transfer in the rat brain: Effects of serotype, promoter and purification method*. Mol Ther* 16(1): 89-96.

283. Mingozzi F & High KA (2011) Therapeutic in vivo gene transfer for genetic disease using AAV: Progress and challenges*. Nat Rev Genet* 12(5): 341-355.

284. Ghashghaei HT, Lai C & Anton ES (2007) Neuronal migration in the adult brain: Are we there yet?*. Nat Rev Neurosci* 8(2): 141-151.

285. Suh H, Deng W & Gage FH (2009) Signaling in adult neurogenesis*. Annu Rev Cell Dev Biol* 25: 253-275.

286. Suzuki SO & Goldman JE (2003) Multiple cell populations in the early postnatal subventricular zone take distinct migratory pathways: A dynamic study of glial and neuronal progenitor migration*. J Neurosci* 23(10): 4240-4250.

287. Zerlin M, Milosevic A & Goldman JE (2004) Glial progenitors of the neonatal subventricular zone differentiate asynchronously, leading to spatial dispersion of glial

clones and to the persistence of immature glia in the adult mammalian CNS. *Dev Biol* 270(1): 200-213.

288. Aguirre A & Gallo V (2004) Postnatal neurogenesis and gliogenesis in the olfactory bulb from NG2-expressing progenitors of the subventricular zone. *J Neurosci* 24(46): 10530-10541.

289. Ellis P, *et al* (2004) SOX2, a persistent marker for multipotential neural stem cells derived from embryonic stem cells, the embryo or the adult. *Dev Neurosci* 26(2-4): 148-165.

290. Beech RD, *et al* (2004) Nestin promoter/enhancer directs transgene expression to precursors of adult generated periglomerular neurons. *J Comp Neurol* 475(1): 128-141.

291. Jacquet BV, *et al* (2009) Analysis of neuronal proliferation, migration and differentiation in the postnatal brain using equine infectious anemia virus-based lentiviral vectors. *Gene Ther* 16(8): 1021-1033.

292. Eom TY, *et al* (2011) Direct visualization of microtubules using a genetic tool to analyse radial progenitor-astrocyte continuum in brain. *Nat Commun* 2: 446.

293. Beier KT, *et al* (2011) Anterograde or retrograde transsynaptic labeling of CNS neurons with vesicular stomatitis virus vectors. *Proc Natl Acad Sci U S A* 108(37): 15414-15419.

294. Card JP & Enquist LW (2014) Transneuronal circuit analysis with pseudorabies viruses. *Curr Protoc Neurosci* 68: 1.5.1-1.5.39.

295. Murlidharan G, Corriher T, Ghashghaei HT & Asokan A (2015) Unique glycan signatures regulate adeno-associated virus tropism in the developing brain. *J Virol* 89(7): 3976-3987.

296. Mali P, Esvelt KM & Church GM (2013) Cas9 as a versatile tool for engineering biology. *Nat Methods* 10(10): 957-963.

297. Ghashghaei HT, *et al* (2006) The role of neuregulin-ErbB4 interactions on the proliferation and organization of cells in the subventricular zone. *Proc Natl Acad Sci U S A* 103(6): 1930-1935.

298. Carlen M, *et al* (2009) Forebrain ependymal cells are notch-dependent and generate neuroblasts and astrocytes after stroke. *Nat Neurosci* 12(3): 259-267.

299. Jacquet BV, *et al* (2011) Specification of a Foxj1-dependent lineage in the forebrain is required for embryonic-to-postnatal transition of neurogenesis in the olfactory bulb. *J Neurosci* 31(25): 9368-9382.

300. De Wit J, Eggers R, Evers R, Castren E & Verhaagen J (2006) Long-term adeno-associated viral vector-mediated expression of truncated TrkB in the adult rat facial nucleus results in motor neuron degeneration. *J Neurosci* 26(5): 1516-1530.

301. Suh H*, et al* (2007) In vivo fate analysis reveals the multipotent and self-renewal capacities of Sox2+ neural stem cells in the adult hippocampus. *Cell Stem Cell* 1(5): 515-528.

302. Alonso M*, et al* (2008) Turning astrocytes from the rostral migratory stream into neurons: A role for the olfactory sensory organ. *J Neurosci* 28(43): 11089-11102.

303. Enquist LW (2012) Five questions about viral trafficking in neurons. *PLoS Pathog* 8(2): e1002472.

304. Koyuncu OO, Perlman DH & Enquist LW (2013) Efficient retrograde transport of pseudorabies virus within neurons requires local protein synthesis in axons. *Cell Host Microbe* 13(1): 54-66.

305. Hollis ER,2nd, Kadoya K, Hirsch M, Samulski RJ & Tuszynski MH (2008) Efficient retrograde neuronal transduction utilizing self-complementary AAV1. *Mol Ther* 16(2): 296-301.

306. Shih RA, Belmonte PL & Zandi PP (2004) A review of the evidence from family, twin and adoption studies for a genetic contribution to adult psychiatric disorders. *Int Rev Psychiatry* 16(4): 260-283.

307. Guo Z*, et al* (2000) Head injury and the risk of AD in the MIRAGE study. *Neurology* 54(6): 1316-1323.

308. Plassman BL*, et al* (2000) Documented head injury in early adulthood and risk of alzheimer's disease and other dementias. *Neurology* 55(8): 1158-1166.

309. Moretti L*, et al* (2012) Cognitive decline in older adults with a history of traumatic brain injury. *Lancet Neurol* 11(12): 1103-1112.

310. Johnson VE, Stewart W & Smith DH (2012) Widespread tau and amyloid-beta pathology many years after a single traumatic brain injury in humans. *Brain Pathol* 22(2): 142-149.

311. Low K, Aebischer P & Schneider BL (2013) Direct and retrograde transduction of nigral neurons with AAV6, 8, and 9 and intraneuronal persistence of viral particles. *Hum Gene Ther* 24(6): 613-629.